# Gut microbiota–mediated lipid accumulation as a driver of evolutionary adaptation to blue light toxicity in *Drosophila*

Yuta Takada[1], Toshiharu Ichinose[2,3], Naoyuki Fuse[4], Kokoro Saito[3], Wakako Ikeda-Ohtsubo[1], Hiromu Tanimoto[3], Masatoshi Hori[1]

[1]Graduate School of Agricultural Sciences, Tohoku University, Japan

[2]Frontier Research Institute for Interdisciplinary Sciences, Tohoku University, Japan

[3]Graduate School of Life Sciences, Tohoku University, Japan

[4]Graduate School of Pharmaceutical Sciences, Tohoku University, Japan

Correspondence to Yuta Takada or Masatoshi Hori

yutatakada38@gmail.com

masatoshi.hori.a3@tohoku.ac.jp

## Abstract

Human agriculture has always raced against insect adaptation, requiring updated pest control methods and knowledge of evolutionary processes. Excessive exposure to blue light (BL) kills a wide range of insect species and has attracted attention as an alternative to chemical pesticides. In this study, to understand the evolutionary adaptation of insects under the pressure of BL toxicity, we revealed evolutionary responses to BL toxicity over 70 generations using laboratory selection experiments in *Drosophila melanogaster*. The selected line exhibited an obese phenotype accompanied by midgut elongation, with BL tolerance dependent on gut microbiota–mediated lipid accumulation. Whole-genome and transcriptome analyses consistently highlighted interactions between the microbiota and lipogenesis genes. Remarkably, manipulation of lipogenesis via these genes conferred BL tolerance even in the absence of selection. We suggest that the acquisition of BL tolerance occurs through 'adaptive obesity'. Our study introduces a mechanism of evolutionary adaptation of insects against BL-based selective pressure by maximising the benefits from the gut microbiota via midgut elongation.

## Introduction

One of the most challenging issues in pest control is the rapid evolution of insects. Traditional chemical pesticides have led to the development of resistance, environmental contamination and unintended effects on non-target organisms, highlighting the need for alternative approaches[1,2].

Blue light (BL) is within the 400–500 nm range, is abundant in sunlight, and is crucial for insect physiology and ecology because it influences processes such as visual perception, circadian rhythms, and photoreactivation (Fig. S1)[3–6]. However, excessive exposure to BL is lethal in a variety of insect species[7]. We propose the use of BL as a pest control method and have demonstrated that exposure to BL at intensities below 40% of the BL content of sunlight for several days can be lethal to fruit fly *Drosophila melanogaster* (hereinafter referred to as *Drosophila*), mosquito *Culex pipiens* form *molestus,* flour beetle *Tribolium confusum,* and leaf beetle *Galerucella grisescens*[7–9]. Notably, in *Drosophila*, *C. pipiens* f. *molestus*, and *G. grisescens*, BL around 420, 440, and 465 nm has been found to be more lethal than shorter wavelength 375–405 nm[7–9]. In *Drosophila*, BL around 465 nm is particularly toxic to both pupae and adults, with males being more sensitive than females[9]. These results suggest that the sensitivity of BL toxicity cannot be explained by photon energy alone. The BL toxicity is thought to be associated with reactive oxygen species (ROS) generated by mitochondria and other cellular components, leading to oxidative damage[9–14]. This damage can impair fitness and act as a selective pressure in insects, yet tolerance and evolutionary adaptation to this stressor remain largely unexplored. Achieving the societal implementation of chemical-free, BL-based pest control requires the gathering of evolutionary insights.

Laboratory selection has contributed to understanding the evolutionary adaptations of organisms to environmental stressors[15,16]. *Drosophila* is well-suited for laboratory selection experiments due to its short life cycle and the extensive genetic and physiological knowledge available[17]. Importantly, these experiments often reveal both evolutionary responses and trade-offs that were not anticipated at the outset[18]. Observing evolutionary processes in the

laboratory and identifying the phenotypic, genomic and epigenomic factors that lead to tolerance in *Drosophila* are crucial to understanding the mechanisms of evolution in insects. Here, by selecting flies that are tolerant to excessive BL exposure, we established *Drosophila* strain with enhanced BL tolerance. Characterisation of these selected line (SL) flies revealed that obesity is a key adaptive trait for enhanced BL tolerance. Moreover, we found that parental BL exposure and selection under BL toxicity induce midgut elongation and that increased gut bacterial load is critical for acquired BL tolerance. This study highlights that maximising the benefits of the gut microbiota has been key to evolutionary adaptation in the host.

# Results

## *Drosophila* evolved BL tolerance through laboratory selection

Reproductive capacity is one of the most important determinants of fitness. We investigated the effects on ovarian development to determine whether damage caused by BL toxicity acts as a selective pressure. Older flies are known to be more sensitive to BL toxicity[13], but our results showed that even very young flies, such as those on the first day after eclosion with underdeveloped ovaries, were particularly susceptible (Fig. S2a and Data S1)[19]. BL toxicity consistently suppressed ovarian development at all stages between days 1 and 10 post eclosion (Fig. S2a). Even after a recovery period of up to 7 days post-BL exposure, ovarian recovery remained minimal (Fig. S2b and Data S1). These results highlight that BL toxicity has a dramatic effect on fitness.

First, we generated a *Drosophila* strain with BL tolerance through laboratory selection. In brief, we derived two experimental strains from the same population: one maintained without selective pressure and the other reared under BL toxicity-driven selection (Fig. 1 a). This procedure was replicated in three independent lines for each strain and each line was repeated for over 70 generations (Fig. 1 a). For laboratory selection, a Canton Special (Canton-S) strain, which is a long-inbred strain of the common wild type, was used as the

ancestral population (for details, see "Laboratory selection for BL tolerance -Artificial selection-" in Methods)[20]. Over the generations, 1–5 day-old flies were exposed for 3 days to BL at around 465 nm, a wavelength highly toxic to *Drosophila* adults, at a photon flux density at which approximately 50% of individuals exhibited the “low impact” phenotype, which was defined as being capable of climbing after a 2-day recovery (Fig. 2b and Fig. S1 and Fig. S3a)[9]. We then selected the low impact flies and let them breed to develop the SL lines (Fig. 1b). The unselected control line (UCL), maintained without BL irradiation, served as a negative control for comparative analyses with the SL. In the negative control group, 3 days of BL irradiation were replaced by darkness and UCL parents were randomly chosen (Fig. 1b and Fig. S3a). Although not selected, a subset of UCL flies in each generation was exposed to BL under the same conditions as the SL to serve as a positive control group (Fig. S3a). Across generations, no strain-specific differences in climbing ability were observed without BL irradiation (Fig. S3b and Data S1). In SL, both male and female flies showed greater climbing ability after BL irradiation following a single selection event (Fig S3a). In contrast, fecundity in SL remained suppressed by BL toxicity even after more than 10 generations of selection (Fig. 2a). After around 20 generations, SL flies began to show improved adaptability, with fecundity maintained at similar levels to flies in the non-irradiated UCL (Fig. 2a–c, Data S2 and Data S3). Ovarian development was affected little by BL exposure in the SL flies but severely in the UCL flies (Fig. 2b and Data S3). Moreover, fecundity in SL flies was slightly increased in response to BL irradiation, whereas that in UCL flies was reduced (Fig. 2c and Data S3). Additionally, SL flies survived longer than UCL flies under continuous BL irradiation (Fig. 2d and Data S3). After 73 generations of selection, the lifespan was further extended, with disparity from the UCL increasing as light intensity decreased (Fig. 2d, e, Fig. S4 and Data S3). These results collectively suggest that we have successfully established a new *Drosophila* strain with enhanced BL tolerance.

## SL flies exhibited obese phenotype, lipid accumulation, and

## oxidative stress resistance

Next, we examined the phenotypic characteristics of the SL flies in non-irradiated conditions. We noticed that they exhibited an obese phenotype characterised by abdomen bloating, increased body weight, and well-developed fat bodies with markedly increased lipid droplets (Fig. 3a, b and Fig. 4a–b' and Fig. S5a and Data S4). They also showed an elongated midgut and shortened wings (Fig. 4c and Fig. S5b and Data S4). Additionally, we observed a slightly low number of oocytes in the SL flies (Fig. S5c and Data S4) and a strong inter-individual correlation between oocyte number and body weight in the UCL flies (Fig. S5d and Data S4). SL flies maintained higher body weight than UCL flies despite similar food consumption levels (Fig. 4d and Data S4). Taken together, these results show that the increased body weight of SL flies was not due to larger ovaries or higher food intake but may instead be associated with increased lipid reserves and elongated midguts. SL flies were rich in major lipids, including fatty acids (fatty acid methyl esters, FAMEs) and triacylglycerol (TAG), and were starvation resistant, providing evidence of lipid accumulation (Fig. 4e–g and Data S4)[21,22]. Consistent with previous reports that lipid droplets and their constituent TAG may protect against oxidative damage[23–25], resistance to oxidative stress was higher in SL flies than in UCL flies (Fig. 4h and Data S4). We did not find any physical traits associated with light reflection by cellular melanin, despite previous reports suggesting these as adaptive traits to phototoxicity (Fig. S6)[26]. These results suggest that BL tolerance in SL flies is acquired physiologically through obesity, rather than through physical traits.

## Increased bacterial abundance in SL flies

Gut microbiota–derived acetate serves as a potential substrate for de novo lipogenesis in the host via acetyl-CoA[27,28]. Considering the elongated midgut and accumulated lipids in SL flies, we compared the gut microbiota profiles and amounts in SL and UCL flies. In both strains, 16S rRNA gene sequencing of whole-body DNA revealed that a single species of *Acetobacter* (*A. persici)*, a common gut bacteria in *Drosophila*, dominated (>99%) the

141 microbiota (Fig. S7a and Data S5)[29–31]. *Wolbachia* was not detected in our microbiota
142 analyses (Data S5). *A. persici* has also been detected in wild flies, and several studies have
143 reported that in some cases more than 90% of the microbiota consisted of this or other
144 *Acetobacter* species[30–34]. Relatedly, several studies have reported that *Acetobacter* can
145 dominate the gut microbiota in natural environments[35,36]. Notably, bacterial counts were
146 higher in SL flies than in UCL flies, and a mild positive relationship between body weight and
147 bacterial abundance was observed, with no change in microbiota profiles (Fig. 5a–a' and Fig.
148 S7b, b' and Fig. S8 and Data S5 and Data S6). All randomly sequenced colonies were
149 identified as *A. persici* (Data S6). These results consistently show that while both strains
150 colonise the same species, SL has the higher bacterial abundance.
151

## 152 Gut microbiota promotes BL tolerance and lipid accumulation 153 in SL flies

154 Acetic acid bacteria, including *Acetobacter*, are known to influence fecundity and TAG levels
155 in *Drosophila*[37–45]. In addition, both bacterial abundance and body weight were drastically
156 reduced in SL flies following BL irradiation, suggesting that the sensitivity of these flies to BL
157 toxicity may be related to the gut microbiota (Fig. S8). To test the hypothesis that gut
158 microbiota play a role in shaping the phenotype of SL flies, we used an antibiotic mixture
159 (Abx) that depletes the bacterial abundance (Fig. S9a). Interestingly, we found that BL
160 tolerance in the SL flies, as measured by fecundity, was totally abolished by Abx treatment,
161 suggesting the critical role of gut microbiota (Fig. 5b and Data S6). Feeding the Abx-treated
162 SL flies with the gut contents of SL flies rescued these phenotypes, whereas feeding with
163 those of UCL flies barely did (Fig. S9b–d, Fig. 5b, Data S6 and Data S7). Consistently, Abx
164 treatment significantly reduced the body weight and the TAG level selectively in the SL flies
165 (Fig. 5c–e and Data S6). This result highlights the dependence of SL flies' body weight and
166 lipid accumulation on their gut microbiota.

167 The midgut of Abx-treated SL flies was longer than that of UCL flies regardless of treatment,
168 and it was even longer in non-treated SL flies (Fig. 5f and Data S7). A positive correlation
169 between body weight and midgut length in non-treated SL flies (Fig. S10 and Data S7)
170 suggested that gut microbiota may contribute to midgut elongation. Furthermore, enhanced
171 oxidative stress resistance was observed only in non-treated SL flies (Fig. S11a, b and Data
172 S7). These observations align with previous reports that gut microbiota is linked to gut
173 morphology and oxidative stress resistance[29,46,47]. Overall, these results suggest that the
174 characteristic phenotype in SL flies is shaped by their gut microbiota.
175

## 176 Parental exposure to BL affects gut microbiota–associated
## 177 traits in progeny

178 We investigated why only the gut contents from SL flies could rescue BL tolerance in infection
179 experiments, despite the dominance of the same gut bacterial species across strains (Fig.
180 S7a and Fig. 5b). We noticed that the flies used for gut contents had different parental
181 experiences depending on whether they belonged to the UCL or SL. Additionally, parental
182 exposure to BL has been reported to alter the transcriptome of the progeny[48]. Thus, we
183 hypothesised that parental exposure to BL irradiation might influence gut microbiota–
184 associated traits in the progeny, leading to quantitative or qualitative changes in gut
185 microbiota. We exposed adult males and females from both strains to the same BL toxicity
186 used in the selection experiment for 3 days, followed by a 3-day recovery period. We then
187 randomly picked flies to be the parent, producing progeny that were influenced by the
188 parental experience (Fig. 6a). First, we examined the body weight and BL tolerance in Abx-
189 treated SL flies that were fed with gut contents from flies whose parents had or had not
190 received BL irradiation. Abx-treated SL flies fed with gut contents from SL flies whose parents
191 had experienced BL irradiation showed the greatest increase in body weight (Fig. S12a–b
192 and Data S8). However, flies fed with gut contents from *A. persici* in different cocktails, each

193 standardized in concentration, exhibited similar body weight increases (Fig. S12c and Data
194 S8). This suggests that quantitative rather than qualitative changes in gut microbiota due to
195 parental BL irradiation are responsible for the increases in host body weight. Furthermore,
196 gut contents from UCL flies whose parents had experienced BL irradiation also rescued the
197 phenotypes of Abx-treated SL flies, restoring fecundity to the level conferred by gut contents
198 from SL flies (Fig. S13a–b and Data S8). These results indicate that parental BL irradiation
199 affects the progeny's bacterial abundance. Consistent with this idea, parental BL irradiation
200 increased the progeny's body weight, bacterial abundance, and midgut length in both UCL
201 and SL flies (Fig. S14, Fig. 6b, c and Data S8). Notably, even without parental BL irradiation,
202 the midgut of SL flies was longer than that of non-irradiated UCL flies, suggesting that this
203 inherited trait had been conserved during the laboratory selection of SL flies (Fig. 6c). In both
204 strains, parental BL irradiation induced midgut elongation even after antibiotic treatment,
205 suggesting that in *Drosophila* this is a common response dependent on parental experience.
206 The increased abundance of beneficial bacteria under BL toxicity may improve fitness,
207 highlighting the dependence of BL tolerance in SL flies on gut microbiota.
208

## 209 Host genome and transcriptomic profiles explain the 210 characteristic phenotype of SL flies

211 To investigate how the SL flies develop their phenotypes through interactions with the gut
212 microbiota, we first performed whole-genome resequencing aimed at detecting genetic
213 characteristics unique to SL. The first approach was to explore genes that show strain-
214 specific variation to understand the genetic variation of SL. We identified 1,917 genes with
215 SL-specific variation above 5% for the full sequence length of each gene (Fig. 7a and Data
216 S9 and Data S10). Kyoto Encyclopedia of Genes and Genomes (KEGG) enrichment analysis
217 of these variations revealed their association with detoxification and antioxidant response
218 such as *Glutathione S transferase* (e.g. *GstD4*, *GstD5, GstD6, GstD7, GstD10, GstE1, GstE2,*

219 *GstE5, GstE6, GstE8, GstE11, GstE14, GstO2, GstT3*) (Fig. 7b and Data S10)[49]. Given the
220 role of oxidative stress in BL toxicity[9,11,13], the variation in these detoxification enzymes
221 suggests functional changes and the effect of selective pressures. The original of Canton-S
222 strain is isogenic in the 1920-1930s, although it has already accumulated variants due to long
223 laboratory breeding (note that the sequencing data is from the Canton-S strain obtained from
224 the Bloomington *Drosophila* Stock Center (Fig. S15a))[20,50]. Even in UCL, the detection of
225 694,867 total sites with heterozygous and homozygous variants across the three replicate
226 lines supports the possibility that multiple standing variants were present (Fig S15b–d). We
227 analysed strain-specific homozygous variants to further elucidate the genetic basis of SL.
228 Homozygous variants shared among the three replicate lines in SL and absent in UCL and
229 in the Canton-S strain were identified (Fig. S16). SL-specific SNPs and indels were detected
230 in 658 and 2,625 genes, respectively, giving a total of 2,970 genes, and the majority of
231 alterations were located outside the coding sequences (CDS) (Fig. 7c and Data S11). KEGG
232 enrichment analysis identified the Notch signaling and the Hippo signaling pathway as
233 enriched pathways (Fig. 7d), consistent with their known function in organ size regulation[51–
234 53]. In particular, the presence of CDS variants in genes that regulate or interact with the Hippo
235 signaling pathway (*Par-1* (missense mutation), *misshapen* (frameshift mutation)), together
236 with the elongated midgut observed in Abx-treated SL flies, suggests that midgut elongation
237 was potentially influenced by these variants (Data S11, Fig. 5f and Fig. 6c)[52,54,55].
238 Furthermore, the Toll and Imd pathways of the immune system were identified as enriched
239 pathways of 4,612 genes with SL genetic characteristics (Fig. 7e and Data S12)[56,57]. The
240 genetic features of SL suggest that the acquisition of gut microbiota-dependent phenotypes
241 may have been facilitated by midgut elongation and immune system modifications.
242 Because variations located outside the CDS are generally thought to influence gene
243 expression and because gut microbiota may alter host phenotypes through changes in the
244 host transcriptome[37,58,59], we performed transcriptome analysis on the whole body of non-
245 irradiated UCL and SL flies, with or without the Abx treatment. We identified 1,242

246 differentially expressed genes (DEGs), of which 1,192 (96%) were specific to non-treated SL
247 flies (Fig. S17a, b, Fig. 8a and Data S13). KEGG enrichment analysis of the 1192 DEGs
248 revealed gene enrichment in oxidative phosphorylation, metabolic pathways and the
249 tricarboxylic acid (TCA) cycle (Fig. 8b and Data S13). Suppressed mitochondrial metabolism
250 is known to lead to lipid accumulation in various animal species[60,61]. Consistent with this fact,
251 non-treated SL flies showed downregulation of most of the genes involved in oxidative
252 phosphorylation and the TCA cycle, which are associated with mitochondrial metabolism (Fig.
253 8c). In addition, several genes whose downregulation is known to induce lipid accumulation
254 were also specifically downregulated in non-treated SL flies (Fig. 8c)[21,22,62], including
255 *Tachykinin* (*Tk*), which also harbored mutation in the SL flies (Fig. 8c and Data S13). Actually,
256 *Tk* expression is known to be modulated in response to acetate produced by gut microbiota,
257 thereby regulating lipid utilisation in enterocytes[37,63]. As expected, approximately 30% of
258 DEGs (387 genes) reflected the distinctive genomic profile of SL, with the Toll and Imd
259 signaling pathways appearing most enriched (Fig. S18a–d). Of these, 276 genes contained
260 homozygous variants, including 6 genes associated with the Toll and Imd signaling pathways,
261 such as *Toll* (Fig. S18b and Data S14). Our results suggest that the phenotypes of SL flies
262 are influenced by the Hippo signaling pathway, *Tk*, and mitochondrial genes, and by their
263 interactions with gut microbiota.
264

## 265 Lipid accumulation via genetic manipulation confers BL
## 266 tolerance

267 Our finding suggest that SL has acquired a gut microbiota-driven lipid accumulation (Fig.4,
268 Fig. 5 and Fig. 8c). To prove the causal relationship between lipid accumulation and BL
269 tolerance, we examined BL tolerance in genetically manipulated flies that are reported to
270 have increased TAG levels[21,22]. We used a range of mutants and GAL4/UAS-mediated
271 manipulations, including knockdowns of *Tk*, *AkhR*, and *Lipid storage droplet-1 (Lsd-1)*, which

were downregulated in the SL flies (Fig. 8c, Data S13 and Data S15). Interestingly, knocking down these genes enhanced BL tolerance to a level comparable to that in the SL flies (Fig. 9a). Furthermore, BL tolerance was also enhanced by other genetic manipulations that are known to increase lipid levels but were not detected as DEGs in our transcriptome analysis (Fig. 8c), such as knockdown of *brummer* (*bmm*), *Phosphatase and tensin homolog* (*Pten*), and *Stromal interaction molecule* (*Stim*), and overexpression of *Insulin-like receptor* (*InR*), *Lk6 kinase* (*Lk6*), and *Lipid storage droplet-2* (*Lsd-2*) (Fig. 9a). Indeed, we found a significant positive relationship between fecundity and TAG levels among flies with all of these genetic modifications (Fig. 9b), which strongly suggests that lipid accumulation is a trait that confers BL tolerance (Fig. 9c).

## The transcriptome of *A. persici* in the host and the growth patterns vary between the host strains

Finally, we tried to investigate the possible mechanisms underlying the contribution of *Acetobacter*. To our knowledge, seventeen *Acetobacter* species have been identified as gut bacteria in *Drosophila* and are known to affect host metabolism and fitness[31,33,35,38,41–46,64,65]. Phylogenetic analysis based on reported full-length 16S rRNA gene sequences suggesting that *A. persici* is closely related to *A. malorum* and *A. cerevisiae* (Fig. 10a). In both UCL and SL, the dominant OTU ID (397 bp) representing 89-98% of the microbiota was identified as *A. persici* Dm-48 strain with 99.75% sequence identity (Fig. 10a, Fig. S19). Analysis of the complete genome of *A. persici* using publicly available data showed that its chromosome is 3,230,507 bp, while its plasmid is 526,169 bp, containing 2,898 and 492 CDS, respectively (Fig. 10b). To characterise the transcriptomic profile of *A. persici* within the host, we first extracted reads that were not mapped to the host genome in the RNA-seq data and subsequently mapped them to the complete genome of *A. persici*. As this mRNA was obtained by poly(A) selection of the host, there is a possibility of bias in the results. However, the sequencing depth was approximately 10X, ensuring a minimum number of reads for

comparative analysis (Fig. 10c, Fig. S20a and Data S16). This approach primarily captured extreme variation and may have missed low-expressed genes. Nevertheless, a total of 225 DEGs were detected, including 124 downregulated and 101 upregulated genes (Fig. S20b and Fig. 10d). Gene Ontology (GO biological process) enrichment analysis revealed a frequent enrichment of metabolic pathways, suggesting that the colonisation state of the *A.persici* within the SL differs from that in the UCL (Fig. S20c and Data S16). *A. persici* harbours 15 genes involved in acetic acid production[66]. Interestingly, key genes such as *Alcohol dehydrogenase* (*ADH*) and *Acetyl-CoA hydrolase* (EC 3.1.2.1) were found to be specifically upregulated in the SL (Fig. 10d and Data S16). These upregulated genes may contribute to the microbiota-dependent lipid accumulation of SL. The top 5 genes with the lowest *p*-values were all upregulated and included potentially oxidative stress-related genes such as *NADPH-dependent FMN reductase* and *Paraquat-inducible protein* (Fig.10d). The ability of *A. tropicalis*, a close relative of *A. persici*, to restore host survival via microbiota-mediated detoxification was previously documented (Fig. 10a)[64]. Given that antioxidant mechanisms are thought to contribute to resilience to BL toxicity, it is noteworthy that genes associated with the oxidation-reduction process were detected as enriched DEGs (Fig. 10f and Data S16). The upregulation of oxidoreductases and translocases indicates their potential antioxidant role by neutralising ROS and transporting key metabolites that support cellular redox balance (Fig. 10f). These results suggest that *A. persici* in SL has a different transcriptomic profile, especially in metabolism. However, it remains uncertain whether this difference is due to bacterial genomic variation, differences in bacterial colonisation state or host-mediated effects. We then investigated whether *A. persici* showed phenotypic differences by analysing the growth patterns of isolates from each host strain. Fifty colonies were cultured from each host strain. Consistent with the transcriptomic variation, *A. persici* isolates from the UCL and SL strains showed divergent growth patterns (Fig. 10g–g''' and Data S16). In the SL, 26% (13 colonies) failed to grow, whereas only 8% (4 colonies) failed to grow in the UCL. Additionally, UCL showed a higher variance, whereas SL showed a lower

326 variance (Fig. 10g''). This phenotypic difference indicated a potential bias towards SL-
327 dominant bacterial strains. Overall, these results suggest that BL toxicity may have acted as
328 a selective pressure shaping bacterial strain dynamics or driving host-microbiota co-evolution.
329

330 # Discussion

331 In this study, we established BL-tolerant *Drosophila* strains through laboratory selection,
332 demonstrating that excessive BL exposure drives the 'adaptive obesity', particularly lipid
333 accumulation mediated by gut microbiota. This supports the increasingly recognized role of
334 microbiota in host adaptation to environmental stress, in which specific bacterial populations
335 contribute to adaptive host phenotypes[33,43,67–69]. Our findings further reveal that elongation
336 of the host midgut in response to parental BL toxicity facilitates an increase in beneficial
337 bacteria, ultimately enhancing host fitness via lipid accumulation under excessive BL
338 exposure (Fig. S21).
339

340 ## Lipid storage is one of the factors that determines BL tolerance

341 SL flies exhibited increased lipid accumulation (Fig. 4), and genetic manipulation that
342 increased lipid contents conferred BL tolerance (Fig. 9). This acquisition of BL tolerance can
343 be explained by the role of lipid accumulation in protecting against ROS, which are produced
344 upon BL irradiation[12,13]. Intracellular lipid droplets play a critical role in shielding cells from
345 oxidative stress, as reduced TAG levels are associated with increased sensitivity to such
346 stress[23–25,70]. Indeed, the accumulation of lipid droplets in response to intracellular ROS has
347 been observed in many species[25,70]. Additionally, lipid droplets are closely linked to fecundity,
348 as higher TAG levels are associated with improved fecundity, whereas reduced TAG levels
349 can lead to oocyte degeneration[71,72]. Thus, lipid accumulation not only helps defend against
350 BL toxicity but also supports the maintenance of fecundity. Furthermore, the transcriptome of
351 SL flies revealed a broad downregulation of genes for mitochondrial metabolism (Fig. 8c).
352 Mitochondria, while crucial for energy production, also contribute to ROS generation[73]. It has

353 been reported that BL toxicity causes a decrease in ATP production[12,13]. Therefore, inhibition
354 of both mitochondrial metabolism and lipid utilisation may be an adaptive strategy to
355 accumulate lipids while minimising oxidative stress, and obesity may serve to compensate
356 for insufficient ATP levels.
357

358 **The potential of the gut microbiota for benefit enhancement in *Drosophila***

359 *Acetobacter* is generally the dominant bacteria in *Drosophila*[34–36,41,42]. The bacterial
360 composition and relative abundance within the microbiota varied between laboratories, with
361 *Acetobacter* sometimes accounting for over 90% of the community[30,32–34]. Generally, the
362 microbiota of laboratory flies is influenced by factors such as the host genome and
363 environmental conditions, including diet[34,36,42]. We identified *A. persici* as the predominant
364 bacterial species and showed the critical role of its increased abundance in the acquisition
365 of BL tolerance. *Acetobacter* species, which are well-known symbionts of *Drosophila* and
366 other insects, are recognized for their acetate production[74]. Acetyl-CoA, derived from acetate,
367 is essential for lipid utilisation[28,75] and also plays a crucial role in the acetylation of both
368 histone and non-histone proteins, facilitating adaptive responses through tissue
369 plasticity[37,76,77]. The elevated TAG levels observed in SL flies may be explained by the
370 increased acetyl-CoA pool resulting from gut microbiota–derived acetate. The increased
371 expression of acetic acid production genes in *A. persici* from the SL supports this hypothesis
372 (Fig. 10d)[66]. Additionally, gut microbiota might act as a barrier against physiological stress
373 induced by BL toxicity. The significant reduction in gut microbiota following BL irradiation in
374 SL flies suggests the evolution of mechanisms that utilise bacteria as a direct nutritional
375 resource or as enzymes (Fig. S8 and Fig. 10f). These findings align with previous research
376 showing that *Acetobacter* enhances the fitness of the host fly[29,35,43–45]. Notably, *Acetobacter*
377 infection enhances oxidative stress tolerance in *Drosophila*, whereas oxidative stress
378 reduces *Acetobacter* abundance, consistent with the findings of Brown *et al.* 2021 (Fig. S8
379 and Fig. S11)[64]. Several studies in *Pseudomonadota*, including *Acetobacter*, have shown

380 that gut bacterial enzymes in nematodes and insects adaptively contribute to host stress
381 tolerance[33,64,78,79]. Consistently, our transcriptome analysis revealed that antioxidant
382 enzymes are part of the upregulated cluster in *A. persici* from SL (Fig. 10d, f and Data S16),
383 suggesting their potential role as bacterial metabolism benefiting the host. In addition, the
384 infection experiments primarily suggested that bacterial abundance strongly influenced the
385 outcome; yet infection with gut contents did not fully rescue the fecundity of SL (Fig. 5b and
386 Fig. S13b). This implies that in addition to bacterial abundance, qualitative differences in *A.*
387 *persici* (such as colonisation status, within the host response, metabolism and bacterial
388 strains) may also play a critical role in host BL tolerance. Given that bacterial evolution is
389 likely to be faster than host genetic change, it is plausible that some genetic differences have
390 arisen in SL-derived *A. persici*. This is suggested by the slightly higher weight gain rate
391 observed for SL-derived *A. persici* in infection experiments with standardised bacterial
392 concentrations, and by differences in the growth patterns of isolated bacteria, with SL strains
393 showing less variance (Fig. S12c and Fig.10g, g''). However, the rate of microbiome evolution
394 during the experimental evolution process is unknown. The difference in bacterial
395 phenotypes highlights the importance of investigating bacterial strain dynamics in response
396 to BL toxicity and host-microbiota co-evolution in future studies.
397

398 **Acquisition of BL tolerance in SL via adaptive obesity**

399 When specific bacteria are implicated in host fitness-related phenotypes, their relative
400 enrichment often leads to reduced microbiota diversity[33,68]. Given that the microbiota
401 composition did not differ between strains (Fig. S7a), the initial diversity of the gut microbiota
402 in our study was probably low. Despite low microbiota diversity, increased abundance of *A.*
403 *persici*, possibly together with reduced strain diversity (dominance of specific strains),
404 appears to confer an adaptive phenotype in SL. Characteristic features such as shortened
405 wings and an elongated midgut were also observed in the SL phenotype. We propose that
406 gut elongation plays a key role in evolutionary adaptation driven by the gut microbiota. Both

407 scenarios could contribute to the formation of the SL phenotype: changes in organ size may
408 be influenced by independent pathways or result from a trade-off in resource allocation. The
409 increase in bacterial abundance appears to be associated with midgut elongation and genetic
410 changes, particularly those in the Hippo signaling pathway and the Toll and Imd signaling
411 pathways (Fig. 4c, Fig. 5f, Fig. 6c, Fig. 7d, e and Fig. S18b). Because our bacterial
412 quantification was based on CFU measurements from whole-body homogenates, the direct
413 relationship between midgut elongation and bacterial abundance remains uncertain.
414 Nevertheless, the observation that SL flies retain an elongated midgut after Abx treatment,
415 but experience a significant reduction in body weight, suggests that gut microbiota are
416 necessary for the acquisition of obesity (Fig. S10). The resulting phenotype from laboratory
417 selection may have been influenced by a combination of epigenetics, de novo mutations,
418 genetic drift, and variant selection. We are not able to separate these contributions, and
419 further analysis will be needed to clarify the underlying mechanisms. The *Drosophila* total
420 sequence length is approximately 140 Mbp[80], with a de novo single nucleotide mutation
421 (SNM) rate of $3.3 \times 10^{-9}$ per site per generation[81]. This corresponds to an estimated 0.462 de
422 novo SNMs per generation across the genome. Over 44 generations (as in the WGS
423 performed), this amounts to approximately 26 de novo SNMs. However, we identified SL-
424 specific homozygous variants at 1,985 sites (corresponding to 658 genes) shared by the
425 three replicate lines, a level that cannot be explained by the accumulation of naturally
426 occurring variants alone. Although de novo mutations may have occurred, we predict that
427 most of the SL-specific variants, including both SNPs and indels, are derived from standing
428 variations already present in the ancestral population. The possibility that BL toxicity
429 increases the SNM rate cannot be ruled out and requires further investigation of the
430 molecular evolutionary process. We also found that parental irradiation with BL, when
431 combined with accumulated mutations in later generations of SL flies, is critical for the midgut
432 elongation and bacterial abundance (Fig. 6b, c). This is consistent with previous studies
433 showing that parental exposure to environmental stressors, such as starvation and BL toxicity,

434 induces epigenetic inheritance or alternations in the transcriptome[48,82]. In *Drosophila*, the
435 midgut undergoes plastic elongation or shortening in response to environmental
436 conditions[83,84]. This physical expansion of the gut, which increases spatial capacity, offers
437 several advantages, including more efficient nutrient absorption, increased bacterial
438 abundance, and maintenance of gut homeostasis[71,85–89]. However, midgut elongation alone,
439 even after one generation with parental exposure to BL toxicity, is insufficient for BL tolerance
440 (Fig. 2a and Fig. 6c). Full BL tolerance requires both midgut enlargement and specific genetic
441 changes. Among these genetic factors, the genes for the neuropeptide *Tk* and its receptor
442 *TkR99D* are particularly important (Fig. 8c, Fig. 9 and Data S11), as they may regulate lipid
443 utilisation in response to acetate produced by the gut microbiota[37,62]. Laboratory evolution
444 studies typically use genetically diverse populations, such as wild populations or multiple
445 lines from the *Drosophila* Genetics Reference Panel[90]. As we used Canton-S (low genetic
446 diversity), it is possible that microbiota-mediated lipid accumulation was more optimal than
447 the development of dedicated lipid synthesis systems driven by host genetic changes.
448 Microbiota-mediated evolutionary adaptation and co-evolution under low host genetic
449 diversity remain interesting topics for future research.
450

451 **Implications of our findings for pest control**

452 BL toxicity indicates wavelength-specific effects across insect species and developmental
453 stages[9]. Reports also show no changes in sensitivity between mutant or overexpression
454 models of photoreceptors[10], suggesting a complex underlying mechanism. Our study
455 identifies lipid storage and gut microbiota as critical factors in BL tolerance. In addition, we
456 have shown that BL toxicity strongly inhibits ovarian development and exerts persistent
457 suppressive effects even in the absence of lethality (Fig. S2). In the context of pest control,
458 the combination of BL irradiation with treatments that disrupt insect lipid storage and gut
459 microbiota could potentially improve efficacy. In parallel with the development of these

methods, research into whether similar tolerance mechanisms exist in other insect species could lead to more effective chemical-free BL pest control.

## Conclusion

Our findings highlight the importance of gut microbiota–mediated lipid accumulation as an adaptive trait for BL tolerance. The elongation of the midgut, associated with an increased abundance of beneficial bacteria, turns out to be a key factor in this evolutionary adaptation. Such phenotypes may be driven by genetic and epigenetic changes from selective pressures and parental BL exposure. These evolutionary responses to excessive BL exposure demonstrate how host traits evolve under a toxic BL environment by maximising the benefits provided by gut microbiota. Our study reveals an insect evolutionary process via the microbiome and presents a concept of evolutionary adaptation initiated by midgut elongation.

# Methods

## Fly cultures and diet

Flies were maintained at 23–26°C on a 16:8 hour light:dark cycle using cold cathode fluorescent lamps as the light source. Detailed light conditions are provided in Fig. S1. The fly diet consisted of 5 g glucose (Fujifilm Wako Pure Chemicals Co., Osaka, Japan), 6 g dry brewer's yeast (Asahi Group Holdings Ltd., Tokyo, Japan), 1 g agar (Fujifilm Wako Pure Chemicals Co.), 0.4 mL propionic acid (Fujifilm Wako Pure Chemicals Co.), 0.4 mL 70% ethanol (Fujifilm Wako Pure Chemicals Co.), 0.01 g butyl *p*-hydroxybenzoate (Fujifilm Wako Pure Chemicals Co.), and 100 mL distilled water.

## BL irradiation

Virgin flies aged 1–5 days were used. Unless otherwise specified, flies were exposed to 462 nm BL for 3 days. BL irradiation conditions varied across experiments:

Fig. 2b–c, Fig. 5b, Fig. 6b, c, Fig. S2a, b, Fig. S3a, Fig. S8, Fig. S9c, d, Fig. S12b, c and Fig. S13b: Photon flux density $10.3 \times 10^{18}$ photons·$m^{-2}$·$s^{-1}$ for females.

Fig. 2a, c, Fig. S3a: $6.5 \times 10^{18}$ photons·$m^{-2}$·$s^{-1}$ for males.

Fig. 2d: Continuous BL irradiation for 5 days, $8 \times 10^{18}$ photons·$m^{-2}$·$s^{-1}$ for males and $10 \times 10^{18}$ photons·$m^{-2}$·$s^{-1}$ for females.

Fig. S4: Continuous BL irradiation for 10 and 4 days, $5 \times 10^{18}$ photons·$m^{-2}$·$s^{-1}$ and $15 \times 10^{18}$ photons·$m^{-2}$·$s^{-1}$ for females.

Fig. 9: 465 nm BL, $9.5 \times 10^{18}$ photons·$m^{-2}$·$s^{-1}$ for females.

Irradiation was performed in a multi-room incubator (LH-30CCFL-8CT; Nippon Medical & Chemical Instruments Co., Ltd, Osaka, Japan) at 24–26°C, with LED panels (IS-mini®, ISL-150 × 150 Series; CCS Inc., Kyoto, Japan) installed on the ceiling. Photon flux density was measured using a high-resolution spectrometer HSU-100S (Asahi Spectra Co., Ltd., Tokyo, Japan) with ND 0050 filter (Asahi Spectra Co., Ltd) and spectroradiometer MS-730 (EKO

500 Instruments Co., Ltd., Tokyo, Japan). For details see Fig. S1. All light condition
501 measurements used in the experiment are included in the source data (Light condition).
502

## 503 Laboratory selection for BL tolerance

### 504 Artificial selection

505 We used the Canton-S strain of *Drosophila* as the ancestral population for laboratory
506 selection. The Canton S strain used in this study was obtained from Tokyo Metropolitan
507 University in 2016. It has been maintained under laboratory conditions for at least 30 years
508 and has been bred in our laboratory in over 1,000 populations over 6 years. Two strains
509 were established, SL and UCL; the former was subjected to BL toxicity every generation
510 and the latter was used for controls. Each strain included three replicate lines. For each
511 strain, 60–100 virgin flies aged 1–5 days were placed in two 60 mm × 90 mm glass Petri
512 dishes for BL irradiation. SL and UCL flies (positive control group) were exposed to 462 nm
513 BL for 3 days. Instead of BL irradiation, the UCL, used as a negative control group, was
514 kept in darkness for 3 days. We followed this standard approach as dark conditions are
515 commonly used as a control in BL toxicity studies[7,10,11,48].

### 516 Climbing assay

517 Irradiated flies were placed in a breeding environment (for details, see “Fly cultures and diet”
518 in Methods) for a 2-day recovery period. For the data shown in Fig. S3a and Fig. S9c, the
519 impact of BL toxicity was assessed in a 4-minute climbing assay and the flies were
520 categorized into four states:
521 “Low impact”:
522 1. Intact: capable of climbing
523 “High impact” (unable to climb):
524 2. Phase 1: alive but unable to climb
525 3. Phase 2: alive but non-ambulatory
526 4. Phase 3: dead

527 **Artificial selective breeding and evaluation of fecundity**

528 "Low impact" SL flies were allowed 5 days for mating and egg-laying. In the early stages of
529 selection, there was no clear difference in climbing ability, and fecundity was low; thus, we
530 used as many intact individuals as possible as parents. From the 17th generation, when
531 tolerance began to emerge, we prioritised intact individuals that climbed above the 2 cm
532 threshold and selected preferentially for higher tolerance. Each vial containing 3 mL of diet
533 medium 3-mL contained 9–13 pairs, with a total of 4–8 vials (for details, see Source data
534 (Fig. 2a)). After 5 days, the diet medium containing eggs and larvae was transferred to a
535 larger plastic box (40 mL diet medium, 72 × 72 × 100 mm; Insect Breeding Square Dish,
536 SPL Life Sciences, Gyeonggi-do, Korea) to ensure sufficient food supply. One box was
537 used for every 4 or 5 vials. UCL parents were randomly chosen from the negative control
538 group (for details, see "Laboratory selection for BL tolerance -Artificial selection-" in
539 Methods) and reared under the same conditions as the SL flies. The total number of pupae
540 was counted and divided by the number of parents to determine the fecundity per female
541 for each generation.

542

543 **Negative geotaxis climbing assay in non-irradiated conditions**

544 Young adult flies, which typically climb 4 cm in 4 seconds, were tested for negative
545 geotaxis[91]. In Fig. S3b, ten flies aged 5–10 days were placed in an empty vial, gently
546 tapped three times to ensure they reached the bottom and given 10 seconds to climb.
547 Climbing rate was defined as the flies reaching a 6 cm reference line within this time. Each
548 vial was tested three times with a 1-minute interval between trials and the mean climbing
549 rate was calculated.

550

551 **Survival assays**

552 Virgin flies aged 5–10 days were used. In the continuous BL irradiation assay, 50 or 42 flies
553 were placed in each glass Petri dish containing standard diet medium and exposed to 462

554 nm BL (Fig. 2d and Fig. S4). In the starvation assay (Fig. 4g), 10 flies were placed in each
555 vial with 1% (w/v) agar (Fujifilm Wako Pure Chemicals Co.) in distilled water. In the
556 oxidative stress assay, 10 flies were placed in each vial with a medium prepared with either
557 10 mM paraquat dichloride standard (Fujifilm Wako Pure Chemicals Co.) (Fig. 4h) or 10
558 mM 1,1'-dimethyl-4,4'-bipyridinium dichloride (Tokyo Chemical Industry Co., Ltd., Tokyo,
559 Japan) (Fig. S11a, b), 5% (w/v) glucose (Fujifilm Wako Pure Chemicals Co.), and 1% (w/v)
560 agar (Fujifilm Wako Pure Chemicals Co.) in distilled water. The surviving flies were
561 manually counted every 2 h. Survival curves were visualised using the KaplanMeierfitter
562 from the lifelines (Python version 3.8.3 version 0.25.9).
563

564 **Measurement of fecundity**

565 To measure fecundity (Fig. 2a, Fig. 5b, Fig. 9, and Fig. S13b), after 3 days of darkness
566 (non-irradiation) or BL irradiation followed by a 3-day recovery period, 5 surviving females
567 were randomly chosen and mated with 5 non-irradiated virgin males (aged 1–10 days) in
568 individual pairs within vials containing 5 mL of diet medium for 4 days of egg-laying. The
569 total numbers of pupae and emerged adults were counted to evaluate fecundity and
570 emergence rate (in Fig. 2a and Fig. 2c, only the total number of pupae was measured).
571 Fig. 2c, Fig. 5b and Fig. S13b used non-irradiated Abx-treated males from the UCL or SL
572 and Fig. 9 used non-irradiated Canton-S males.
573

574 **Measurement of body weight, organ size and oocyte number**

575 Phenotypic measurements were performed on non-irradiated flies in Fig. 3a, b, Fig. 4c, Fig.
576 5a, d, f, Fig. 6c, Fig. S8 and Fig. S14 and on BL-irradiated flies in Fig. 2b, Fig. S2a, b and
577 Fig. S8. As ovarian development can progress with age, we ensured that phenotypic
578 comparisons between strains were made at the same chronological age[19]. Virgin flies aged
579 4–12 days were anesthetized by chilling on ice. Body weight was measured using an
580 AUW220D balance (Shimadzu, Kyoto, Japan). Wings or ovaries were dissected and

581 photographed under a SteREO Discovery.V12 stereomicroscope and an Axiocam 305
582 color camera (Carl Zeiss, Oberkochen, Germany). Wing length was measured as the
583 distance between the alula opening and the distal edge of the 3rd longitudinal vein, using
584 Fiji ImageJ2 (version 2.3/1.54f), following a previous method[92]. Stage 14 oocytes were
585 counted under the stereomicroscope. Midgut lengths of regions R1 to R5 were measured
586 manually from the midgut images using Fiji ImageJ2[89].
587

588 **Lipid droplet staining and imaging**

589 In Fig. 4b and b', we performed dissection and fluorescence microscopy to visualise lipid
590 droplets in the fat body of the abdominal epithelium of virgin female flies aged 6–12 days
591 kept in non-irradiated conditions. After removing other tissues from the abdomen, we fixed
592 the abdominal epithelium in PBS containing 4% paraformaldehyde (Fujifilm Wako Pure
593 Chemicals Co.) for 20 minutes. After fixation, we washed the samples twice with PBS
594 (Gibco, Carlsbad, CA, USA) for 15 minutes each time. The fixed abdominal epithelium was
595 stained with Nile Red (Fujifilm Wako Pure Chemicals Co.) at a concentration of 10 μg/mL
596 overnight according to a previous method[93]. Following this, we washed the samples twice
597 with PBS for 10 minutes each time and then stained them with NucBlue (Thermo Fisher
598 Scientific, Waltham, MA, USA) for 3 minutes, followed by a 5-minute wash with PBS. All
599 staining procedures were conducted in a light-shielded environment at room temperature.
600 Imaging was performed under an Eclipse Ti2 microscope equipped with a DS-Ri2 camera
601 (Nikon, Tokyo, Japan). The images were analysed using the Python package OpenCV
602 (Python version 3.8.3 version 4.5.3.56) to obtain the mean fluorescent intensity of Nile Red.
603

604 **Lipid extraction and derivatization of fatty acids**

605 Lipids were extracted using the Bligh and Dyer method[94,95]. Two virgin female flies aged 6–
606 12 days and kept in non-irradiated conditions were homogenised in 100 μL of PBS (Gibco),
607 added 600 μL of methanol (Fujifilm Wako Pure Chemicals Co.) and chloroform (Fujifilm

608 Wako Pure Chemicals Co.) in a 2:1 (v/v) ratio, vortexed for 1 minute, and shaken at 1000
609 rpm for 2 h at 4°C. Next, we added 200 μL of chloroform and 250 μL of distilled water,
610 vortexed for 1 min, centrifuged at 9000 rpm for 2 min, and collected the organic lower
611 phase. We then added 400 μL of chloroform to the remaining mixture, vortexed for 1
612 minute, and centrifuged as above. The two organic extracts were pooled and dried under
613 vacuum. The dried lipids were derivatized using the Fatty Acid Methylation Kit (Nacalai
614 Tesque, Inc., Tokyo, Japan) and the Fatty Acid Methyl Ester Purification Kit (Nacalai
615 Tesque, Inc.). FAMEs were collected.
616

617 **Gas chromatography mass spectrometry (GC-MS) analysis**

618 The FAMEs were analysed using a GC-MS instrument (GCMS-QP2010 Ultra (Shimadzu))
619 equipped with a DB-5 ms column (30 m × 0.25 mm ID, 0.25 μm film thickness) (J&W
620 Scientific, Folsom, CA, USA). Helium was used as the carrier gas at a pressure of 100 kPa.
621 The column oven was set at 40°C for 5 minutes. The temperature was increased at a rate
622 of 10°C/min to 280°C and maintained at 280°C for 10 minutes. The injection port
623 temperature was 220°C, and the analysis was performed in split mode. Fatty acids were
624 identified using a similarity search against the standards Supelco F.A.M.E. Mix C4-C24
625 (Supelco, Bellafonte, PA, USA) and relevant references[96,97]. The total ion chromatogram
626 area for each compound was measured. On the basis of the obtained data, we compared
627 the total amount of FAMEs. The log-transformed average values of each compound in each
628 replicate line were visualized using a cluster map. Clusters were classified by hierarchical
629 clustering using the Ward method based on Euclidean distances between compound
630 amounts[98].
631

632 **Measurement of TAG**

633 Relative TAG levels were measured by homogenising 10 virgin female flies aged 6–12
634 days and kept in non-irradiated conditions, in 1 mL of PBS (Fujifilm Wako Pure Chemicals

635 Co.) containing 0.1% Triton X-100 (Nacalai Tesque Inc.). The homogenate was heated at
636 70°C for 10 minutes and then centrifuged at 20,000 × *g* for 15 minutes at 4°C. A 10-μL
637 aliquot of the supernatant was used for TAG measurement using the LabAssay Triglyceride
638 kit (Fujifilm Wako Pure Chemicals Co.). For protein normalization, protein concentration
639 was measured using the Bradford method with the Protein Assay CBB Clean Up Kit and
640 Protein Assay CBB Solution (both from Nacalai Tesque Inc.), with the standard calibration
641 curve prepared using bovine serum albumin solution (Nacalai Tesque Inc.). Absorbance
642 was measured using the BioTek Synergy H1 Multimode Reader (Agilent Technologies Inc.,
643 Santa Clara, CA, USA). Relative TAG levels were normalised to protein content, adjusted
644 on the basis of the average values from UCL (Fig. 4f and Fig. 9) or non-treated UCL (Fig.
645 5e), and the $Log_2$ fold change was computed accordingly.
646

647 **Measurement of reflectance and transmittance**

648 Virgin female flies, aged 6–12 days and kept in non-irradiated conditions, were
649 anesthetized on ice. The abdominal reflectance and transmittance were measured by
650 capturing hyperspectral images under a BX51WI microscope (Olympus, Tokyo, Japan)
651 fitted with an SC-108 hyperspectral imaging system (EBA Japan Co., Ltd., Tokyo, Japan).
652

653 **DNA extraction**

654 Virgin female flies, aged 5–8 days and kept in non-irradiated conditions, were used. For
655 Fig. 7 and Fig. S7a, the same sample of 30 flies was used, with 10 flies used specifically for
656 Fig. S7b'. The flies were rinsed in a 1.5-mL tube with 99% ethanol (Fujifilm Wako Pure
657 Chemicals Co.) for 30 seconds. Then, 180 μL of PBS and beads were added, and the flies
658 were homogenised at 3500 rpm for 30 seconds using the Micro Smash MS100R (Tomy
659 Seiko Co., Ltd., Tokyo, Japan) while keeping the mixture cold. DNA was extracted using
660 the DNeasy Blood & Tissue Kit (Qiagen, Hilden, Germany) according to the kit protocols.
661

662 **16S rRNA amplicon sequencing (V3–V4 hypervariable region)**

663 Virgin female adult flies were used after surface sterilisation under non-irradiated
664 conditions. For details of DNA samples, see “DNA extraction” in Methods. Quality checks
665 were performed using the 2100 BioAnalyzer (Agilent Techologies Santa Clara, CA, USA),
666 followed by library preparation with the NEBNext® Ultra™ II DNA Library Prep Kit (Illumina,
667 San Diego, CA, USA). DNA amplification was performed by PCR using the V3-V4 region
668 primers 341F (5'-CCTAYGGGRBGCASCAG-3') and 806R (5'-
669 GGACTACNNGGGTATCTAAT-3'). PCR cycling conditions were as follows: 95°C for 3
670 minutes, followed by 25 cycles of 95°C for 30 seconds, 55°C for 30 seconds, 72°C for 30
671 seconds, with a final extension at 72°C for 5 minutes and holding at 4°C. Amplicon
672 sequencing was conducted on an Illumina NovaSeq 6000 with the following parameters:
673 paired-end reads of 250 bp × 2 (PE250) and an output of 50,000 reads per sample. In silico
674 analyses were performed on a Mac OS (Catalina version 10.15) terminal using Jupyter
675 Notebook (Python version 3.9 version 6.4.11). Quality was assessed with FastQC (version
676 0.11.8). Data were analysed using QIIME 2 (version 2023.7) with the Silva 138 99% OTUs
677 full-length database (MD5: b8609f23e9b17bd4a1321a8971303310). The QIIME dada2
678 denoise-paired parameters were set as follows: --p-trim-left-f 30, --p-trim-left-r 30, --p-trunc-
679 len-f 250, and --p-trunc-len-r 250. To improve classification accuracy, taxonomic filtering
680 was performed by removing all unassigned taxa using the qiime taxa filter-table command,
681 resulting in a refined feature table. Sequences of operational taxonomic units were
682 classified to determine gut microbiota composition. Relative abundance calculations were
683 performed using the qiime feature-table relative-frequency function.

684

685 **Bacterial abundance and identification**

686 Body weights of 4 virgin adult females were measured after 3 days of non-irradiation or BL
687 irradiation followed by a 3-day recovery period (Fig. 5a–a’, Fig. 6b, Fig. S8). 4 surviving
688 females aged 6–12 days were randomly chosen, immersed in 70% ethanol for 1 minute,

689 washed three times with PBS homogenised in 500 μL of PBS in a 2-mL tube (stock
690 solution), and diluted 1:100 with PBS. A 10-μL aliquot was plated onto an MRS agar plate
691 (5.5 g MRS broth (Becton, Dickinson and Company, Franklin Lakes, NJ, USA), 1 g agar
692 (Fujifilm Wako Pure Chemicals Co.), and 100 mL distilled water). The plates were
693 incubated for 72 hours at 30–31°C, and colony-forming units (CFU) were counted. Single
694 bacterial colonies were isolated, and their 16S rRNA genes were amplified by PCR using
695 universal bacterial primers 27F (5' AGAGTTTGATCCTGGCTCAG 3') and 1492R (5'
696 GGTTACCTTGTTACGACTT 3'). PCR cycling conditions were as follows: 95°C for 3
697 minutes, followed by 30 cycles of 94°C for 30 seconds, 55°C for 45 seconds, 72°C for 1
698 minute, with a final extension at 72°C for 7 minutes and holding at 4°C. Sequencing of the
699 amplified 16S RNA gene fragments was performed on an ABI3500 Sanger sequencing
700 platform (Thermo Fisher Scientific) using the BigDye™ Terminator v3.1 Cycle Sequencing
701 Kit (Thermo Fisher Scientific)[99,100]. Bacterial species were identified using Microbial
702 Nucleotide BLAST.
703

704 **Abx treatment**

705 The Abx was prepared according to established protocols[101]; the diet was supplemented
706 with 100 μg/mL streptomycin sulfate (Fujifilm Wako Pure Chemicals Co.), 50 μg/mL
707 tetracycline hydrochloride (Fujifilm Wako Pure Chemicals Co.), and 200 μg/mL rifampicin
708 (Fujifilm Wako Pure Chemicals Co.). Flies were reared on a diet containing Abx from the
709 embryo stage to adult.
710

711 **Capillary feeding (CAFE) assay**

712 The assay was adapted from a previous study with minor modifications[102]. Briefly, a group
713 of four male flies, aged 5-8 days, was kept in a plastic vial with two glass capillaries
714 inserted (BF100-50-15, Sutter Instrument, CA, USA). The gender was selected because
715 female flies often lay eggs inside the capillaries, which prevents precise measurement.

716 Flies were fed for 24h with liquid food (5% sucrose, 2% yeast extract, 0.25% nipagin in
717 ethanol, and 0.005% Sulforhodamine B sodium salt (red dye) in water), and images of the
718 capillaries were taken before and after the experiments. Reduction in liquid volume was
719 quantified to estimate consumption. To account for evaporation, control capillaries without
720 flies were included and their loss of fluid was used as a correction.
721

722 **Parental experience of BL irradiation**

723 Virgin flies aged 1–5 days were BL-irradiated for 3 days (462 nm BL, $6.5 \times 10^{18}$
724 photons·$m^{-2}$·$s^{-1}$ for males and $10.3 \times 10^{18}$ photons·$m^{-2}$·$s^{-1}$ for females) and allowed to
725 recover for 3 days. Non-irradiated parents were used as controls to ensure that the
726 offspring had no parental experience of irradiation. Flies exposed to BL irradiation were
727 assumed to experience BL toxicity. Parental choice was made without assessing
728 differences in survival status, such as climbing ability, to produce offspring with different
729 parental experiences. Randomly chosen males and females were allowed to mate and lay
730 eggs for 4 days.
731

732 **Infection with gut contents or *A. persici* cocktails**

733 In Fig. 5b, Fig. S12a and Fig. S13, 30 virgin female flies aged 5–8 days were immersed in
734 70% ethanol for 1 minute, washes three times with PBS and homogenised in 500 μL of
735 PBS in a 2-mL tube (stock solution). The latter was diluted 1:10 with PBS. To infect with the
736 gut microbiota, 20 μL of the diluted stock solution was added to the diet, and virgin females
737 aged 1–4 days were maintained on this diet for 4 days. PBS was used as a control. Body
738 weight was measured before and after infection. Climbing ability and fecundity were
739 evaluated after 3 days of non-irradiation or BL irradiation followed by a 3-day recovery
740 period. In Fig. S12b, *A. persici* was cultured and isolated on MRS plates for 48 hours.
741 These isolates, along with the standard strain of *A. persici* (JCM 25330), were cultured in
742 200 μL of MRS broth (5.5 g MRS broth (Becton, Dickinson and Company) and 100 mL

743 distilled water) in 96-well plates for 72 hours. Bacterial suspensions were centrifuged to
744 obtain pellets, and the 10-μL bacterial culture pellet was diluted 1:30 with PBS and
745 inoculated into 20 μL of diet. Autoclaved MRS was also diluted 1:30 with PBS, and 20 μL of
746 this mixture was used as the control.
747

## 748 Whole-genome resequencing, variation estimation, variant identification, 749 and enrichment analysis

750 Thirty virgin adult females were used after surface sterilisation under non-irradiated
751 conditions. For details of DNA samples, see “DNA extraction” in Methods. Quality checks
752 were performed using a BioAnalyzer, followed by library preparation with the NEBNext®
753 Ultra DNA Library Prep Kit (Illumina). Sequencing was conducted on an Illumina NovaSeq
754 6000 with the following parameters: paired-end reads of 150 bp (PE150), a data output of
755 10 G bases per sample, and approximately 66.7 million reads per sample. In silico
756 analyses were performed using a macOS (Catalina version 10.15.7) terminal and Jupyter
757 Notebook (Python version 3.9 version 6.4.11). The quality of the fastq files was assessed
758 using seqkit stat (version 0.16.1) and then fastqc (version 0.11.8). Reads were trimmed
759 using Trimmomatic (version 0.39) with the following parameters: LEADING:20,
760 TRAILING:20, SLIDINGWINDOW:4:15, and MINLEN:20, based on Illumina adapter
761 sequences (CTGTCTCTTATACACATCT,
762 AGATCGGAAGAGCACACGTCTGAACTCCAGTCA,
763 AGATCGGAAGAGCGTCGTGTAGGGAAAGAGTGT). Trimmed reads were re-evaluated
764 with seqkit stat and fastqc to confirm their quality. Mapping was performed using the
765 reference genome BDGP6.46, INSDC Assembly GCA_000001215.4 (details provided in
766 Data S9). Indexing and mapping were conducted using bwa (version 0.7.17), followed by
767 conversion from SAM to BAM format using samtools (version 1.10). PCR duplicates were
768 marked with GATK (version 4.2.6.1), and alignment statistics were calculated from the BAM
769 file. Paired-end reads were merged using samtools, and the merged BAM file was sorted.

770 Consensus sequences for UCL, SL, and Canton-S strains were generated using the
771 reference genome and VCF files. Gene sequences were extracted based on BDGP
772 6.32.109.chr.gtf3 annotations and processed using BioPython's SeqIO module. Gene
773 sequence alignments between strains were performed using BioPython's AlignIO module,
774 MAFFT (version 7.0), and variation for each gene were calculated using Canton-S
775 (SRX8038113)[50] as a reference. Variation was calculated as (the number of mismatched
776 bases to the reference gene / the total sequence length of the gene) × 100. Gaps were
777 counted as 0.5 to account for insertions, deletions and sequencing errors. SL-specific
778 variation was determined by subtracting the variation of each SL replicate line from the
779 mean variation of UCL replicate lines 1-3. Genes with a mean variation of more than 5%
780 across replicate lines 1-3 were classified as SL-specific variation. Variants were called
781 using sambamba (version 1.0.1) and varScan (version 2.4.6) with the following parameters:
782 sambamba mpileup, Heterozygous: SNP; pileup2snp --min-coverage 10 --min-var-freq 0.20
783 --p-value 0.05 (filter; default), Indel; pileup2indel --min-coverage 10 --min-var-freq 0.20 --p-
784 value 0.10 (filter; --min-reads2 4 --min-var-freq 0.15 --p-value 0.05), Homozygous: SNP;
785 pileup2snp --min-coverage 10 --min-var-freq 0.90 --p-value 0.05 (filter; default), Indel;
786 pileup2indel --min-coverage 10 --min-var-freq 0.90 --p-value 0.10 (filter; --min-reads2 4 --
787 min-var-freq 0.15 --p-value 0.05). Homozygous variants were identified by extracting rows
788 with matching Cons and VarAllele values. Common chromosomes and positions across
789 replicates (lines 1, 2, and 3) within each strain were defined to identify strain-specific
790 shared homozygous variants. Shared and unique homozygous variants among UCL, SL,
791 and Canton-S[102] were analysed. homozygous variants were annotated using SnpEff
792 (version 5.0) and visualized using IGV (version 2.8.12). Variants classified as having a low
793 impact ("LOW") by SnpEff were excluded from the analysis list (full list available in Data
794 S11). Enrichment analysis was conducted with DAVID (version 2023q4) and KEGG
795 (version 108.1).
796

797 **RNA extraction**

798 Ten virgin female flies, aged 5–8 days and kept in non-irradiated conditions, were frozen in
799 liquid nitrogen and homogenised in Trizol (Molecular Research Center, Inc., Cincinnati, OH,
800 USA). Chloroform (Fujifilm Wako Pure Chemicals Co.) was then added, and the mixture
801 was vortexed twice and centrifuged at 20,000 × *g* for 10 minutes at 4°C. The upper
802 aqueous phase was transferred to a new tube, and 200 μL of isopropyl alcohol was added.
803 The mixture was vortexed, incubated at room temperature for 10 minutes and centrifuged
804 again at 20,000 × *g* for 10 minutes at 4°C; the supernatant was discarded. To wash the
805 RNA pellet, 400 μL of 75% ethanol (prepared with DEPC-treated water) was added,
806 followed by vortexing. The sample was then centrifuged at 20,000 × *g* for 5 minutes at 4°C.
807 The supernatant was discarded, and the pellet was centrifuged once more for 1 minute.
808 The pellet was air-dried and resuspended in DEPC-treated water.
809

810 **RNA-sequence and enrichment analysis**

811 Quality assessment was initially performed using a BioAnalyzer. Library preparation was
812 conducted with the NEBNext Ultra II Directional RNA Library Prep Kit (Illumina) and the
813 NEBNext Poly(A) mRNA Magnetic Isolation Module (New England Biolabs, Ipswich, MA,
814 USA). Sequencing was performed on an Illumina NovaSeq 6000, with a read length of
815 PE150 (150 bp × 2 paired-end), generating a data output of 6 G bases per sample and
816 approximately 40 million reads per sample. In silico analyses and read trimming followed
817 the protocols described in the "Whole-genome resequencing, variant identification, and
818 enrichment analysis" section in Methods. Poly(A) tails were removed using cutadapt, and
819 mapping was conducted with hisat2 (version 2.2.1) using the BDGP6.46 reference genome
820 (INSDC Assembly GCA_000001215.4) (for details, see Data S13). Gene-wise read
821 counting was accomplished using HTSeq (version 2.0.4) with the dmel-all-r6.54.gtf
822 annotation file. Read counts were normalised with edgeR (version 3.40.2) using the
823 trimmed mean of M values method. Subsequent principal component analysis and

824 differential expression analysis were carried out with edgeR and scikit-learn (version 1.0.2).
825 DEGs were identified by comparing non-treated SL with non-treated UCL, Abx-treated SL,
826 or Abx-treated UCL groups, applying a false discovery rate–adjusted *p*-value threshold of
827 <0.05. Python libraries such as pandas (version 2.0.3), numpy (version 1.25.2), scipy
828 (version 1.11.2), and stats were used to filter DEGs with *p*-values below 0.05. For the
829 DEGs, $\log_2$-fold change values and Z scores normalised within the range of −2 to 2 were
830 calculated. These Z scores were then used to create a cluster map using the Ward method,
831 which classified genes and treatments on the basis of their similarity patterns. Enrichment
832 analysis was performed using DAVID and KEGG. Gene lists related to specific biological
833 functions were retrieved from KEGG (for TCA cycle, oxidative phosphorylation and Toll and
834 Imd signaling pathways) and FlyBase (for lipid metabolic processes). In Fig. 8c and Fig.
835 S18d, heatmaps illustrating functional profiles were generated using $\log_2$-fold change
836 values. These values were compared for each gene and each group and normalised
837 against the mean value of the non-treated UCL group.
838

839 **Genetics and evaluation of TAG levels and BL tolerance**

840 We collected genetically engineered flies with known elevated TAG levels and reared them
841 at 23–25°C under a 12-hour light/dark cycle. Using the GAL4/UAS system and null
842 mutants, we generated flies with RNAi knockdown or overexpression of target genes. The
843 following strains from the Bloomington *Drosophila* Stock Center were used (see Data S15):
844 Null mutants: *w;Akh* (84448), w;*Bmm* (15828), *yw,Pdgy* (19990), *yw;Chico* (14337), *w;InR*
845 (8267), *w;Ilp 2 3 5* (30889), *w;Lk6* (87087)
846 GAL4 drivers: *yw;Lsp2* (6357), *w;ppl* (58768), *w;Tk* (51973)
847 UAS strains: *yv;UAS-AkhR*$^{RNAi}$ (51710), *yv;UAS-Pect*$^{RNAi}$ (63710), *yv;UAS-Pten*$^{RNAi}$
848 (33643), *yv;UAS-Bmm*$^{RNAi}$ (25926), *y sc v sev;UAS-Stim*$^{RNAi}$ (52911), *y sc v sev;UAS-Lsd-*
849 *1*$^{RNAi}$ (65020), *yv;UAS-Tk*$^{RNAi}$ (25800), *yw;UAS-Gbb* (63059), *yw;UAS-InR* (8263), *w;UAS-*
850 *Lsd-2* (98116), *w;UAS-Lk6* (8709), *w,UAS-Rpr1* (5823)

851 We used F1 progenies for the experiments, obtained by crossing GAL4 driver males with
852 UAS effector females. As controls, we used wild-type Canton-S and w1118 genetically
853 washed by crossing with the Canton-S flies, F1 progenies from crosses of w1118 with UAS
854 effectors, and F1 progenies from crosses of GAL4 drivers with *y sc v;eGFP*$^{RNAi}$ (41555) and
855 *y sc v;eGFP*$^{RNAi}$ (41556) UAS effectors. Virgin female flies aged 1–5 days were irradiated
856 with either darkness or BL for 3 days and recovered for 3 days. Their survival rates were
857 assessed, and 5 flies were randomly chosen to mate with 5 Canton-S males for 4 days (for
858 details, see "Measurement of fecundity" in Methods). TAG storage was measured in virgin
859 female flies aged 7–12 days. Relative TAG levels are presented as $\log_2$-fold changes
860 relative to the mean values across all treatments. Fecundity was calculated as $\log_2$-fold
861 changes relative to the non-irradiation condition for each treatment. Data are from SL and
862 UCL (replicate lines 1, generation 57).
863

## 864 Phylogenetic tree based on the 16S rRNA gene

865 16S rRNA gene sequences were obtained from the Integrated Microbial Genomes (IMG)
866 database, with the addition of *A. persici* DS-1 strain[66] for *A. persici*. Based on previous
867 studies, *Neokomagataea thailandica* and *Swingsia samuiensis* were used as outgroups[103].
868 Sequence lengths ranged from 1,391 to 1,498 bp. The phylogenetic tree in Fig. S19 was
869 constructed by including the *A. persici* sequence (397 bp) from the dominant OTU ID,
870 which accounted for 89-98% of the microbiome analysis in Fig. S7a. Based on these
871 results, the phylogenetic position of *A. persici* in our laboratory was inferred in Fig. 10a.
872 Phylogenetic analyses were performed using MEGA (version 11.013), with alignments
873 performed using ClustalW. A maximum likelihood (ML) method with 1,000 bootstrap
874 replicates was used (substitution type: general time reversible model; ML heuristic method:
875 Nearest-Neighbour Interchange; initial tree for ML: NJ/BioNJ). The resulting phylogenetic
876 tree was visualised using iTOL (version 7.0).
877

878 ***A.persici* circular genome visualisation and transcriptome analysis**

879 The complete genome of *A. persici* (GCA_002006565.1_ASM200656v1) was used for
880 circular genome visualisation and transcriptome analysis for reference genome. The
881 circular genome representation was generated using GenoVi (version 0.2.16)[104]. After
882 mapping to the host genome, reads that unmatched to the host were extracted and
883 subsequently mapped to the complete *A. persici* genome. Unmapped reads were filtered
884 from the SAM file using Samtools (samtools view -b -f 4), followed by conversion to FASTQ
885 format. Sequence quality was assessed using FastQC and overrepresented sequences,
886 excluding *A. persici*, were removed. Reads were trimmed using Trimmomatic with the
887 following parameters: LEADING:20, TRAILING:20, SLIDINGWINDOW:4:15, and
888 MINLEN:20. The *A. persici* genome index was generated using HISAT2, and reads were
889 aligned using parameters: hisat2 -x reference genome index -1 -2 -k 3 --mp 2.1 --np 1 --rdg
890 10.5 --rfg 10.5 --seed 42 --score-min L,0,-0.9) (for details, see Data S16). Gene expression
891 was quantified using featureCounts (subread-1.5.2.-MacOSX-x86_64, version 2.0.8) and
892 parameters: featureCounts -t CDS -g gene_id -a genomic.gft (GCA_002006565.1) -M -p.
893 Gene expression levels were quantified using transcripts per million (TPM). Reads per
894 kilobase (RPK) were calculated as expression / (length / 1000). TPM values were then
895 derived by normalising the RPK of each gene to the total RPK within its respective GeneID.
896 Sequence depth was estimated using the formula (total bases mapped to the gene) /
897 (target gene length). DEGs were identified by comparing the UCL and SL groups using an
898 FDR adjusted *p*-value threshold of <0.05. To quantify changes in gene expression, we
899 calculated the $\log_2$FC of the transcripts. The mean TPM was calculated for each gene in
900 the UCL group, and the fold change was determined as the ratio of individual sample TPM
901 values to this mean. The dataset was then $\log_2$ transformed. Enrichment analysis was
902 performed using ShinyGO (version 0.82) and Gene ontology (GO) biological process
903 (version Ensembl 92). Gene lists related to oxidation-reduction process was retrieved from
904 GO biological process. The genomic.gft (GCA_002006565.1), UniProt (version 2025_01)

905 and KEGG databases were used to determine protein identities, enzyme classifications and
906 functional annotations for each gene. For details of the host transcriptome analysis and
907 visualisation, see “RNA-sequence and enrichment analysis” in Methods.
908

## 909 Growth experiments of isolated *A. persici*

910 *A. persici* was isolated from 10 adult females and cultured on MRS plates for 48 hours. 50
911 isolates were pre-cultured in 200 μL MRS broth (5.5 g MRS broth and 100 mL distilled
912 water) in 96-well plates for 72 hours. Bacterial growth was then assessed by culturing in 50
913 mL of MRS broth with continuous shaking at 60 rpm. Cultures were maintained at 30-31°C
914 throughout the incubation period. Optical density (OD) was measured using a compact
915 rocking incubator equipped with a spectrophotometer (TVS062CA ADVANTEC Tokyo,
916 Japan).
917

## 918 Statistical analysis

### 919 State space model and Bayesian estimation

920 The state space model is a statistical framework designed to analyse time series data with
921 autocorrelation, based on state and observation equations[105–107]. It was applied to estimate
922 fecundity across generations, incorporating replicate lines as random effects. In Fig. 2a,
923 intergenerational fecundity data were analysed using a Bayesian state space model
924 implemented with pystan (Python 3.9, version 2.17.0.0). This model included the following
925 components:
926 Data block: Defined the number of generations (length of the time series data), a vector of
927 explanatory variables, and three outcome variables corresponding to each replicate line,
928 each following a normal distribution.
929 Parameters block: Estimated a vector of levels with drift components (*mu*), vectors of
930 random effects (*r1*, *r2*, *r3*), coefficients of the explanatory variables (*b1*, *b2*, *b3*), the

standard deviation representing the magnitude of the drift component (*s_z*), and the standard deviations of the random effects (*s_r1*, *s_r2*, *s_r3*).

Transformed parameters block: Calculated the expected values for each outcome variable (*lambda1*, *lambda2*, *lambda3*) as the sum of the level with drift component (mu), the product of the explanatory variables' coefficients (*b*) and values (*ex*), and the random effects (*r*).

Model block: Assumed that the random effects followed a normal distribution with a mean of 0 and a given standard deviation. The state equation, *mu[i] ~ normal(2 * mu[i-1] - mu[i-2], s_z*), expressed changes in the level with drift components using a second-order local linear regression. The observation equations, *y1[i] ~ normal(lambda1[i], sigma1), y2[i] ~ normal(lambda2[i], sigma2)*, and *y3[i] ~ normal(lambda3[i], sigma3)*, defined the observed values as following a normal distribution.

Generated quantities block: Sampled the predicted values for each outcome variable using the normal distribution.

Random numbers were generated according to the posterior distribution using the Markov Chain Monte Carlo (MCMC) method with parameters set to iter=10000, chains=4, and control={'adapt_delta': 0.8, 'max_treedepth': 20}. Convergence was confirmed by ensuring that the *R*hat of the predicted values was <1.10 and by examining the trace plots (for details, see Data S2).

**Hierarchical Bayesian model**

Unless otherwise specified, hierarchical uncertainty estimation, accounting for random effects, was performed using Hierarchical Bayesian Model (HBM)[108]. The model specification and execution used the following tools and versions:

Software: R (version 4.0.1), rstan (version 2.32.2, Stan version 2.26.1), brms (version 2.20.4), and bayesplot (version 1.10.0).

Bayesian model comparison: The Bayes factor ($BF_{10}$) quantifies the strength of evidence for the alternative hypothesis ($H_1$) over the null hypothesis ($H_0$)[109]. A $BF_{10} > 1$ indicates

958 support for $H_1$, whereas a $BF_{10} < 1$ favours $H_0$. Guidelines for interpretation are as follows:
959 $BF_{10} > 3$ indicates moderate evidence, $BF_{10} > 10$ indicates strong evidence, and $BF_{10} > 100$
960 provides conclusive support for $H_1$. Conducted using $BF_{10}$ with the loo function, computing
961 *exp(0.5 * (elpd1 - elpd2))*, where elpd1 denotes the model's expected log pointwise
962 predictive density (elpd_loo) and elpd2 denotes that of the null model.
963 MCMC sampling: Parameters were set to seed=1, chains=4, iter=20000, warmup=5000,
964 and thin=4. If convergence was not attained, adjustments were made to iter=25000 and
965 warmup=10000, ensuring that *R*hat values remained below 1.10.
966 Prior distributions: Uniformly set to Gaussian.
967 Model details: Comprehensive details including the response variable, predictors, random
968 effects, and estimation results are available in Data S1, Data S3, 4, Data S6–8, Data S16.
969 Results included posterior median estimates, Bayesian 95% credible intervals (CI), and
970 approximate *p*-values (*p*MCMC) computed from posterior sampling.
971 Posterior sampling and *p*MCMC calculation: To test whether the posterior distribution of the
972 difference in each treatment was above or below 0, we followed references[110–113]. Posterior
973 samplings of each parameter were stored in diff_samples, and pairwise comparisons of
974 treatments were made using the formula: *p*MCMC = 2 * min(mean(diff_samples > 0),
975 mean(diff_samples < 0)).
976 **Logistic function**
977 Lethal dose: The survival rate at each dose was calculated by assigning a value of 1 if the
978 survival time exceeded the median survival time of UCL at $10 \times 10^{18}$ photons·$m^{-2}$·$s^{-1}$ (88 h)
979 and 0 otherwise. The $LD_{50}$ was estimated using a logistic function: The logistic function,
980 defined as $f(x) = 100 / (1 + \exp(slope \times (x - LD_{50})))$, describes the survival probability as a
981 sigmoidal function of dose.
982 Bacterial growth curves: modelled using a logistic function defined as $f(t) = K / (1 + \exp(-r \times$
983 $(t - t_0)))$, where $K$ is the maximum optical density (OD), $r$ is the growth rate, and $t_0$ is the
984 midpoint of the growth phase. Parameter estimation was performed by fitting this function

985 to the OD measurements over time.

986 **Correlation and Regression analysis**

987 The Pearson correlation coefficient or linear regression and 95% confidence intervals were
988 calculated using the pearsonr function or linregress function from the scipy.stats library.

989

## 990 Data availability

991 16S rRNA amplicon sequencing, whole-genome resequencing, and RNA-sequence data
992 have been deposited in the DNA Data Bank of Japan (DDBJ). All raw read data have been
993 uploaded to DDBJ under BioProject PRJDB19030, PRJDB19027, and PRJDB19028. The
994 source data for all figures are available in the supplementary files. Detailed experimental
995 methods are available on reasonable request from the corresponding author, Y.T.

## 996 Code availability

997 The code for all analyses and visualisations is available on reasonable request from the
998 corresponding author Y.T.

999

# References


1. Mallet, J. The evolution of insecticide resistance: Have the insects won? *Trends Ecol. Evol.* **4**, 336-340 (1989). doi: 10.1016/0169-5347(89)90088-8

2. Barathi, S., Sabapathi, N., Kandasamy, S. & Lee, J. Present status of insecticide impacts and eco-friendly approaches for remediation-a review. *Environmental Research* **240**, 117432 (2024). doi: 10.1016/j.envres.2023.117432

3. Spitschan, M., Aguirre, G. K., Brainard, D. H. & Sweeney, A. M. Variation of outdoor illumination as a function of solar elevation and light pollution. *Sci. Rep.* **6**, 26756 (2016). doi: 10.1038/srep26756

4. Song, B. M. & Lee, C. H. Toward a mechanistic understanding of color vision in insects. *Front. Neural Circuits.* **12**, 16 (2018). doi: 10.3389/fncir.2018.00016

5. Numata, H., Miyazaki, Y. & Ikeno, T. Common features in diverse insect clocks. *Zool. Lett.* **1**, 10 (2015). doi: 10.1186/s40851-014-0003-y

6. Kavakli, I. H., Ozturk, N. & Gul, S. DNA repair by photolyases. *Adv. Protein. Chem. Struct. Biol.* **115**, 1–19 (2019). doi: 10.1016/bs.apcsb.2018.10.003

7. Hori, M., Shibuya, K., Sato, M. & Saito, Y. Lethal effects of short-wavelength visible light on insects. *Sci. Rep.* **4**, 7383 (2014). doi: 10.1038/srep07383

8. Hori, M. & Suzuki, A. Lethal effect of blue light on strawberry leaf beetle, *Galerucella grisescens* (Coleoptera: Chrysomelidae). *Sci. Rep.* **7**, 2694 (2017). doi: 10.1038/s41598-017-03017-z

9. Shibuya, K., Onodera, S. & Hori, M. Toxic wavelength of blue light changes as insects grow. *PLoS One* **13**, e0199266 (2018). doi: 10.1371/journal.pone.0199266

10. Nash, T. R. *et al.* Daily blue-light exposure shortens lifespan and causes brain neurodegeneration in *Drosophila*. *npj Aging Mech. Dis.* **5**, 8 (2019). doi: 10.1038/s41514-019-0038-6

11. Hall, H., Ma, J., Shekhar, S., Leon-Salas, W. D. & Weake, V. M. Blue light induces a neuroprotective gene expression program in *Drosophila* photoreceptors. *BMC Neurosci.* **19**, 43 (2018). doi: 10.1186/s12868-018-0443-y

12. Yang, J. *et al.* Chronic blue light leads to accelerated aging in *Drosophila* by impairing energy metabolism and neurotransmitter levels. *Front. Aging* **3**, 983373 (2022). doi: 10.3389/fragi.2022.983373

13. Song, Y. *et al.* Age-dependent effects of blue light exposure on lifespan, neurodegeneration, and mitochondria physiology in *Drosophila melanogaster*. *npj Aging* **8**, 11 (2022). doi: 10.1038/s41514-022-00092-z

14. Stanhope, S. C. *et al.* Proteome-wide quantitative analysis of redox cysteine availability in the *Drosophila melanogaster* eye reveals oxidation of phototransduction machinery during blue light exposure and age. *Redox Biol.* **63**, 102723 (2023). doi: 10.1016/j.redox.2023.102723

15. Scheiner, S. M. Selection experiments and the study of phenotypic plasticity. *J Evol. Biol.* **15**, 889–898 (2002). doi: 10.1046/j.1420-9101.2002.00468.x

16. Martínez, A. A. & Lang, G. I. Identifying targets of selection in laboratory evolution experiments. *J. Mol. Evol.* **91**, 345–355 (2023). doi: 10.1007/s00239-023-10096-2

17. Harshman, L. G. & Hoffmann, A. A. Laboratory selection experiments using *Drosophila*: What do they really tell us? *Trends Ecol. Evol.* **15**, 32-36 (2000). doi: 10.1016/S0169-5347(99)01756-5

18. Watson, M. J. O. & Hoffmann, A. A. Acclimation, cross-generation effects, and the response to selection for increased cold resistance in *Drosophila*. *Evolution* **50**, 1182–1192 (1996). doi: 10.1111/j.1558-5646.1996.tb02359.x

19. Zhao, R., Xuan, Y., Li, X. & Xi, R. Age-related changes of germline stem cell activity, niche signaling activity and egg production in Drosophila. *Aging Cell* **7**, 344–354 (2008). doi: 10.1111/j.1474-9726.2008.00379.x

20. Lindsley, D. L. & Grell, E. H. Genetic Variations of *Drosophila melanogaster*. 2nd edn 431 *Carnegie Institution of Washington Publication* (1968).

21. Chatterjee, N. & Perrimon, N. What fuels the fly: Energy metabolism in *Drosophila* and its application to the study of obesity and diabetes. *Sci. Adv.* **7**, eabg4336 (2021). doi: 10.1126/sciadv.abg433

22. Heier, C. & Kühnlein, R. P. Triacylglycerol metabolism in *Drosophila melanogaster*. *Genetics* **210**, 1163–1184 (2018). doi: 10.1534/genetics.118.301583

23. Akhmetova, K., Balasov, M. & Chesnokov, I. *Drosophila* STING protein has a role in lipid metabolism. *eLife* **10**, e67358 (2021). doi: 10.7554/eLife.67358

24. Bailey, A. P. *et al.* Antioxidant role for lipid droplets in a stem cell niche of *Drosophila*. *Cell* **163**, 340–353 (2015). doi: 10.1016/j.cell.2015.09.020

25. Moulton, M. J. *et al.* Neuronal ROS-induced glial lipid droplet formation is altered by loss of Alzheimer's disease-associated genes. *Proc. Natl. Acad. Sci. U.A.S.* **118**, e2112095118 (2021). doi: 10.1073/pnas.2112095118

26. Bastide, H., Yassin, A., Johanning, E. J. & Pool, J. E. Pigmentation in *Drosophila melanogaster* reaches its maximum in Ethiopia and correlates most strongly with ultra-violet radiation in sub-Saharan Africa. *BMC Evol. Biol.* **14**, 179 (2014). doi: 10.1186/s12862-014-0179-y

27. Paiva, P. *et al.* Animal fatty acid synthase: a chemical nanofactory. *Chem. Rev.* **121**, 9502–9553 (2021). doi: 10.1021/acs.chemrev.1c00147

28. Miao, T. *et al.* Acetyl-CoA-mediated autoacetylation of fatty acid synthase as a metabolic switch of de novo lipogenesis in *Drosophila*. *Proc. Natl. Acad. Sci. U.S.A.* **119**, e2212220119 (2022). doi: 10.1073/pnas.2212220119

29. Onuma, T. et al. Recognition of commensal bacterial peptidoglycans defines *Drosophila* gut homeostasis and lifespan. *PLoS Genet.* **19**, e1010709 (2023). doi: 10.1371/journal.pgen.1010709

30. Sekihara, S., Shibata, T., Hyakkendani, M. & Kawabata, S. I. RNA interference directed against the Transglutaminase gene triggers dysbiosis of gut microbiota in Drosophila. *J. Biol. Chem.* **291**, 25077–25087 (2016). doi: 10.1074/jbc.M116.761791

31. McMullen, J. G., Bueno, E., Blow, F. & Douglas, A. E. Genome-inferred correspondence between phylogeny and metabolic traits in the wild *Drosophila* gut microbiome. *Genome Biol. Evol.* **13**, (2021). doi: 10.1093/gbe/evab127

32. Suyama, R., Cetraro, N., Yew, J. Y. & Kai, T. Microbes control *Drosophila* germline stem cell increase and egg maturation through hormonal pathways. *Commun. Biol.* **6**, (2023). doi: 10.1038/s42003-023-05660-x

33. Henry, L. P., Fernandez, M., Webb, A. & Ayroles, J. F. Host evolutionary history and ecological context modulate the adaptive potential of the microbiome. Preprint https://doi.org/10.1101/2020.09.21.306779 (2020).

34. Wong, A. C. N. *et al.* The host as the driver of the microbiota in the gut and external environment of *Drosophila melanogaster*. *Appl. Environ. Microbiol.* **81**, 6232–6240 (2015). doi: 10.1128/AEM.01442-15

35. Pais, I. S., Valente, R. S., Sporniak, M. & Teixeira, L. *Drosophila melanogaster* establishes a species-specific mutualistic interaction with stable gut-colonizing bacteria. *PLoS Biol.* **16**, e2005710 (2018). doi: 10.1371/journal.pbio.2005710

36. Staubach, F., Baines, J. F., Künzel, S., Bik, E. M. & Petrov, D. A. Host species and environmental effects on bacterial communities associated with *Drosophila* in the laboratory and in the natural environment. *PLoS One* **8**, e70749 (2013). doi: 10.1371/journal.pone.0070749

37. Jugder, B. E., Kamareddine, L. & Watnick, P. I. Microbiota-derived acetate activates intestinal innate immunity via the Tip60 histone acetyltransferase complex. *Immunity* **54**, 1683-1697.e3 (2021). doi: 10.1016/j.immuni.2021.05.017

38. Chaston, J. M., Newell, P. D. & Douglas, A. E. Metagenome-wide association of microbial determinants of host phenotype in *Drosophila melanogaster*. *mBio* **5**, e01631-14 (2014). doi: 10.1128/mbio.01631-14

39. Newell, P. D. & Douglas, A. E. Interspecies interactions determine the impact of the gut microbiota on nutrient allocation in *Drosophila melanogaster*. *Appl. Environ. Microbiol.* **80**, 788–796 (2014). doi: 10.1128/AEM.02742-13

40. He, Y. *et al.* Oxidative fermentation of acetic acid bacteria and its products. *Front. Microbiol.* **13**, 879246 (2022). doi: 10.3389/fmicb.2022.879246

41. Shin, S. C. *et al. Drosophila* microbiome modulates host developmental and metabolic

homeostasis via insulin signaling. *Science* **334**, 670–674 (2011). doi: 10.1126/science.1212782

42. Chaston, J. M., Dobson, A. J., Newell, P. D. & Douglas, A. E. Host genetic control of the microbiota mediates the *Drosophila* nutritional phenotype. *Appl. Environ. Microbiol.* **82**, 671–679 (2016). doi: 10.1128/AEM.03301-15

43. Gould, A. L. *et al*. Microbiome interactions shape host fitness. *Proc. Natl. Acad. Sci. U.S.A.* **115**, E11951–E11960 (2018). doi: 10.1073/pnas.1809349115

44. Elgart, M. *et al*. Impact of gut microbiota on the fly's germ line. *Nat. Commun.* **7**, 11280 (2016). doi: 10.1038/ncomms11280

45. Henriques, S. F. *et al*. Metabolic cross-feeding in imbalanced diets allows gut microbes to improve reproduction and alter host behaviour. *Nat. Commun.* **11**, 4236 (2020). doi: 10.1038/s41467-020-18049-9

46. Dodge, R. *et al*. A symbiotic physical niche in *Drosophila melanogaster* regulates stable association of a multi-species gut microbiota. *Nat. Commun.* **14**, 1557 (2023). doi: 10.1038/s41467-023-36942-x

47. Broderick, N. A., Buchon, N. & Lemaitre, B. Microbiota-induced changes in *Drosophila melanogaster* host gene expression and gut morphology. *mBio* **5**, e01117-14 (2014). doi: 10.1128/mBio.01117-14

48. Huang, J. *et al.* Systematic assessment of transcriptomic and metabolic reprogramming by blue light exposure coupled with aging. *PNAS Nexus* **2**, 1–15 (2023). doi: 10.1093/pnasnexus/pgad390

49. Tu, C. P. D. & Akgül, B. *Drosophila* glutathione S-transferases. *Methods Enzymol.* **401**, 204–226 (2005). doi: 10.1016/S0076-6879(05)01013-X

50. Wierzbicki, F.*, Schwarz, F.*, Cannalonga, O. & Kofler, R. Novel quality metrics allow identifying and generating high-quality assemblies of piRNA clusters. *Mol. Ecol. Resour.* **22**, 102–121 (2022). doi: 10.1111/1755-0998.13455

51. Yu, F. X., Zhao, B. & Guan, K. L. Hippo pathway in organ size control, tissue homeostasis, and cancer. *Cell* **163**, 811–828 (2015). doi: 10.1016/j.cell.2015.10.044

52. Li, Q. et al. Ingestion of food particles regulates the mechanosensing Misshapen-Yorkie pathway in *Drosophila* intestinal growth. *Dev. Cell* **45**, 433-449.e6 (2018). doi: 10.1016/j.devcel.2018.04.014

53. Yu, F. X., Meng, Z., Plouffe, S. W. & Guan, K. L. Hippo pathway regulation of gastrointestinal tissues. *Annu. Rev. Physiol.* **77**, 201–227 (2015). doi: 10.1146/annurev-physiol-021014-071733

54. Huang, H. L. *et al. Par-1* regulates tissue growth by influencing Hippo phosphorylation status and Hippo-Salvador association. *PLoS Biol.* **11**, e1001620 (2013). doi:

10.1371/journal.pbio.1001620

55. Li, Q. et al. The conserved Misshapen-Warts-Yorkie pathway acts in enteroblasts to regulate intestinal stem cells in *Drosophila*. *Dev. Cell* **31**, 291–304 (2014). doi: 10.1016/j.devcel.2014.09.012

56. Valanne, S., Wang, JH. & Rämet, M. The *Drosophila* Toll Signaling Pathway. *J. Immunol.* **186**, 649–656 (2011). doi: 10.4049/jimmunol.1002302

57. Myllymäki, H., Valanne, S. & Rämet, M. The *Drosophila* Imd Signaling Pathway. *J. Immunol.* **192**, 3455–3462 (2014). doi: 10.4049/ jimmunol.1303309

58. Albert, F. W. & Kruglyak, L. The role of regulatory variation in complex traits and disease. *Nat. Rev. Genet.* **16**, 197–212 (2015) doi: 10.1038/nrg3891

59. Massouras, A. *et al.* Genomic variation and its impact on gene expression in *Drosophila melanogaster*. *PLoS Genet* **8**, e1003055 (2012) doi: 10.1371/journal.pgen.1003055

60. Moschandrea, C. *et al*. Mitochondrial dysfunction abrogates dietary lipid processing in enterocytes. *Nature* **625**, 385–392 (2024). doi: 10.1038/s41586-023-06857-0

61. Byrns, C. N. et al. Senescent glia link mitochondrial dysfunction and lipid accumulation. *Nature* **630**, 475–483 (2024). doi: 10.1038/s41586-024-07516-8

62. Song, W., Veenstra, J. A. & Perrimon, N. Control of lipid metabolism by *Tachykinin* in *Drosophila*. *Cell Rep*. **9**, 40–47 (2014). doi: 10.1016/j.celrep.2014.08.060

63. Kamareddine, L., Robins, W. P., Berkey, C. D., Mekalanos, J. J. & Watnick, P. I. The *Drosophila* immune deficiency pathway modulates enteroendocrine function and host metabolism. *Cell Metab.* **28**, 449-462.e5 (2018). doi: 10.1016/j.cmet.2018.05.026

64. Brown, J. B. *et al.* An integrated host-microbiome response to atrazine exposure mediates toxicity in *Drosophila*. *Commun. Biol.* **4**, 1324 (2021). doi: 10.1038/s42003-021-02847-y

65. Chongtham, A. *et al.* Gut bacteria regulate the pathogenesis of Huntington's disease in *Drosophila* model. *Front. Neurosci.* **16**, 902205 (2022). doi: 10.3389/fnins.2022.902205

66. Tripathi, N. M. *et al.* Draft genome sequence of *Acetobacter persici* DS1, a strain for high-acidity vinegar fermentation. *Microbiol. Resour. Announc.* **14**, e01119-24 (2025). doi: 10.1128/mra.01119-24

67. Henry, L. P., Bruijning, M., Forsberg, S. K. G. & Ayroles, J. F. The microbiome extends host evolutionary potential. *Nat. Commun.* **12**, 5141 (2021). doi: 10.1038/s41467-021-25315-x

68. Henry, L. P. & Ayroles, J. F. Meta-analysis suggests the microbiome responds to

evolve and resequence experiments in *Drosophila melanogaster*. *BMC Microbiol.* **21**, 108 (2021). doi: 10.1186/s12866-021-02168-4

69. Bruijning, M., Henry, L. P., Forsberg, S. K. G., Metcalf, C. J. E. & Ayroles, J. F. Natural selection for imprecise vertical transmission in host–microbiota systems. *Nat. Ecol. Evol.* **6**, 77–87 (2022). doi: 10.1038/s41559-021-01593-y

70. Liu, L. *et al.* Glial lipid droplets and ROS induced by mitochondrial defects promote neurodegeneration. *Cell* **160**, 177–190 (2015). doi: 10.1016/j.cell.2014.12.019

71. Reiff, T. *et al*. Endocrine remodelling of the adult intestine sustains reproduction in *Drosophila*. *eLife* **4**, e06930 (2015). doi: 10.7554/eLife.06930

72. Buszczak, M., Lu, X., Segraves, W. A., Chang, T. Y. & Cooley, L. Mutations in the Midway gene disrupt a *Drosophila* Acyl Coenzyme A: diacylglycerol acyltransferase. *Genetics* **160**, 1511–1518 (2002). doi: 10.1093/genetics/160.4.1511

73. Murphy, M. P. How mitochondria produce reactive oxygen species. *Biochem. J.* **417**, 1–13 (2009). doi: 10.1042/BJ20081386

74. Crotti, E. et al. Acetic acid bacteria, newly emerging symbionts of insects. *Appl. Environ. Microbiol.* **76**, 6963–6970 (2010). doi: 10.1128/AEM.01336-10

75. Shi, L. & Tu, B. P. Acetyl-CoA and the regulation of metabolism: mechanisms and consequences. *Curr. Opin. Cell Biol.* **33**, 125–131 (2015). doi: 10.1016/j.ceb.2015.02.003

76. Li, X. & Karpac, J. A distinct Acyl-CoA binding protein (ACBP6) shapes tissue plasticity during nutrient adaptation in *Drosophila*. *Nat. Commun.* **14**, 7599 (2023). doi: 10.1038/s41467-023-43362-4

77. Narita, T., Weinert, B. T. & Choudhary, C. Functions and mechanisms of non-histone protein acetylation. *Nat. Rev. Mol. Cell Biol.* **20**, 156–174 (2019). doi: 10.1038/s41580-018-0081-3

78. Schiffer, J. A. *et al.* Caenorhabditis elegans processes sensory information to choose between freeloading and self-defense strategies. *eLife* **9**, e56186 (2020). doi: 10.7554/eLife.56186

79. Sato, Y. *et al.* Insecticide resistance by a host-symbiont reciprocal detoxification. *Nat. Commun.* **12**, 6432 (2021). doi: 10.1038/s41467-021-26649-2

80. Hoskins *et al*. The release 6 reference sequence of the *Drosophila melanogaster* genome. *Genome Res*. **25**, 445–458 (2015). doi: 10.1101/gr.185579.114

81. Wang, Y. *et al.* Variation in mutation, recombination, and transposition rates in *Drosophila melanogaster* and *Drosophila simulans*. *Genome Res.* **33**, 587–598 (2023). doi: 10.1101/gr.277383.122

82. Fitz-James, M. H. & Cavalli, G. Molecular mechanisms of transgenerational epigenetic inheritance. *Nat. Rev. Genet.* **23**, 325–341 (2022). doi: 10.1038/s41576-021-00438-5

83. Christensen, C. F., Laurichesse, Q., Loudhaief, R., Colombani, J. & Andersen, D. S. *Drosophila* activins adapt gut size to food intake and promote regenerative growth. *Nat. Commun.* **15**, 273 (2024). doi: 10.1038/s41467-023-44553-9

84. Nagai, H. *et al.* Nutrient-driven dedifferentiation of enteroendocrine cells promotes adaptive intestinal growth in *Drosophila*. *Dev. Cell* **58**, 1764–1781 (2023). e10. doi: 10.1016/j.devcel.2023.08.022

85. Karasov, W. H., Martínez, del Rio, C. & Caviedes-Vidal, E. Ecological physiology of diet and digestive systems. *Annu. Rev. Physiol.* **73**, 69–93 (2011). doi: 10.1146/annurev-physiol-012110-142152

86. Stojanović, O., Miguel-Aliaga, I. & Trajkovski, M. Intestinal plasticity and metabolism as regulators of organismal energy homeostasis. *Nat. Metab*. **4**, 1444–1458 (2022). doi: 10.1038/s42255-022-00679-6

87. Miguel-Aliaga, I., Jasper, H. & Lemaitre, B. Anatomy and physiology of the digestive tract of *Drosophila melanogaster*. *Genetics* **210**, 357–396 (2018). doi: 10.1534/genetics.118.300224

88. Chevalier, C. *et al.* Gut microbiota orchestrates energy homeostasis during cold. *Cell* **163**, 1360–1374 (2015). doi: 10.1016/j.cell.2015.11.004

89. Buchon, N. *et al.* Morphological and molecular characterization of adult midgut compartmentalization in *Drosophila*. *Cell Rep.* **3**, 1725–1738 (2013). doi: 10.1016/j.celrep.2013.04.001

90. MacKay, T. F. C. *et al.* The Drosophila melanogaster Genetic Reference Panel. *Nature* **482**, 173–178 (2012). doi: 10.1038/nature10811

91. Gargano, J. W., Martin, I., Bhandari, P. & Grotewiel, M. S. Rapid iterative negative geotaxis (RING): A new method for assessing age-related locomotor decline in *Drosophila*. *Exp. Gerontol.* **40**, 386395 (2005). doi: 10.1016/j.exger.2005.02.005

92. Torquato, L. S., Mattos, D., Matta, B. P. & Bitner-Mathé, B. C. Cellular basis of morphological variation and temperature-related plasticity in *Drosophila melanogaster* strains with divergent wing shapes. *Genetica* **142**, 495–505 (2014). doi: 10.1007/s10709-014-9795-0

93. Lee, J. H., Bassel-Duby, R. & Olson, E. N. Heart- and muscle-derived signaling system dependent on MED13 and Wingless controls obesity in *Drosophila*. *Proc. Natl. Acad. Sci. U.S.A.* **111**, 9491–9496 (2014). doi: 10.1073/pnas.1409427111

94. Bligh, E. G. & Dyer. W. J. A rapid method of total lipid extraction and purification. *Can. J. Biochem. Physiol.* **37**, 911–7 (1959). doi: 10.1139/o59-099

95. Guan, X. L. *et al.* Biochemical membrane lipidomics during *Drosophila* development. *Dev. Cell.* **24**, 98–111 (2013). doi: 10.1016/j.devcel.2012.11.012

96. Shen, L. R. *et al. Drosophila* lacks C20 and C22 PUFAs. *J. Lipid Res.* **51**, 2985–2992 (2010). doi: 10.1194/jlr.M008524

97. Wood, J. G. *et al. Sirt4* is a mitochondrial regulator of metabolism and lifespan in *Drosophila melanogaster*. *Proc. Natl. Acad. Sci. U.S.A.* **115**, 1564–1569 (2018). doi: 10.1073/pnas.172067311

98. Ward, J. H. Hierarchical grouping to optimize an objective function. *J. Am. Stat. Assoc.* **58**, 236–244 (1963). doi: 10.1080/01621459.1963.10500845

99. Weisburg, W. G., Barns, S. M., Pelletier, D. A. & Lane, D. J. 16S Ribosomal DNA amplification for phylogenetic study. *J. Bacteriol*. **173**, 697–703 (1991). doi: 10.1128/jb.173.2.697-703.1991

100. Edwards, U., Rogall, T., Blöcker, H., Emde, M. & Böttger, E. C. Isolation and direct complete nucleotide determination of entire genes. Characterization of a gene coding for 16S ribosomal RNA. *Nucleic Acids Res.* **17**, 7843–7853 (1989). doi: 10.1093/nar/17.19.7843

101. Leftwich, P. T., Clarke, N. V. E., Hutchings, M. I. & Chapman, T. Gut microbiomes and reproductive isolation in *Drosophila*. *Proc. Natl. Acad. Sci. U.S.A.* **114**, 12767–12772 (2017). doi: 10.1073/pnas.1708345114

102. Kanno, M., Hiramatsu, S., Kondo, S., Tanimoto, H. & Ichinose, T. Voluntary intake of psychoactive substances is regulated by the dopamine receptor *Dop1R1* in *Drosophila*. *Sci. Rep.* **11**, 3432 (2021). doi: 10.1038/s41598-021-82813-0

103. Yukphan, P. *et al. Acetobacter garciniae* sp. nov., an acetic acid bacterium isolated from fermented mangosteen peel in Thailand. *Int. J. Syst. Evol. Microbiol.* **71**, 10 (2021). doi: 10.1099/ijsem.0.005052

104. Cumsille, A. *et al.* GenoVi, an open-source automated circular genome visualizer for bacteria and archaea. *PLoS Comput. Biol.* **19**, e1010998 (2023). doi: 10.1371/journal.pcbi.1010998

105. Auger-Méthé, M. *et al.* A guide to state–space modeling of ecological time series. *Ecol. Monogr.* **91**, e01470 (2021). doi: 10.1002/ecm.1470

106. Frühwirth-Schnatter, S. & Wagner, H. Stochastic model specification search for Gaussian and partial non-Gaussian state space models. *J. Econom.* **154**, 85–100 (2010). doi: 10.1016/j.jeconom.2009.07.003

107. Aeberhard, W. H., Flemming, J. M. & Nielsen, A. Review of state-space models for fisheries science. *Annu. Rev. Stat. Appl*. **5**, 215–235 (2018). doi: 10.1146/annurev-statistics-031017-100427

108. Lee, M. D. How cognitive modeling can benefit from hierarchical Bayesian models. *J.*

*Math. Psychol.* **55**, 1–7 (2011). doi: 10.1016/j.jmp.2010.08.013

109. Kass, R. E. & Raftery, A. E. Bayes factors. *J. Am. Stat. Assoc*. **90**, 773–795 (2012). doi: 10.1080/01621459.1995.10476572

110. Bürkner, PC. brms: An R package for Bayesian multilevel models using Stan. *J. Stat. Softw.* **80**, 1–28 (2017). doi: 10.18637/jss.v080.i01

111. Nott, D. J., Drovandi, C. C., Mengersen, K. & Evans, M. Approximation of Bayesian predictive *p*-values with regression ABC. *Bayesian Anal.* **13**, 59–83 (2018). doi: 10.1214/16-BA1033

112. Cornwallis, C. K. *et al*. Symbioses shape feeding niches and diversification across insects. *Nat. Ecol. Evol.* **7**, 1022–1044 (2023). doi: 10.1038/s41559-023-02058-0

113. Hadfield, J. D. MCMC methods for multi-response generalized linear mixed models: The MCMCglmm R package. *J. Stat. Softw.* **33**, 1–22 (2010). doi: 10.18637/jss.v033.i02

## Acknowledgements

We are grateful to Dr. Takema Fukatu, Dr. Yuto Yoshinari, Dr. Takashi Nishimura, and Dr. Koichiro Tamura for their valuable discussions regarding the study. We also thank Dr. Masaki Iwata, Dr. Shuhei Miyashita, Dr. Chisato Kobayashi, Dr. Katsuya Taniyama, Dr. Takashi Makino, Dr. Yuma Takahashi, Dr. Takahisa Ueno, Dr. Masashi Murakami, Dr. Misako Okumura, Dr. Takahiro Chihara Dr. Toshinori Hayashi, Dr. Takeshi Igawa, Dr. Ritsuko Suyama and Dr. Sota Tanaka for their important suggestions. We would like to thank Dr. Atsuhiko Nagasawa and Dr. Yuki Chiba for teaching us the GC-MS analysis, and Dr. Fu Namai for teaching us microbiome analysis. We also thank Mr. Yusaku Hayashi for instructing us on how to dissect the fat body. Ms. Ayako Abe and Mr. Kento Fukuoka provided technical assistance. We extend our gratitude to Dr. Haruki Kitazawa and Dr. Shoichiro Kurata for lending us their laboratories. We thank the Rhelixa, Inc. for conducting the next-generation sequencing and assisting with the data acquisition, ELSS, Inc for proofreading and editing the English language of this manuscript, Bloomington Drosophila Stock Center for providing the *Drosophila* stocks used in this study, and Japan Collection of Microorganisms RIKEN BioResource Research Center for providing the bacterial strains used in this research. This work was supported by JST SPRING, grant numbers JPMJSP2102 and JPMJSP2114 to Y.T.

## Author information

Authors and Affiliations

**Graduate School of Agricultural Sciences, Tohoku University, Sendai, Japan**

Yuta Takada, Wakako Ikeda-Ohtsubo, and Masatoshi Hori

**Frontier Research Institute for Interdisciplinary Sciences, Tohoku University, Sendai, Japan**

Toshiharu Ichinose

**Graduate School of Pharmaceutical Sciences, Tohoku University, Sendai, Japan**

Naoyuki Fuse

**Graduate School of Life Sciences, Tohoku University, Sendai, Japan**

Toshiharu Ichinose, Kokoro Saito, and Hiromu Tanimoto

## Contributions

Y.T. and M.H. conceived and designed the study. Y.T. performed all experiments and analysed all data, wrote the original manuscript, third manuscripts and fourth manuscript. Y.T. and W.I. designed and performed the infection experiment with gut contents and bacterial experiments. Y.T., T.I., and N.F. performed whole-genome and RNA sequencing. Y.T., K.S., T.I., and H.T. designed the genetics and CAFE assays. Y.T. and K.S. performed the CAFE assay. Y.T., W.I., N.F., and T.I. edited the first manuscript. Y.T. and T.I. edited the second manuscript and third manuscript. H.T. and M.H. supervised the study. All authors participated in the discussions and reviewed the manuscript.

**There are no conflicts of interest to declare in relation to this study.**

# Figures

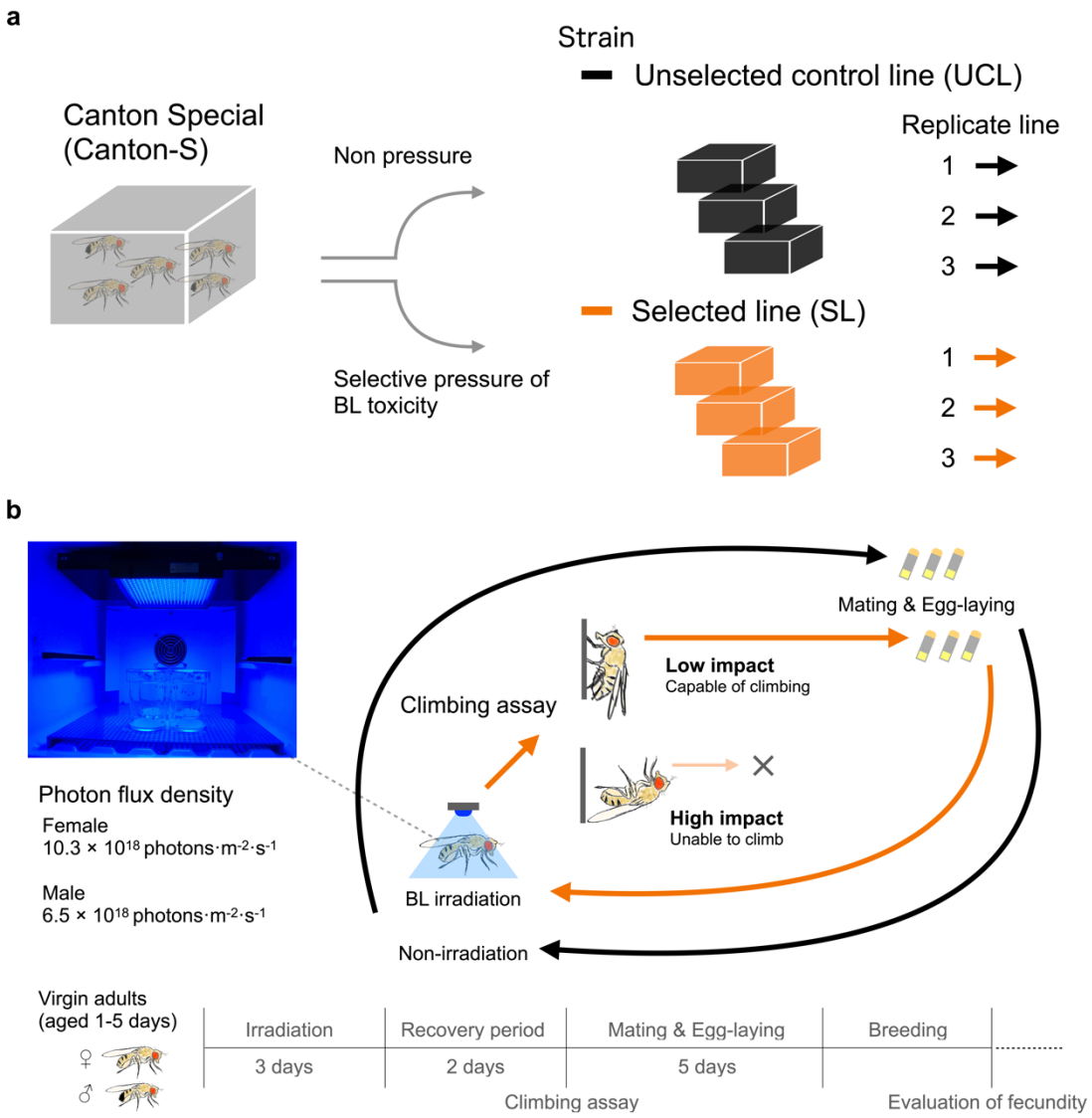


**Fig 1: Experimental design of laboratory selection using blue light (BL) toxicity.**

**a**, Overview of the ancestral population and the laboratory selection experiment. We established two strains from the Canton Special (Canton-S) strain: a selected line subjected to BL toxicity pressure at the adult stage in each generation, and an unselected control line without selection pressure. Each strain was maintained with three replicate lines. **b**, Detail of the selection experiment. Flies were BL-irradiated for 3 days, recovered

1473 for 2 days, and categorized in a climbing assay into those capable of climbing ("low
1474 impact") and those unable to climb ("high impact"). In SL, parents selected from low impact
1475 flies. Flies were allowed 5 days for mating and egg-laying. UCL parents were randomly
1476 chosen from the negative control group and reared under the same conditions as the SL
1477 flies.

1478

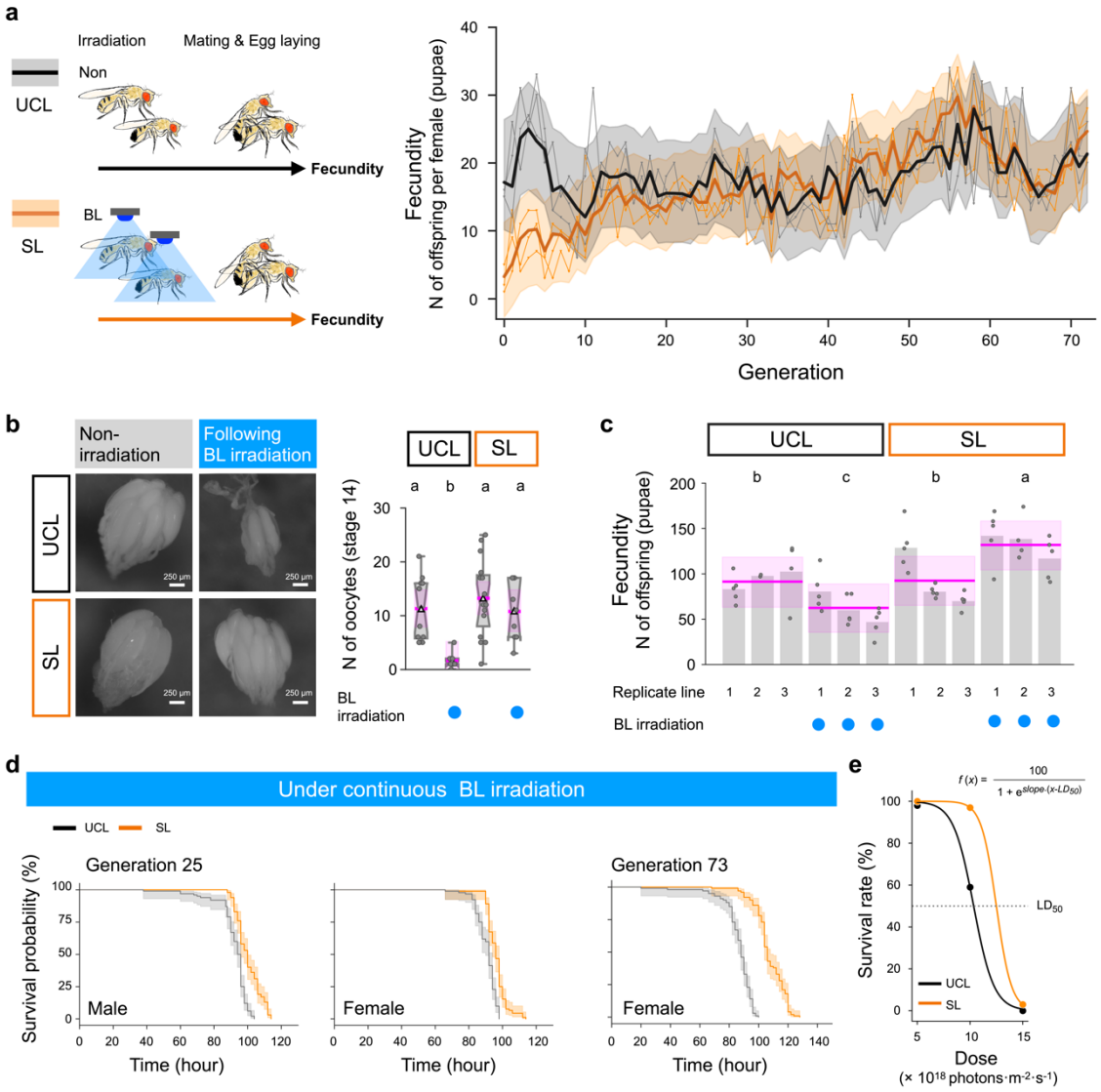


**Fig 2: Establishment of *Drosophila* lines with BL tolerance evolved by laboratory selection.**

**a**, Changes in fecundity across generations. UCL represents fecundity under non-irradiated conditions, while SL represents fecundity after BL irradiation. Fecundity was measured as the number of offspring per female (pupae). $n$ = 3. State space model with Markov Chain Monte Carlo (MCMC) method, posterior median and Bayesian 95% credible intervals (CI). **b**, Ovarian development differences after 3 days of BL irradiation followed by 3 days of recovery. Number of stage 14 oocytes after a 3-day recovery period. $n$ = 9–15. Bayes factor ($BF_{10}$) = 50.74. (Replicate lines 2, generation 25). **c**, Fecundity measured as the

number of offspring (pupae). $n$ = 11–15. $BF_{10}$ > 100, generation 38. **d**, Lifespan under continuous BL irradiation. Male $n$ = 100. $BF_{10}$ >100. Estimates: UCL 90.62 h (89.38–91.82), SL 96.35 h (95.16–97.52), $p$MCMC < 0.001. Female $n$ = 92. $BF_{10}$ = 0.72. Estimates: UCL 92.09 h (90.38–93.78), SL 100.39 h (98.74–102.13), $p$MCMC < 0.001, replicate lines 1, generation 25. Female $n$ = 100. $BF_{10}$ > 100. Estimates: UCL 86.16 h (84.05–88.27), SL 107.18 h (105.09–109.28), $p$MCMC < 0.001, replicate lines 1, generation 73. **e**, Dose-response curve for females exposed to BL. The lethal dose ($LD_{50}$) was estimated by logistic regression: $10.35 \times 10^{18}$ photons-m$^{-2}$-s$^{-1}$ for UCL and $12.50 \times 10^{18}$ photons-m$^{-2}$-s$^{-1}$ for SL. See Fig. S4 for details of lifespan at $5 \times 10^{18}$ photons-m$^{-2}$-s$^{-1}$ and $15 \times 10^{18}$ photons-m$^{-2}$-s$^{-1}$. Statistical analyses for panels **b**–**d** used a Hierarchical Bayesian Model (HBM) with MCMC methods, posterior median, and Bayesian 95% CI. In **b** and **c**, different letters indicate significant differences at $p$MCMC < 0.05. See Data S2 and Data S3 for details of all results, including statistical models.

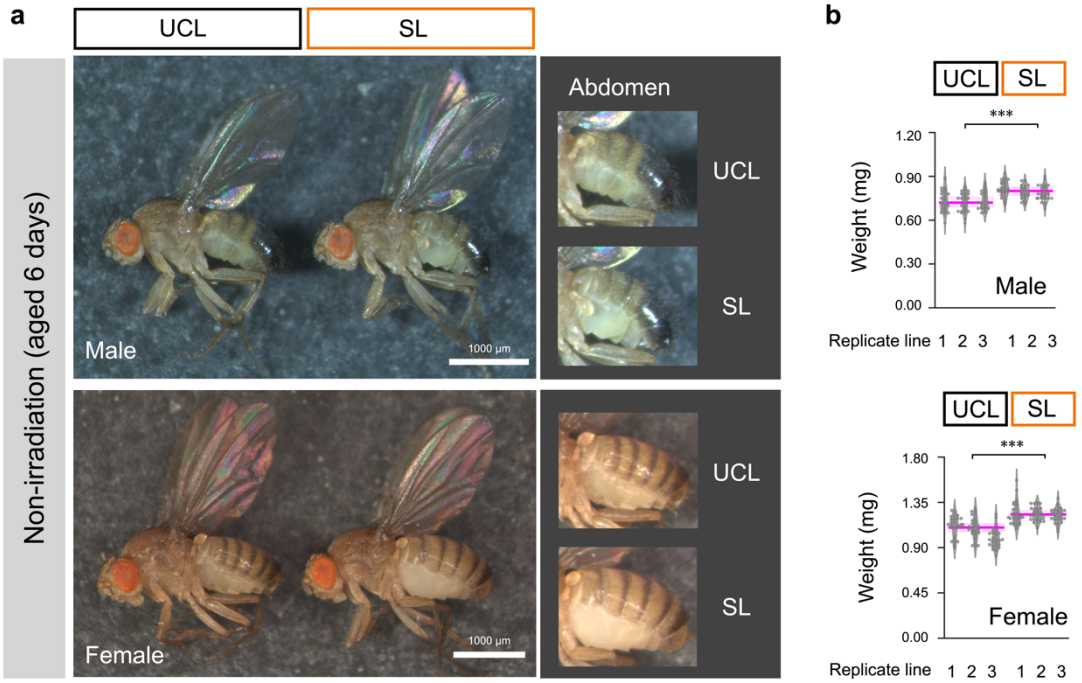


**Fig 3: Selected line (SL) flies characterised by enlarged abdomen and heavier body weight in both sexes.**

**a,** Phenotype of adult virgin male and virgin female aged 6 days. The zoomed view of the abdomen is brightened with maximum exposure. **b**, Body weight, $n$ = 90, $BF_{10}$ >100, generation 39. Statistical analysis for panel **b** was performed using a HBM with MCMC methods, posterior median, and Bayesian 95% CI. Asterisks indicate significance levels: *** $p$MCMC < 0.001. See Data S4 for details of all results, including statistical models.

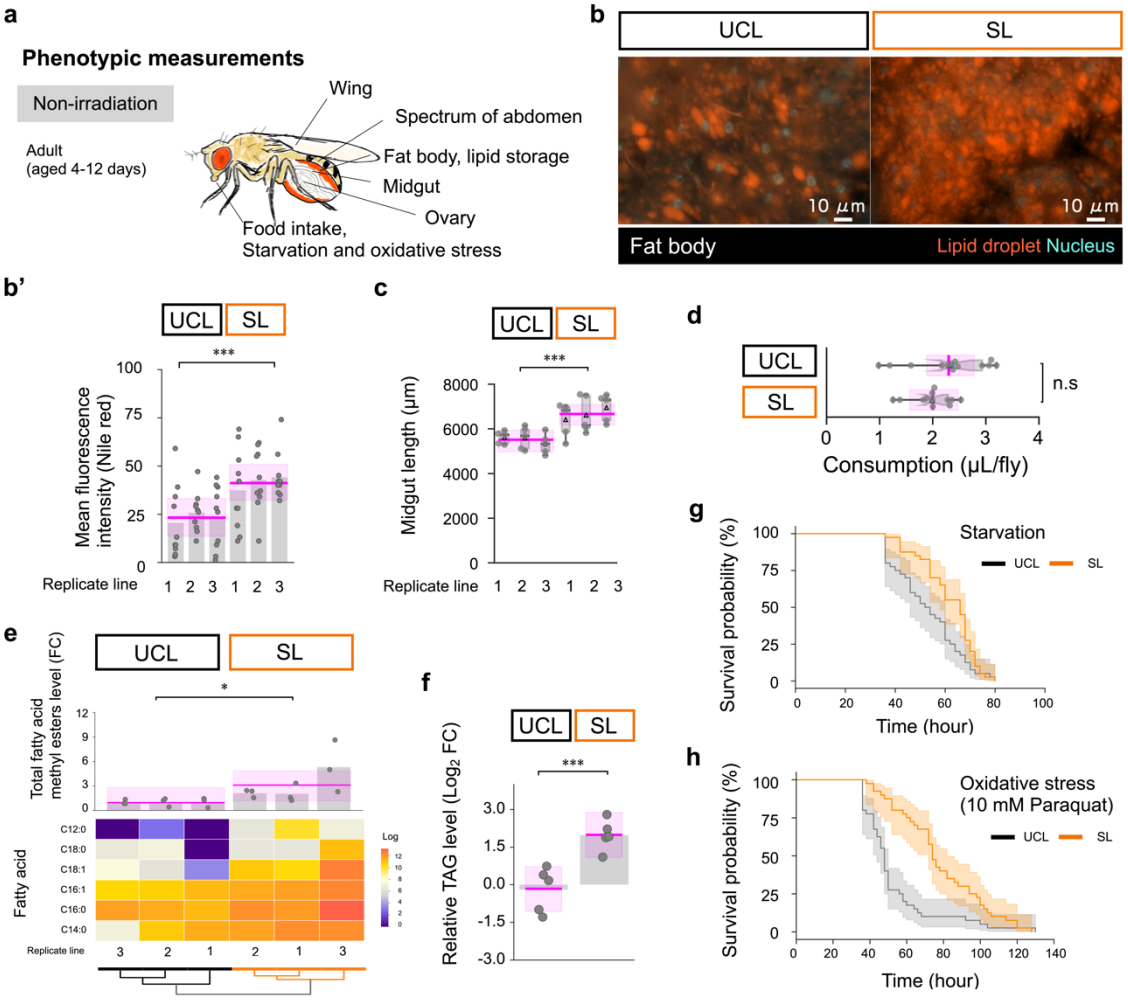


**Fig 4: SL flies exhibited obese phenotype, lipid accumulation, and oxidative stress resistance.**

**a**, Phenotypic measurements of virgin adult females (aged 4-12 days) under non-irradiated conditions (**b-h**). Age matching was performed between strains at the time of measurement. See Fig. S5 and Fig. S6 for details of wing, ovary and abdomen spectrum. **b**, Fluorescence imaging of the abdominal fat body and lipid droplets (lipid droplets: Nile red; nuclei: NucBlue). **b'**, Mean fluorescence intensity from Nile red staining, $n$ = 30, $BF_{10}$ >100, generation 35. **c**, Midgut length, $n$ = 15, $BF_{10}$ >100, generation 45. **d**, Food consumption, $n$ = 12–13, $BF_{10}$ = 1.85, replicate line 1, generation 52. **e**, Gas chromatography mass spectrometry analyses of fatty acid methyl esters (FAMEs), total FAMEs, $n$ = 9, $BF_{10}$ = 1.69, generation 30. **f**, Relative triacylglycerol (TAG) level, $n$ = 5, $BF_{10}$

1525 =15.14, replicate line 1, generation 57. **g**, Starvation resistance, Kaplan–Meier survival
1526 curve, *n* = 40, $BF_{10}$ = 4.49. Estimates: UCL 53.04 h (49.20–56.89), SL 61.91 h (58.09–
1527 65.43), *p*MCMC < 0.01, replicate line 2, generation 43. **h**, Oxidative stress resistance (10
1528 mM paraquat), Kaplan–Meier survival curve, *n* = 40, $BF_{10}$ >100. Estimates: UCL 53.07 h
1529 (45.90–59.03), SL 77.94 h (71.19–84.08), *p*MCMC < 0.001, replicate line 3, generation 43.
1530 Statistical analyses for panels **b** and **d**–**h** were performed using a HBM with MCMC
1531 methods, posterior median, and Bayesian 95% CI. Asterisks indicate significance levels: *
1532 *p*MCMC < 0.05, *** *p*MCMC < 0.001, n.s = not significant. See Data S4 for details of all
1533 results, including statistical models. FC, fold change.
1534
1535

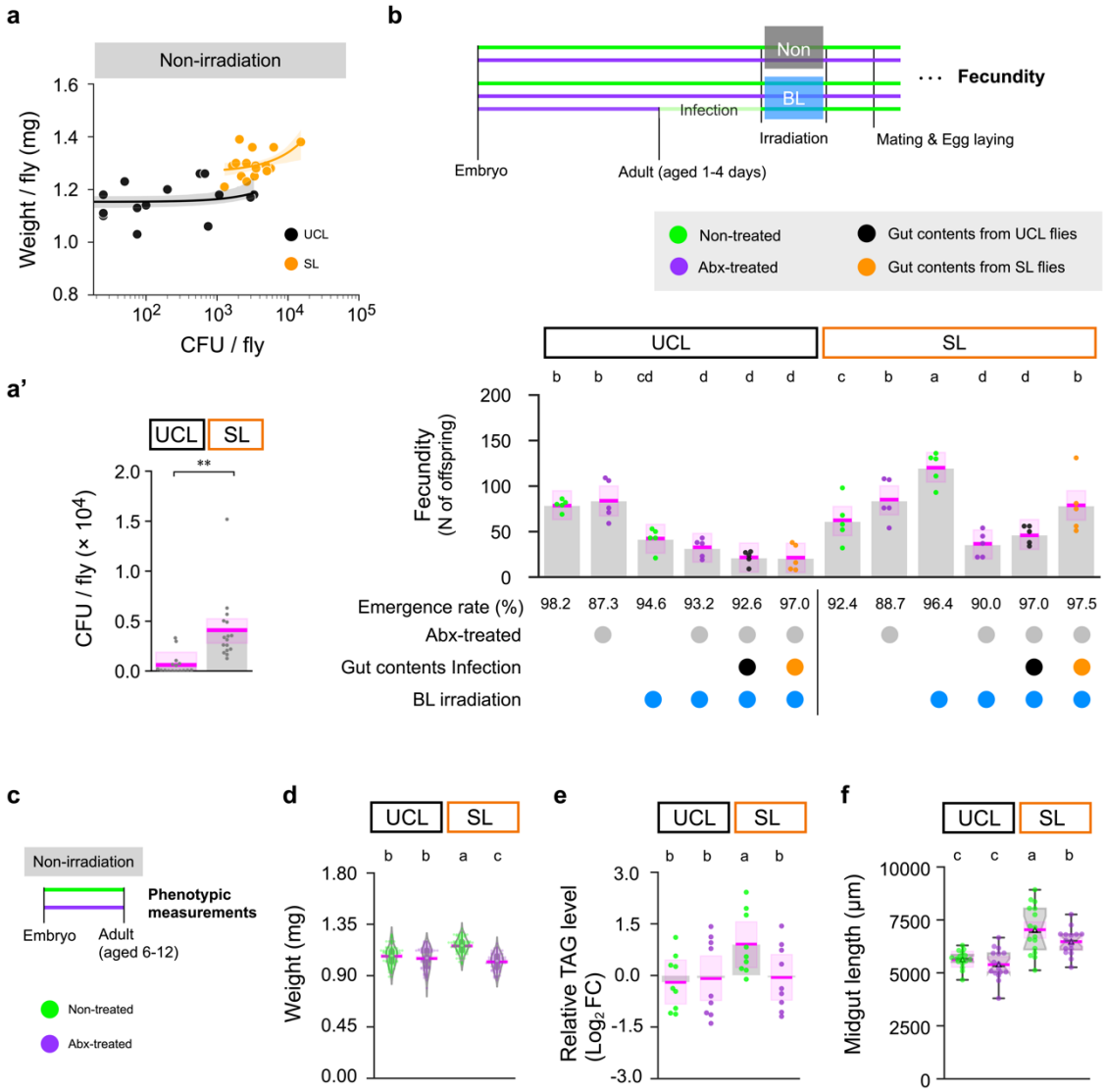


**Fig 5: High bacterial abundance is the key to BL tolerance and lipid accumulation in SL flies.**

**a,** Relating body weight to bacterial abundance. $n$ = 16, UCL; $y = 0.00 \times x + 1.15$, $p$ = 0.54, SL; $y = 0.00 \times x + 1.27$, $p$ = 0.06. Bacterial measurements from virgin adult females (aged 6-12 days) under non-irradiated conditions. After measuring body weight, homogenised samples from four flies were diluted 100-fold and cultured on MRS plates for 72 hours to quantify colony-forming units (CFU). The variance represents the 80% confidence interval. See Fig. S7 for microbiota analysis. **a',** Bacterial abundance. $n$ = 16, $BF_{10}$ = 11.17. Asterisks indicate significance: ** $p$MCMC < 0.01; replicate line 1, generation

1546 48. CFU from same dataset as Fig. 5a. **b,** Impact of antibiotic mixture (Abx) treatment and
1547 gut content infection on fecundity under BL toxicity. Fecundity measured as the number of
1548 offspring (adults), $n$ = 5, $BF_{10}$ >100; replicate line 1, generation 47. **c**, Phenotypic effects of
1549 Abx treatment (**d**–**f**). Abx was administered continuously from the embryo to adult, resulting
1550 in a significant reduction in the adult microbiota. The efficacy of Abx treatment was
1551 confirmed by regular plating of adults on MRS plates, where CFU counts were zero in all
1552 observations. See Fig. S9a for details. **d**, Body weight, $n$ = 100, $BF_{10}$ >100; replicate line 1,
1553 generation 55. **e**, Relative TAG level, $n$ = 10, $BF_{10}$ = 1.47; replicate line 1, generation 55. **f,**
1554 Midgut length, $n$ = 16, $BF_{10}$ >100; replicate line 1, generation 48. Statistical analyses for
1555 panels **a'**–**f** were performed using a HBM with MCMC methods, posterior median, and
1556 Bayesian 95% CI. Different letters indicate significant differences at $p$MCMC < 0.05. See
1557 Data S6 for details of all results, including statistical models.
1558

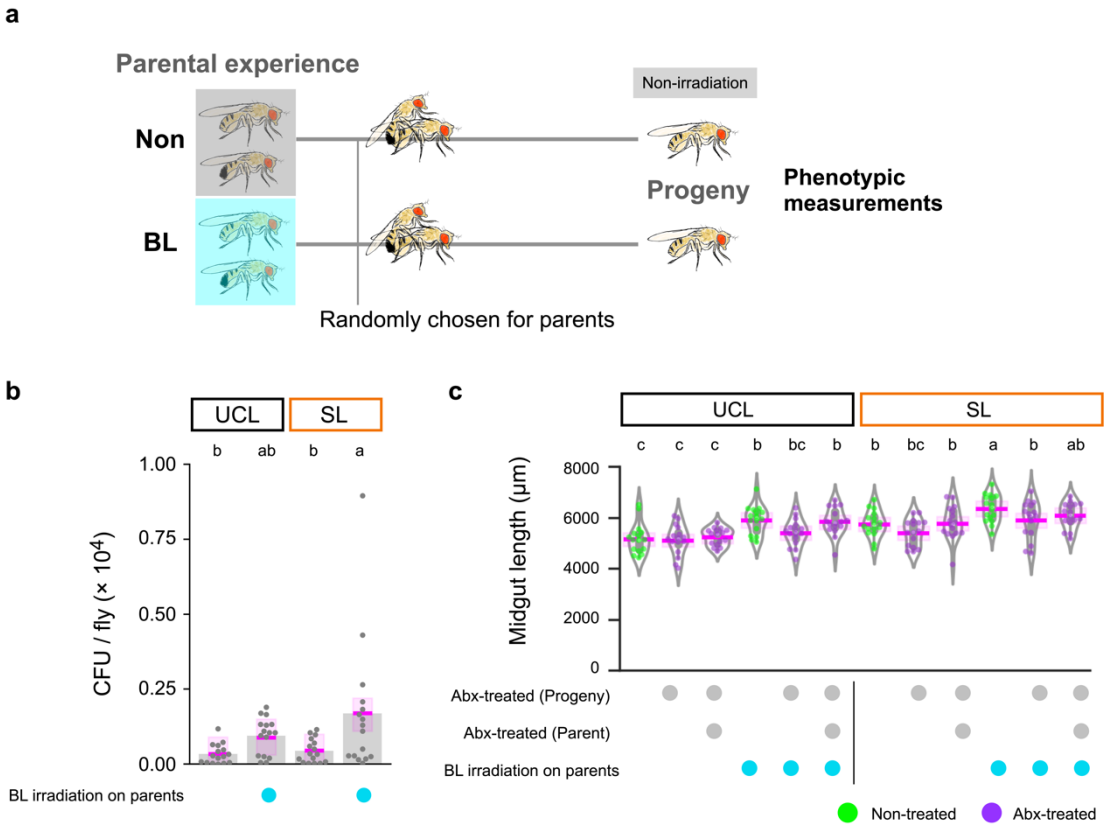


**Fig 6: Parental experience of BL irradiation promotes midgut elongation and increased bacterial abundance in progeny.**

**a**, The effect of parental exposure to BL toxicity on offspring traits. Offspring with different parental experiences were generated. **b**, Bacterial abundance. $n$ = 16. $BF_{10}$ = 8.93; replicate line 1, generation 53. **c**, Midgut length. $n$ = 16, $BF_{10}$ >100; replicate line 1, generation 54. Statistical analyses for panels **b** and **c** were performed using HBM with MCMC methods, posterior median, and Bayesian 95% CI. Different letters indicate significant differences at $p$MCMC < 0.05. For details, see Data S8 for all results, including statistical models.

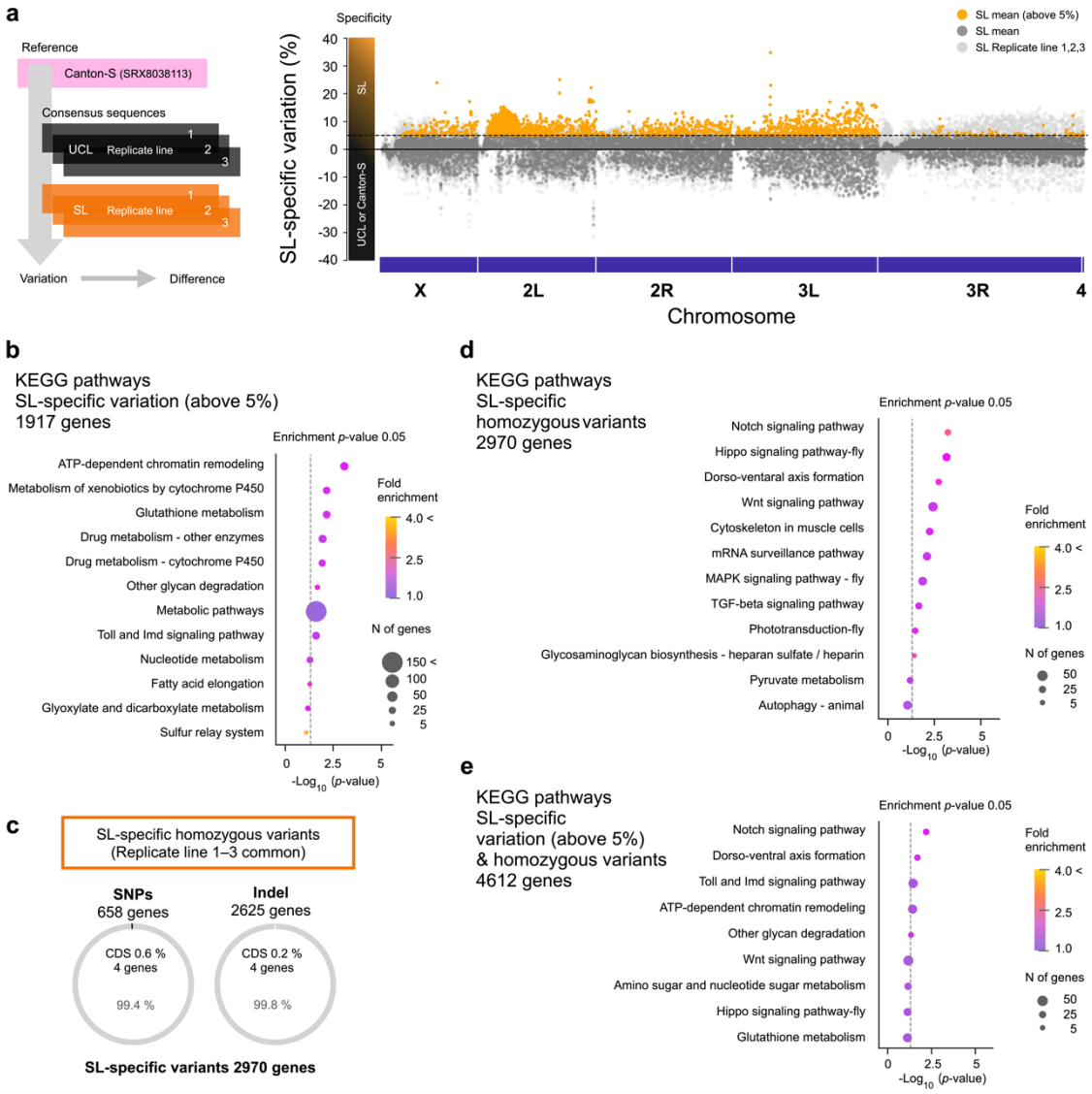


**Fig 7: Genetic characteristics unique to SL are enriched in detoxification, antioxidant response, Hippo signaling pathway and Toll and Imd signaling pathway.**

**a**, Manhattan plot of variation for each gene from whole genome resequencing analysis; generation 44. Variation of genes are referenced to Canton-S strain (SRX8038113). SL-specific variation is defined as the difference between the UCL mean variation and the SL variation per replicate line and mean greater than 5%. Each SL replicate line is shown in light grey, the SL mean is shown in dark grey and SL means with more than 5% variation

1579 are highlighted in yellow. Negative values indicate higher variation in Canton-S or UCL. A
1580 value of zero indicates no difference between UCL and SL. **b**, Enrichment analysis of SL-
1581 specific variation (above 5%) using Kyoto Encyclopedia of Genes and Genomes (KEGG).
1582 **c**, Identification of SL-specific common homozygous variants. CDS, coding sequence. **d**,
1583 Enrichment analysis of SL-specific variants using KEGG. **e**, Enrichment analysis of SL-
1584 specific variation (above 5%) and variants using KEGG. For details, see Data S9–Data S1
1585 2.
1586

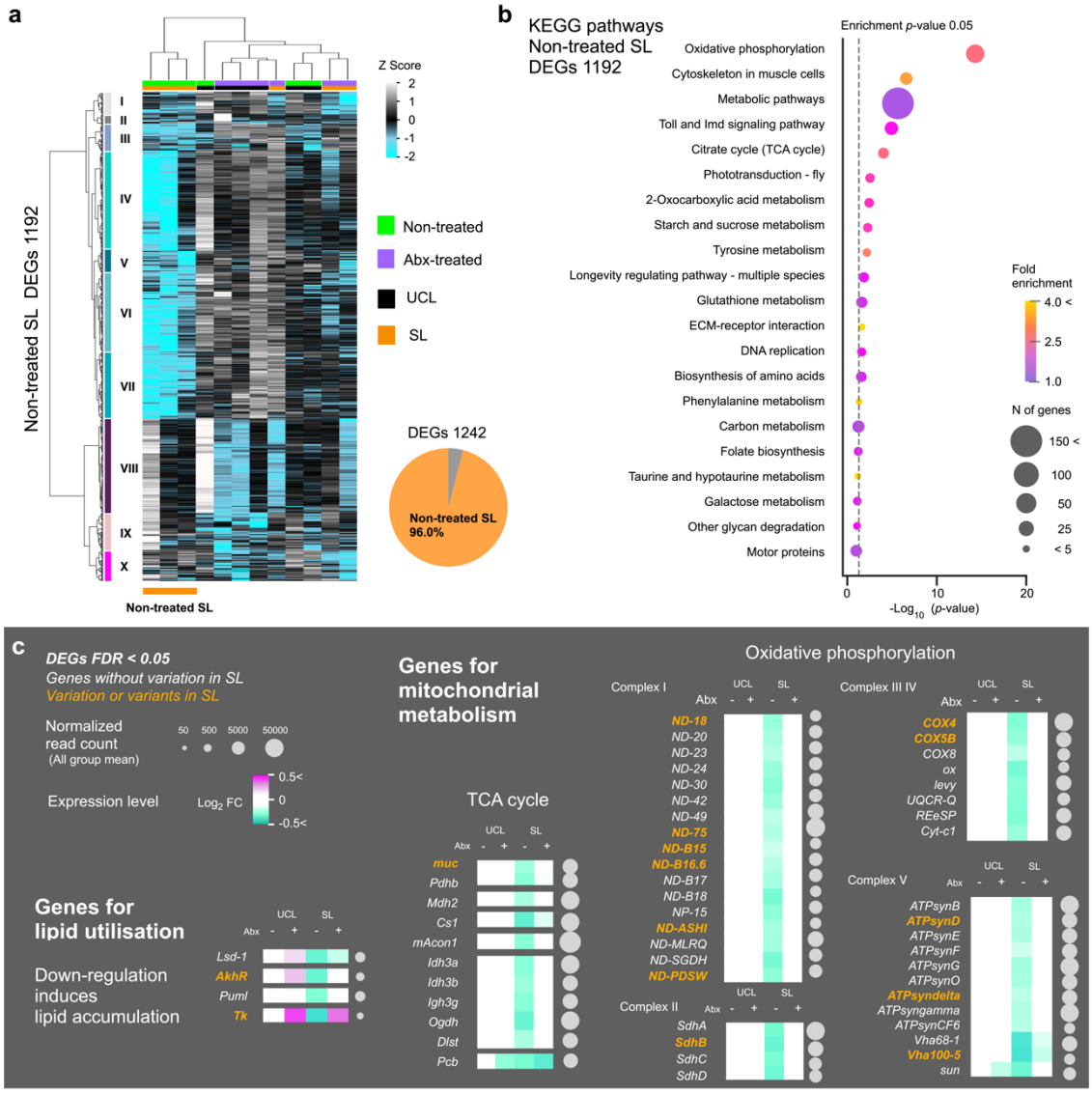


1587

1588 **Fig 8: The characteristic phenotype of SL flies is explained by the host**

1589 **transcriptome.**

1590 **a**, Transcriptome analysis of the whole body of virgin females under non-irradiated

1591 conditions. Cluster map of non-treated SL-specific differentially expressed genes (DEGs)

1592 with a false discovery rate (FDR)-adjusted *p*-value threshold of <0.05. The total number of

1593 DEGs across all comparisons was 1,242, of which 1,192 (96%) were specific to non-treated

1594 SL (pie chart); replicate line 1, generation 50. **b**, Enrichment analysis of non-treated SL

1595 DEGs using KEGG. **c**, Heatmaps illustrating functional profiles. All genes shown are DEGs

1596 (FDR-adjusted *p*-value threshold of < 0.05). Expression levels are presented as mean log2

1597 fold change for each group, calculated by first calculating $\log_2$ FC for individual samples
1598 relative to the average expression in non-treated UCL and then averaging across groups.
1599 The list of genes includes those known to induce lipid accumulation through genetic
1600 manipulation and related mitochondrial metabolism. Genes with orange symbols represent
1601 either SL-specific variations (above 5%) or common homozygous variants in SL. Circles
1602 indicate mean read counts across all groups. For details, see Data S13.
1603

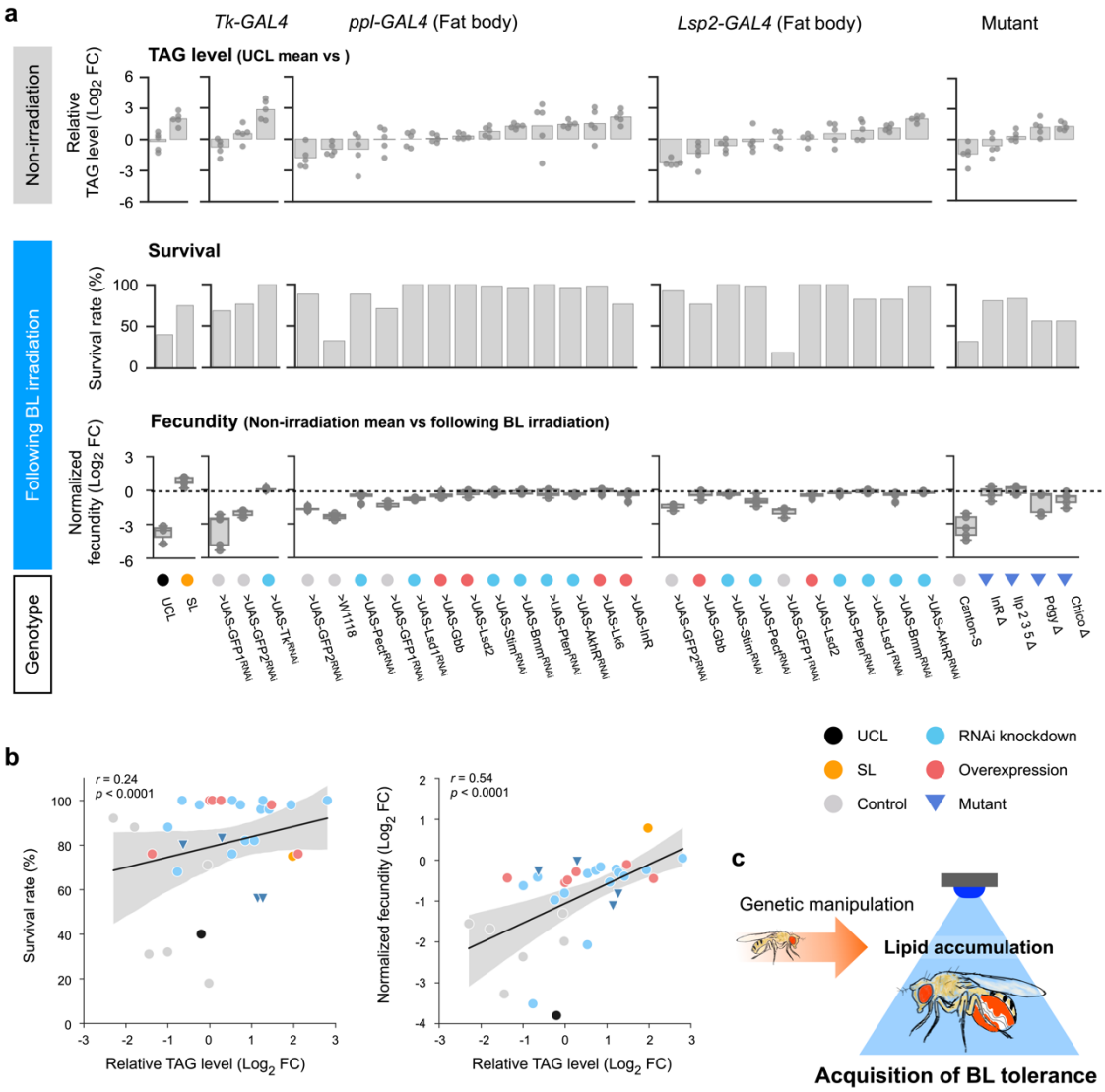


**Fig 9: Lipid accumulation via genetic manipulation confers BL tolerance.**

**a**, Relative TAG levels, survival rates following BL irradiation, and normalised fecundity. TAG levels are presented as $Log_2$ FC values relative to mean UCL levels. Data are arranged in the order of UCL, SL, the *Tachykinin* (neuropeptide) targeting *Tk-GAL4* driver, the fat body targeting *ppl-GAL4* and *Lsp2-GAL4* drivers and mutant lines. The order is sorted by TAG levels, with higher values on the right. Survival rates after 3 days of BL exposure were measured on a minimum of 40 and a maximum of 120 flies per genotype. Genotypes with less than 10% survival were excluded from the data. The full list is available in Data S4. Fecundity was normalised by calculating the $log_2$ FC in the number of offspring after BL

exposure relative to the unexposed control for each genotype. Negative values indicate a reduction in fecundity due to BL toxicity, while zero indicates no effect. Positive values observed in SL only indicate a beneficial effect. Raw fecundity data, including the number of offspring in both non-irradiated and BL irradiated conditions, are presented in Data S7. Genotype labels and colors indicate the effector, the target gene and the type of manipulation (overexpression; red, knockdown; skyblue or null mutation; royalblue). UCL and SL TAG levels were derived from the same dataset as in Fig. 4f (replicate line 1, generation 57). **b**, Correlation analysis. $n$ = 33, Data using mean values for each genotype in Fig.9a. The variance represents the 95% confidence interval. **c**, Summary of experimental results: Lipid accumulation induced by genetic manipulation confers BL tolerance. For details, see Data S15.

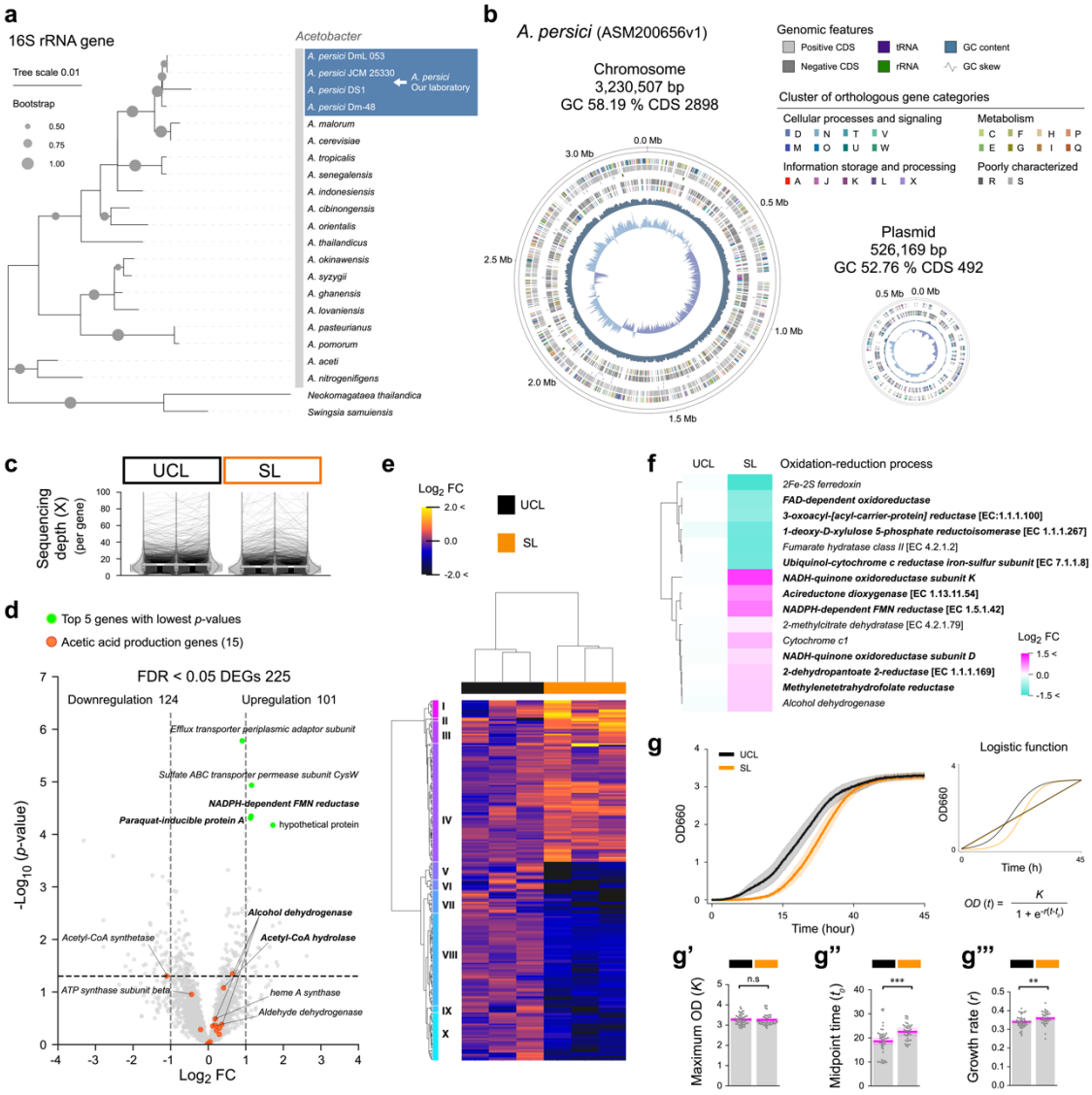


**Fig 10: Phylogenetic relationships, distinct transcriptome and divergent growth patterns of *A. persici* in SL.**

**a**, Phylogenetic tree based on the 16S rRNA gene of *Acetobacter* species identified in the *Drosophila* gut microbiota. *Neokomagataea thailandica* and *Swingsia samuiensis* were used as outgroups. Several strains of *A. persici* were analysed to improve resolution. The arrows indicate the inferred phylogenetic position of the dominant *A. persici* in our laboratory. As the full-length sequence was not available, it was excluded from the phylogenetic tree. See Fig. S19 for the phylogenetic relationships of the *A. persici* strains. The tree was constructed using maximum likelihood with 1,000 bootstrap replicates. **b**,

1636 Complete genome of *A. persici* based on ASM200656v1. The alphabetical annotations
1637 represent functional categories based on the Database of Cluster of Orthologous Genes. **c**,
1638 Sequencing depth calculated from unmapped *Drosophila* reads mapped to *A. persici.*
1639 Sequencing depth estimated from the length per gene length and total bases mapped to
1640 the gene (mean values for UCL: 13.10, SL: 10.63). Genes corresponding to the same locus
1641 are connected by lines. The central white line represents the mean value. See Fig. S19a for
1642 an overview of the depth distribution. See Fig. 8 for host transcriptome data. **d**, Number of
1643 *A. persici* DEGs across host strains and corresponding volcano plot. Genes with the lowest
1644 *p*-values in the top five are shown in lime, while those involved in acetic acid production are
1645 highlighted in red. Genes highlighted in the main text are shown in bold. **e**, Cluster map of
1646 *A. persici* DEGs (FDR-adjusted *p*-value <0.05) in the SL. **f**, List of genes associated with
1647 the oxidation-reduction process (Gene Ontology: biological process). Only DEGs (FDR-
1648 adjusted *p*-value <0.05) are shown. Bold indicates oxidoreductases or translocases. **g**,
1649 Bacterial growth curve between isolates from host strains. $n$ = 44 (UCL), 37 (SL). The
1650 bacterial growth curve shows the mean OD values with a 95% confidence interval,
1651 estimated by bootstrap resampling ($n$ = 10,000, seed = 4). **g'**, Maximum OD ($K$); $BF_{10}$ =
1652 0.52, **g''**, Midpoint time ($t_0$); $BF_{10}$ = 0.37, **g'''**, growth rate ($r$); $BF_{10}$ = 8.94, Asterisks indicate
1653 significance: ** *p*MCMC < 0.01; *** *p*MCMC < 0.001, n.s = not significant; replicate line 1,
1654 generation 52. **g**–**g'''** represent the same dataset. Statistical analyses for panels **g'**–
1655 **g'''**were performed using HBM with MCMC methods, posterior median, and Bayesian 95%
1656 CI. For details, see Data S16 for all results, including statistical models.
1657

# Supplementary information

## Gut microbiota–mediated lipid accumulation as a driver of evolutionary adaptation to blue light toxicity in *Drosophila*

Yuta Takada[1], Toshiharu Ichinose[2,3], Naoyuki Fuse[4], Kokoro Saito[3], Wakako Ikeda-Ohtsubo[1], Hiromu Tanimoto[3], Masatoshi Hori[1]

[1]Graduate School of Agricultural Sciences, Tohoku University, Japan
[2]Frontier Research Institute for Interdisciplinary Sciences, Tohoku University, Japan
[3]Graduate School of Life Sciences, Tohoku University, Japan
[4]Graduate School of Pharmaceutical Sciences, Tohoku University, Japan

Correspondence to Yuta Takada or Masatoshi Hori
yutatakada38@gmail.com
masatoshi.hori.a3@tohoku.ac.jp

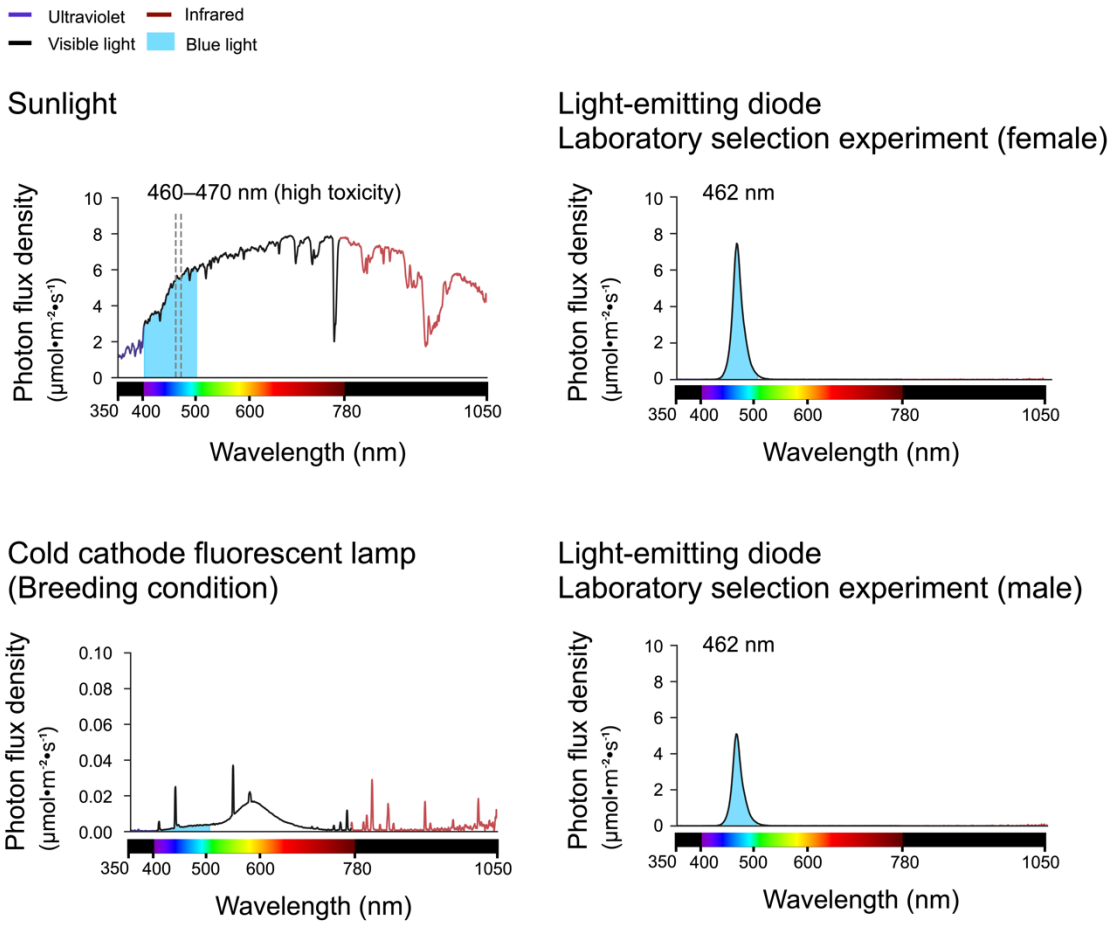


**Fig. S1: Sunlight contains a significant amount of blue light.**

Sunlight photon flux density: Sendai, Japan; 38°N, 140°E, clear sky; November 21, 2021; 11:30 AM (approximately 4000 μmol·m$^{-2}$·s$^{-1}$, blue light (BL): approximately 470 μmol·m$^{-2}$·s$^{-1}$). 460–470 nm is a highly toxic wavelength range for *Drosophila* adults. Laboratory selection experiment (female) light condition photon flux density: approximately 175 μmol·m$^{-2}$·s$^{-1}$, BL: approximately 175 μmol·m$^{-2}$·s$^{-1}$ (10.3 × 10$^{18}$ photons·m$^{-2}$·s$^{-1}$)). Laboratory selection experiment (male) light condition photon flux density: approximately 120 μmol·m$^{-2}$·s$^{-1}$, BL: approximately 120 μmol·m$^{-2}$·s$^{-1}$ (6.5 × 10$^{18}$ photons·m$^{-2}$·s$^{-1}$)). Breeding light condition photon flux density: approximately 3 μmol·m$^{-2}$·s$^{-1}$, BL: approximately 0.3 μmol·m$^{-2}$·s$^{-1}$. For details, see Source data (Light condition and Fig. S1).

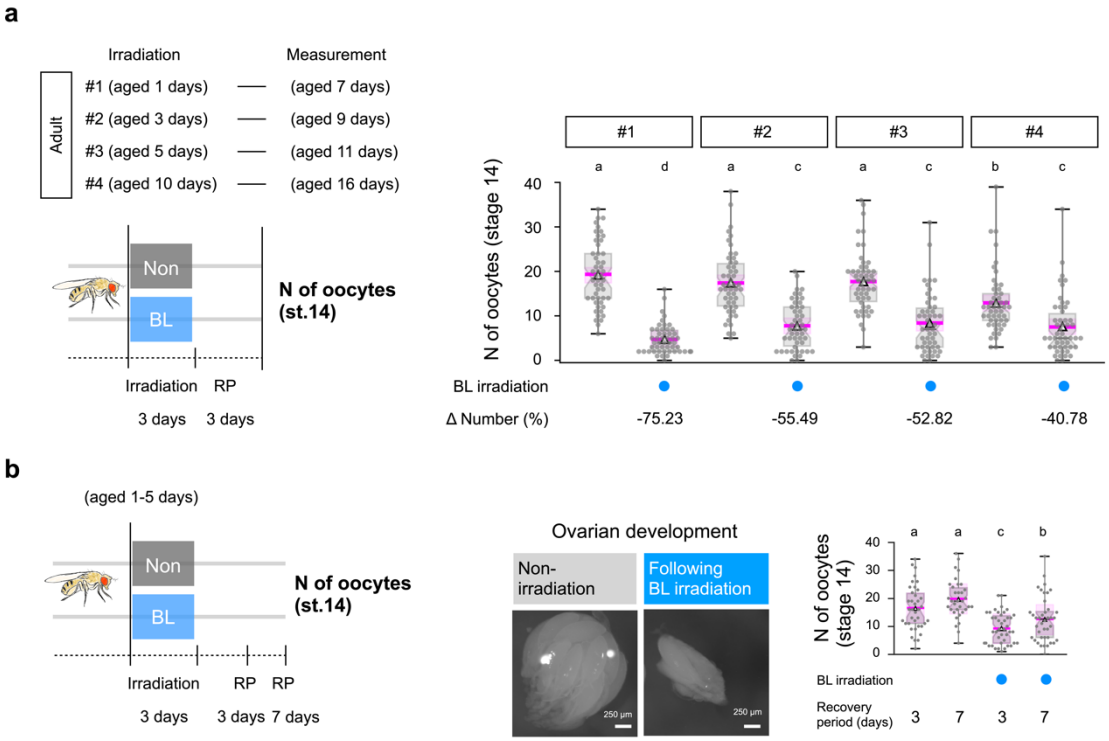


## Fig. S2: Dramatic impact on fitness due to BL toxicity

**a**, Impact of BL toxicity on flies (Canton-S strain) of different ages subjected to a single irradiation for 3 days and a recovery period (RP) of 3 days. $n$ = 50, Bayes factor 10 ($BF_{10}$) > 100. Δ Number is percent change in same age non-irradiation vs following BL irradiation. **b**, Impact of BL toxicity on UCL flies (generation 34) subjected to a single irradiation for 3 days: ovarian development, the number of stage 14 oocytes after recovery. $n$ = 34–42. $BF_{10}$ > 100. Statistical analyses for panels **a** and **b** were performed using Hierarchical Bayesian Model (HBM) with Markov Chain Monte Carlo (MCMC) methods, posterior median, and Bayesian 95% credible intervals (CI). In **a** and **b**, different letters indicate significant differences at $p$MCMC < 0.05. For details, see Data S1 for all results, including statistical models.

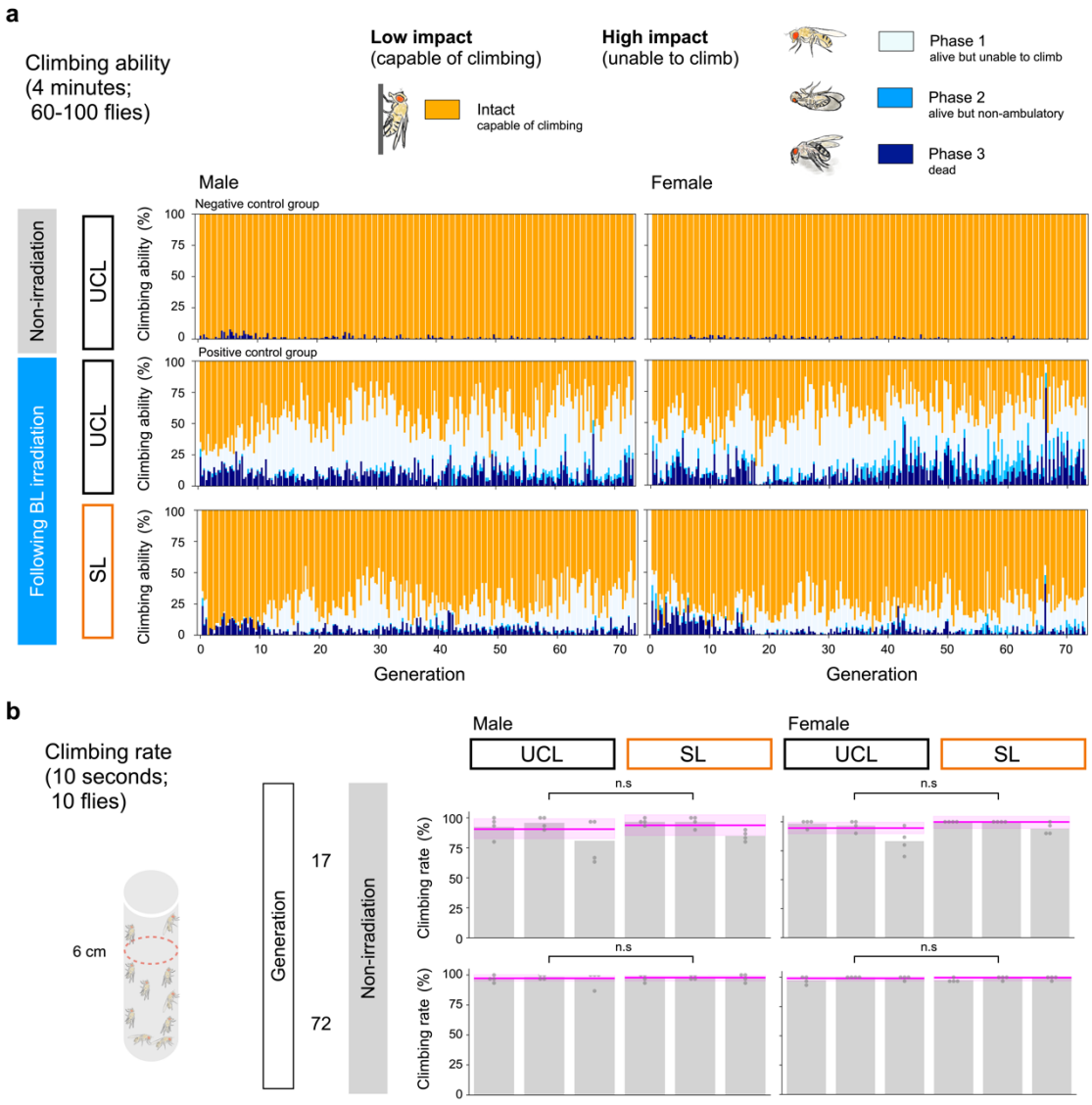


**Fig. S3: SL flies are BL tolerant.**

**a**, Climbing ability and generational changes in male and female flies after exposure to BL irradiation. Climbing ability is represented by a total of 60–100 flies per bar, with bars representing replicate lines 1, 2, and 3. All categories were exposed to BL except the negative control group (top). Negative control group: The UCL flies were kept in darkness for 3 days instead of BL irradiation. Positive control group: A subset of UCL flies in each generation was exposed to BL under the same conditions as SL. **b**, Climbing rate under non-irradiated conditions. The percentage of 10 flies that crossed the 6 cm reference line within 10 seconds of tapping. Each measurement was repeated three times, and the average was taken as the climbing rate. *n* = 12 (corresponding to 120 flies). Statistical analyses for panels **b** were performed using a HBM with MCMC methods, posterior median, and Bayesian 95% CI. n.s = not significant. For details, see Data S1 for all results,

including statistical models. The source data (Light condition) contains all the light condition measurements used in the experiment.

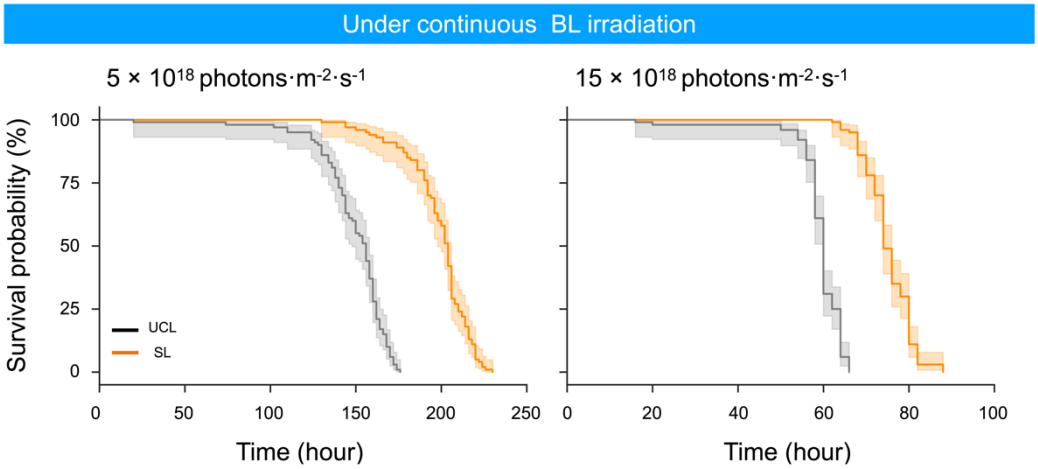


**Fig. S4: The 73rd generation SL flies show high survival under BL irradiation.**

Lifespan under continuous BL irradiation. Kaplan–Meier survival curve, 5 × $10^{18}$ photons·$m^{-2}$·$s^{-1}$, Female *n* = 100, $BF_{10}$ >100. Estimates: UCL 149.25 h (145.09–153.11), SL 198.65 h (194.71–202.77). 15 × $10^{18}$ photons·$m^{-2}$·$s^{-1}$, Female *n* = 100, $BF_{10}$ >100. Estimates: UCL 59.12 h (58.00–60.31), SL 75.28 h (74.01–76.57), *p*MCMC < 0.001. Replicate line 1, generation 73. For details, see Data S3 for all results, including statistical models.

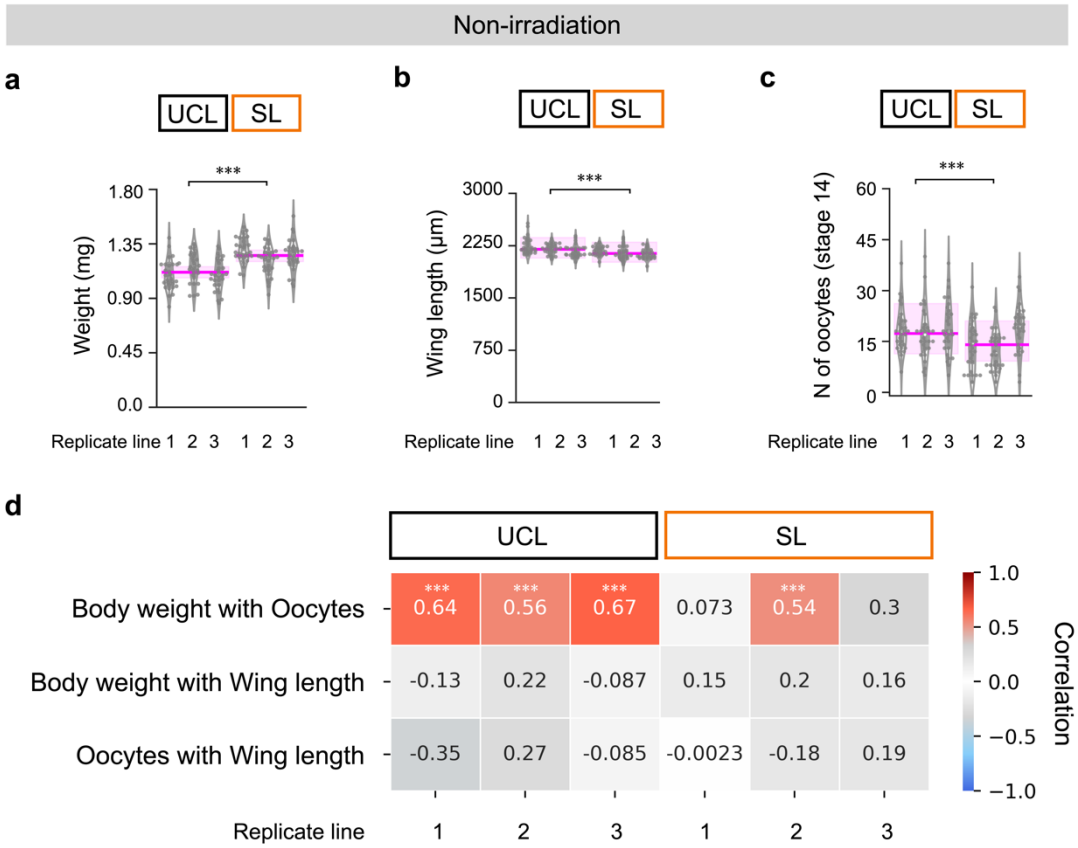


**Fig. S5: SL flies have heavier bodies, shorter wings and fewer oocytes.** **a**, Body weight. $n$ = 90, $BF_{10}$ > 100; generation 28. **b**, Wing length. $n$ = 90, $BF_{10}$ = 91.1; generation 28. **c**, Number of stage 14 oocytes. $n$ = 90, $BF_{10}$ = 2.46; generation 28. **d,** Correlation between traits, based on data from panels **a**–**c**. $n$ = 30. Asterisks indicate significance: *** $p$ < 0.001. Statistical analyses for panels **a**–**c** were performed using a HBM with MCMC methods, posterior median, and Bayesian 95% CI. Asterisks indicate significance levels: *** $p$MCMC < 0.001. See Data S4 for details of all results, including statistical models.

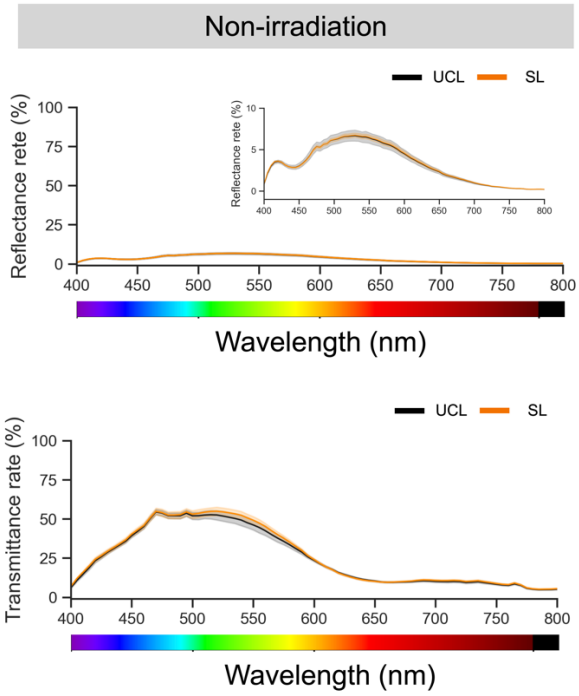


**Fig. S6: No differences in light reflection or transmission due to physical characteristics.**

Reflectance rate and transmittance rate in female abdomens, *n* = 16; replicate line 1, generation 49.

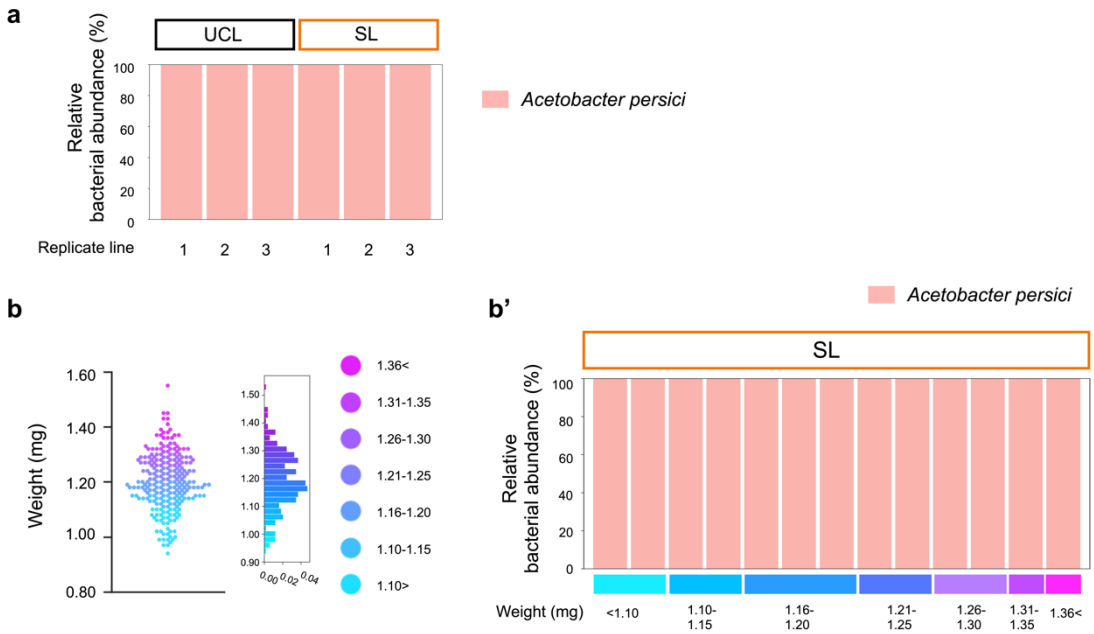


**Fig. S7: The gut microbiota of SL flies consists of a single *Acetobacter* species.**

**a**, Relative bacterial abundance based on 16S rRNA amplicon sequencing in SL and UCL. The DNA samples used were the same as those used for whole-genome resequencing in Fig 6 (generation 44). **b**, Overview of body weight distribution in the SL flies. replicate line 1, *n* = 240; generation 45. **b'**, Relative bacterial abundance based on 16S rRNA amplicon sequencing in SL replicate line 1, generation 45. For details, see Data S5.

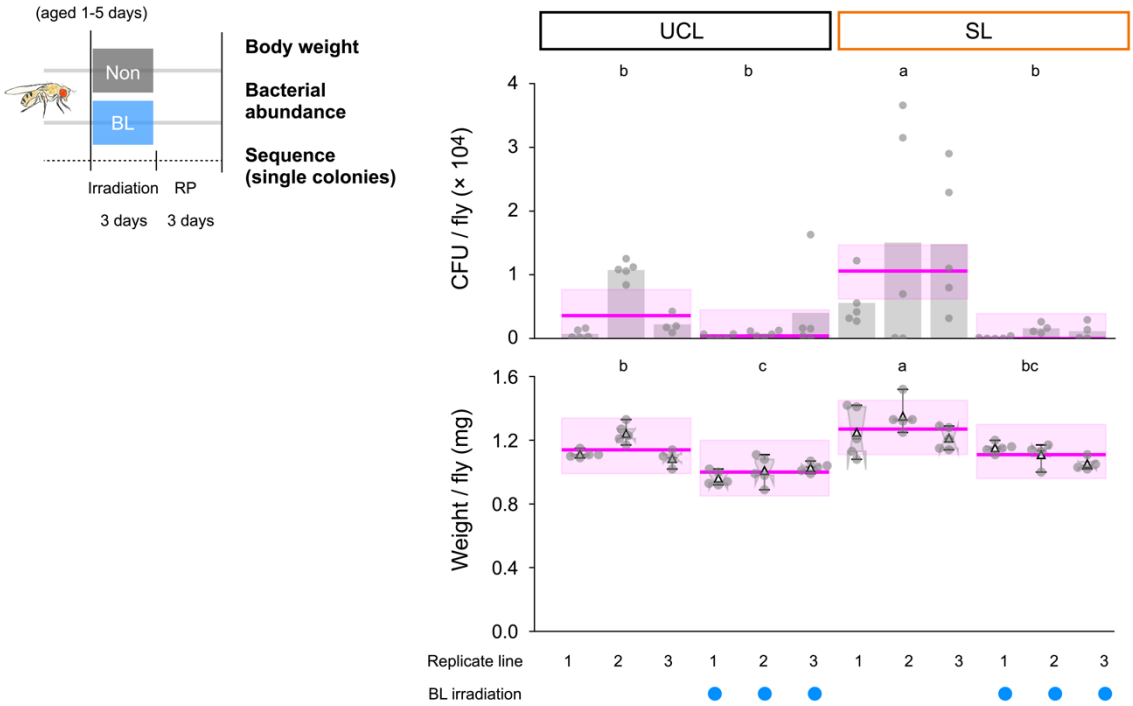


**Fig. S8: Dramatic reduction in gut microbiota and body weight of *Drosophila* after BL irradiation.**

**a**, Bacterial abundance and Body weight, $n$ = 13–15, $BF_{10}$ >100; generation 38. Randomly picked colonies were sequenced for 16S rRNA genes and all bacteria were identified as *A. persici.* Statistical analyses were performed using HBM with MCMC methods, posterior median, and Bayesian 95% CI. Different letters indicate significant differences at *p*MCMC < 0.05. See Data S6 for details of all results, including statistical models.

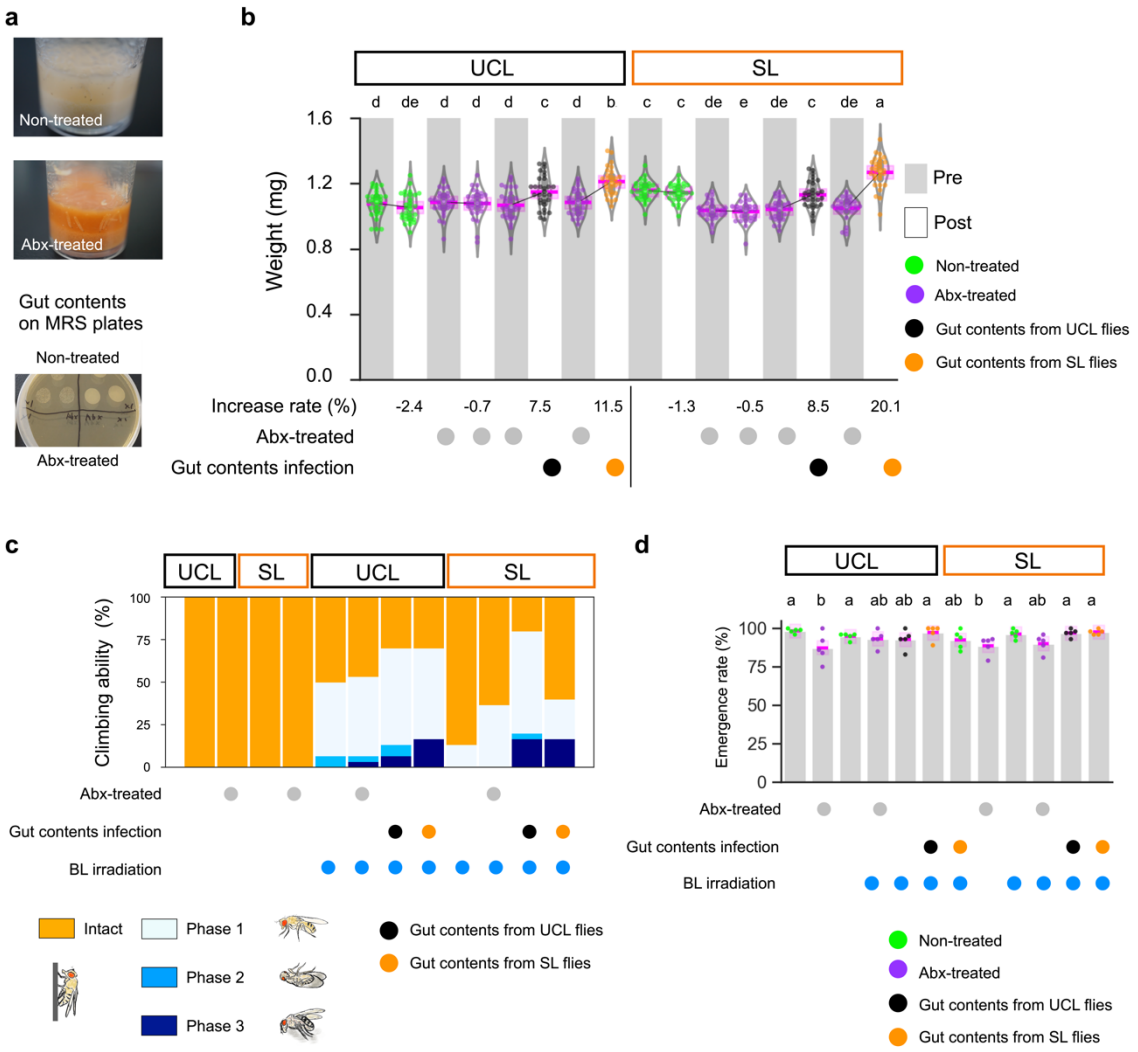


**Fig. S9: The unique phenotypes of SL flies depend on gut microbiota.** **a**, Effect of antibiotic mixture (Abx) treatment on gut microbiota. **b**, Impact of Abx treatment and infection with gut contents on body weight. Grey bars represent pre-infection, while white bars indicate post-infection after 4 days. $n$ = 30, $BF_{10}$ > 100; replicate line 1, generation 47. **c**, Climbing ability following BL irradiation. Each bar represents a total of 30 flies; replicate line 1, generation 47. **d**, Emergence rate, based on data shown in Fig 4B. $BF_{10}$ = 1.30; replicate line 1, generation 47. Statistical analyses for panels **b** and **d** were performed using HBM with MCMC methods. Different letters indicate significant differences at $p$MCMC < 0.05. See Data S7 for details of all results, including statistical models.

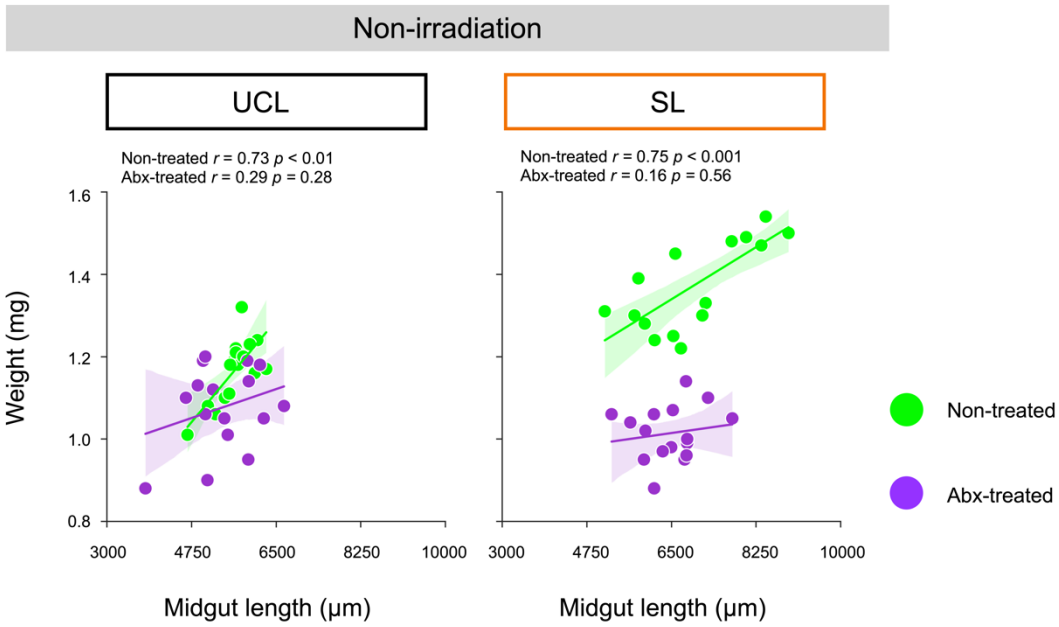


**Fig. S10: *Drosophila* body weight and midgut length positively correlate in the presence of gut microbiota.**

Correlation between body weight and midgut length, based on data from Fig. 5f. $n$ = 16, replicate line 1, generation 48. For details, see Data S7.

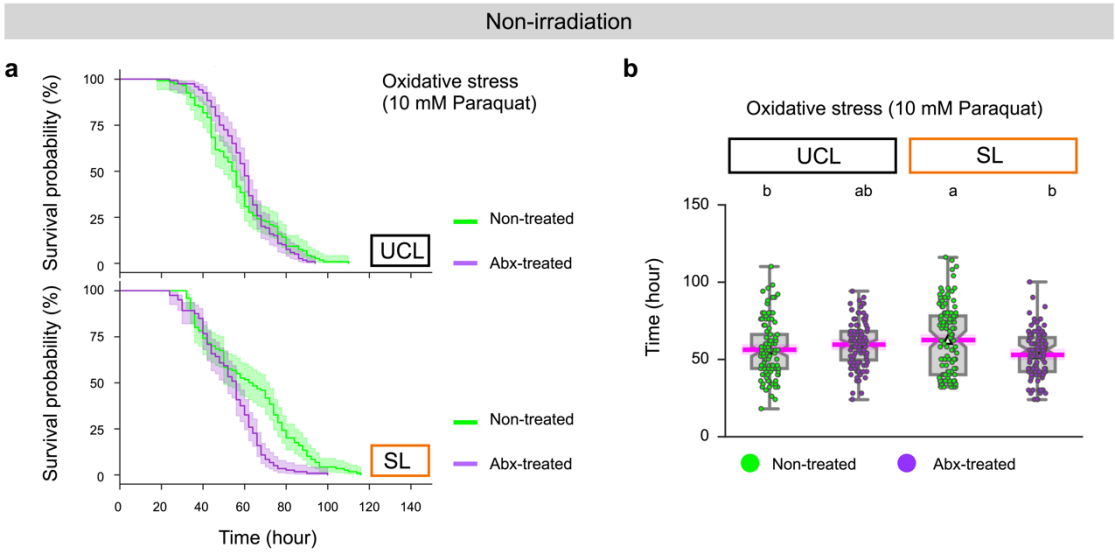


**Fig. S11: Resistance to oxidative stress in SL flies depends on gut microbiota.**

**a**, Oxidative stress resistance in SL flies treated with 10 mM paraquat. Kaplan–Meier survival curve, $n$ = 120; replicate line 1, generation 52. **b**, Oxidative stress resistance in SL and UCL flies treated with 10 mM paraquat. $n$ = 120, $BF_{10}$ = 0.01. Survival: non-treated UCL 56.36 h (53.29–59.43), Abx-treated UCL 59.57 h (56.33–62.61), non-treated SL 62.48 h (59.42–65.64), Abx-treated SL 53.10 h (50.02–56.22); replicate line 1, generation 52. Statistical analysis was performed using HBM with MCMC methods. Different letters indicate significant differences at $p$MCMC < 0.05. See Data S7 for details of all results, including statistical models.

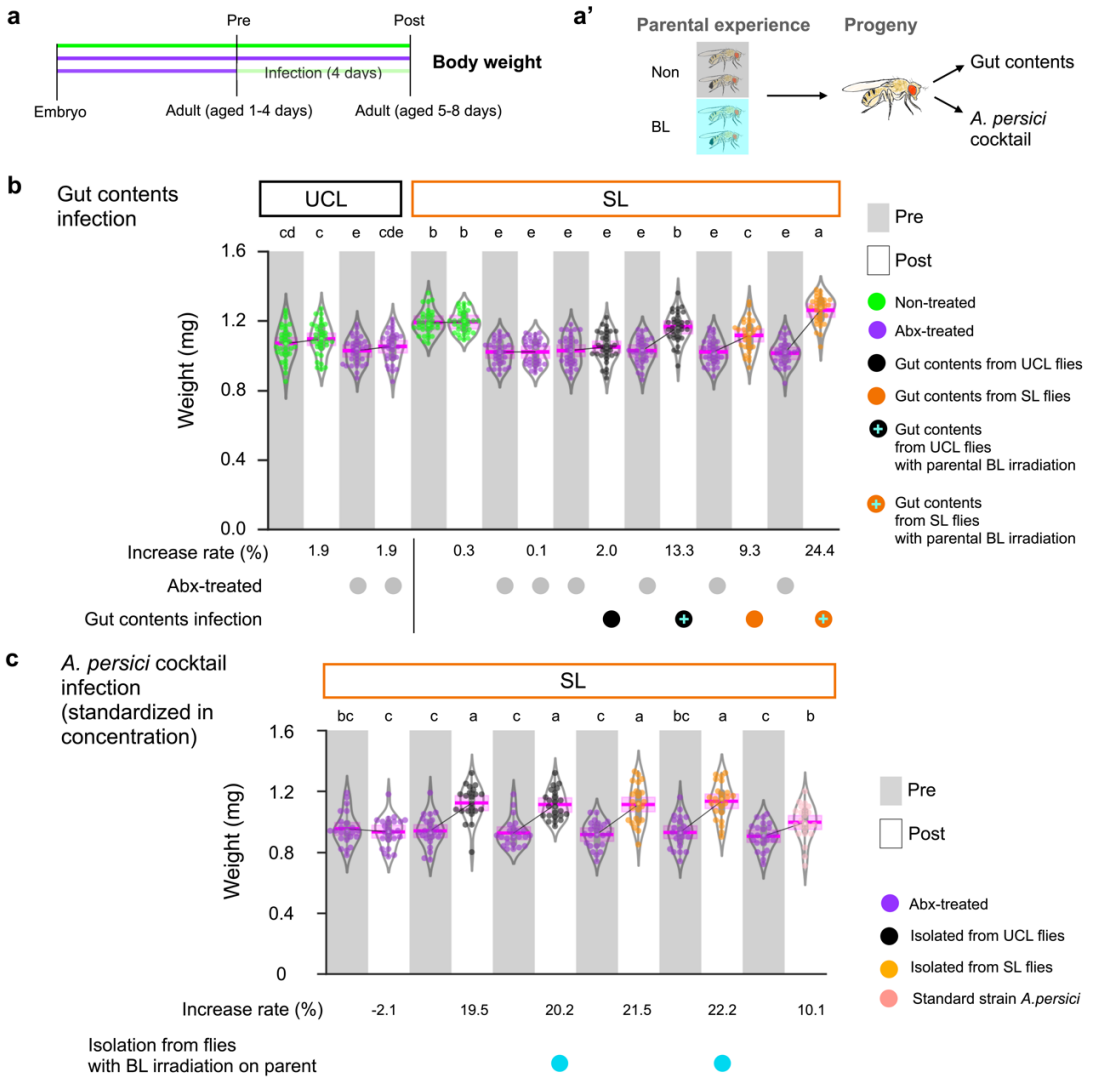


**Fig. S12: Greater bacterial abundance leads to higher body weight.**

**a**, Schematic of the infection experiment. **a'**, Overview of gut contents or isolated *Acetobacter persici* cocktail from offspring of parents exposed to BL. **b**, Impact of infection with gut contents on body weight. $n$ = 30. **c**, Impact of infection with *A. persici* cocktail on body weight. $n$ = 23,24. In both panels, grey bars represent pre-infection; white bars indicate post-infection after 4 days. $BF_{10}$ >100; replicate line 1, generation 53. Statistical analyses were performed using HBM with MCMC methods. Different letters indicate significant differences at $p$MCMC < 0.05. See Data S8 for details of all results, including statistical models.

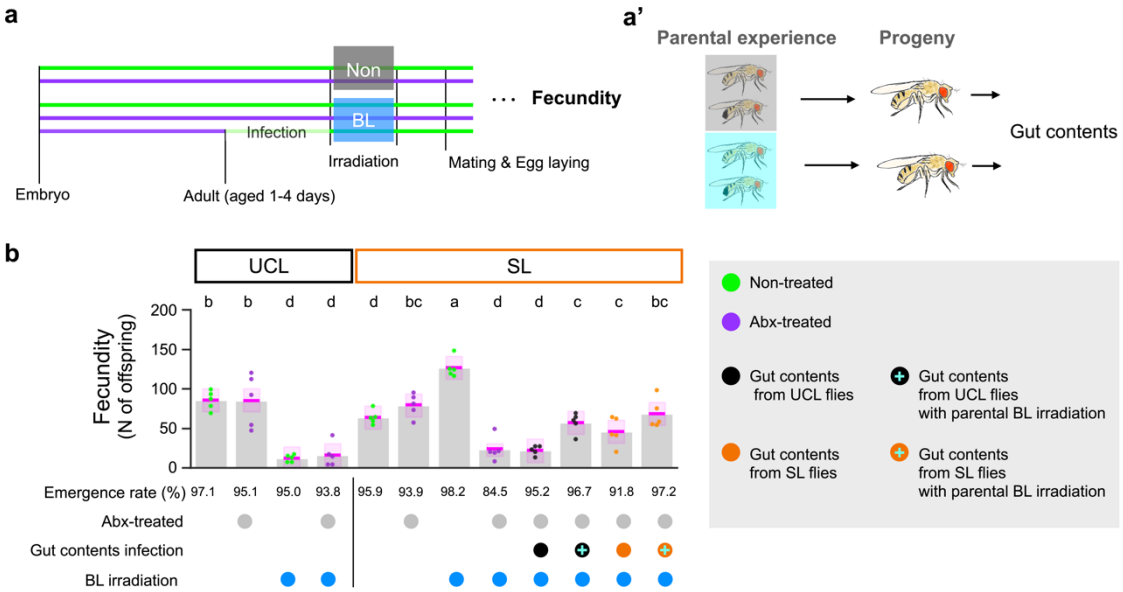


1798

1799 **Fig. S13: Gut contents from BL-exposed UCL parental flies restore**
1800 **fecundity in Abx-treated SL flies.**

1801 **a**, Schematic of the infection experiment. **a'**, Overview of gut contents from offspring of
1802 parents exposed to BL. **b**, Fecundity: number of offspring (adults). $n = 5$. $BF_{10} > 100$; replicate
1803 line 1, generation 53. Statistical analysis was performed using HBM with MCMC methods.
1804 Different letters indicate significant differences at *p*MCMC < 0.05. See Data S8 for details of
1805 all results, including statistical models.

1806

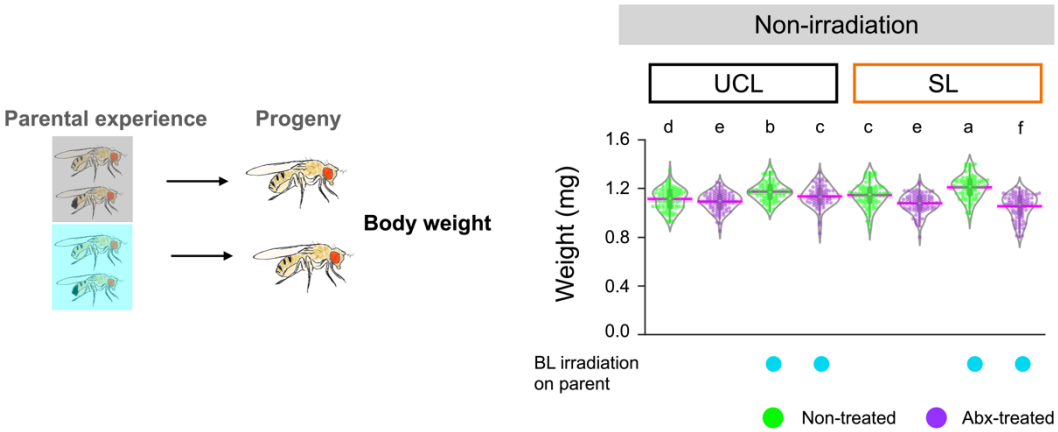


**Fig. S14: Parental BL experience increases body weight in progeny.**

Overview of the offspring of parents exposed to BL. Data is based on female body weight. *n* = 72–90, $BF_{10}$ > 100; replicate line 1, generation 46. Statistical analysis was performed using HBM with MCMC methods. Different letters indicate significant differences at *p*MCMC < 0.05. See Data S8 for details of all results, including statistical models.

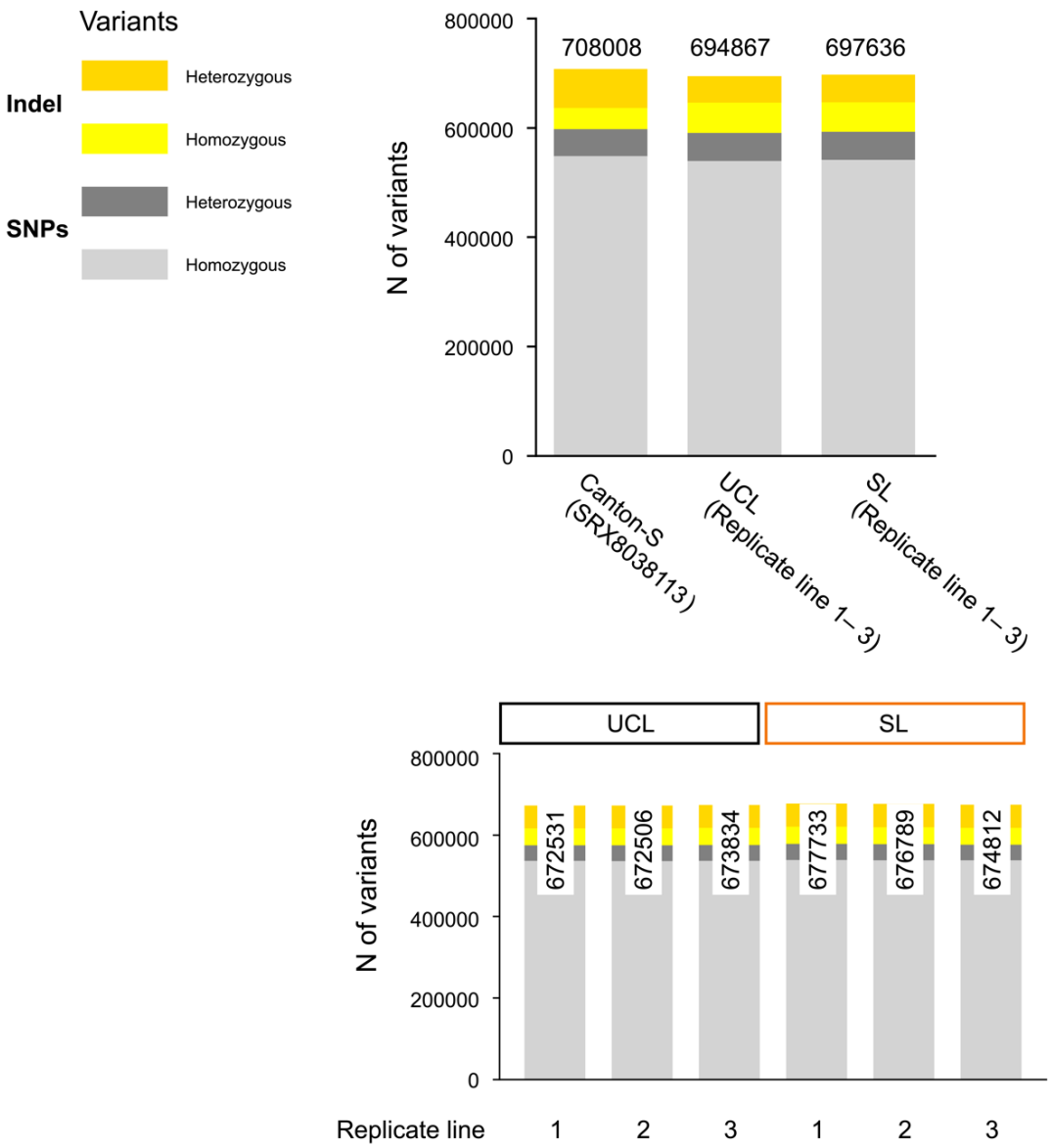


**Fig. S15: Number of variants potentially present in the strains used for the selection experiment.**

Number of variants in the Canton-S strain (SRX8038113), UCL and SL. Variants in UCL and SL are the total number of variants from replicate lines 1 to 3. The bottom panel shows the number of variants for each replicate line. Colour differences indicate SNPs and indels as well as homozygous and heterozygous variants. The numbers on or within the bars represent the total number of variants.

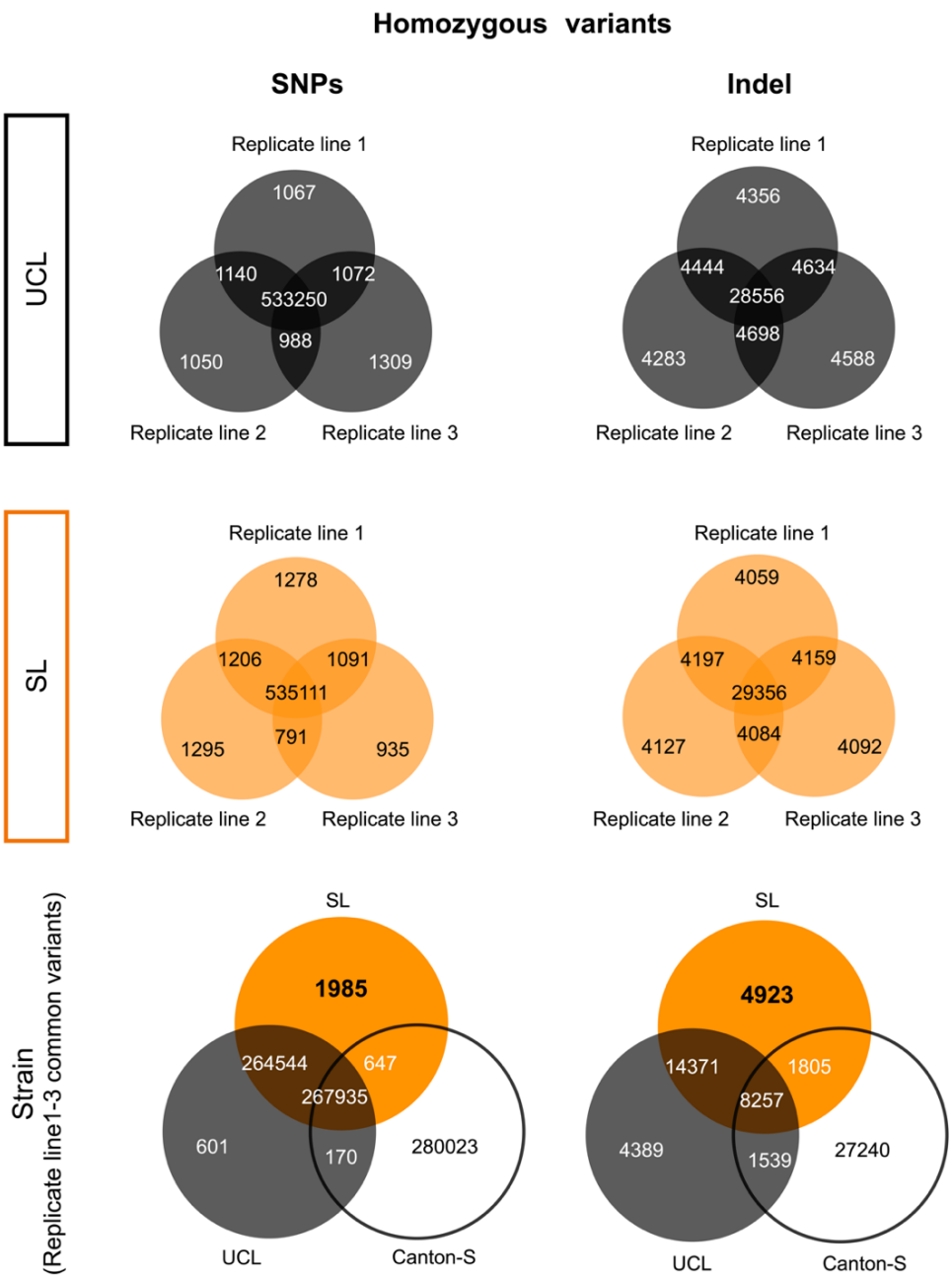


**Fig. S16: Number of homozygous variants specific to SL and shared by all three replicate lines, potentially selected under BL toxicity.**

Common and unique variants identified in each replicate line across different strains. Variants shared within a strain were considered strain-specific, whereas homozygous variants absent in both UCL and Canton-S were defined as SL-specific.

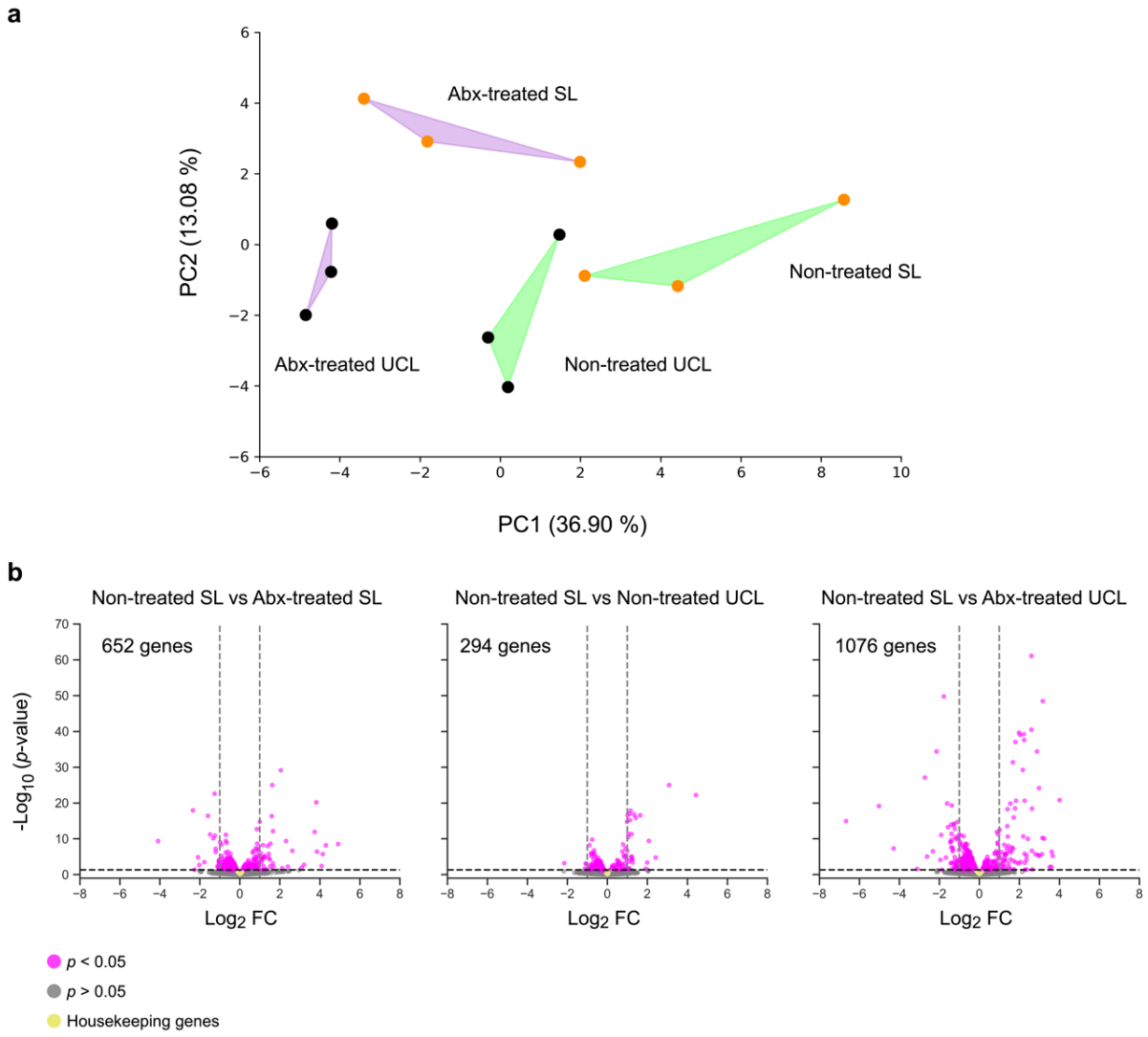


**Fig. S17: Overview of the host transcriptome profiles.**
**a**, Principal component analysis (PCA) of transcriptome profiles using normalised read counts. **b**, Volcano plots comparing non-treated SL with each condition. Differentially expressed genes (DEGs) with a false discovery rate (FDR)-adjusted *p*-value threshold of <0.05 are shown in magenta. Housekeeping genes were defined based on Ferrari and Aitken, 2006, *BMC Genomics*. For details, see Data S13.

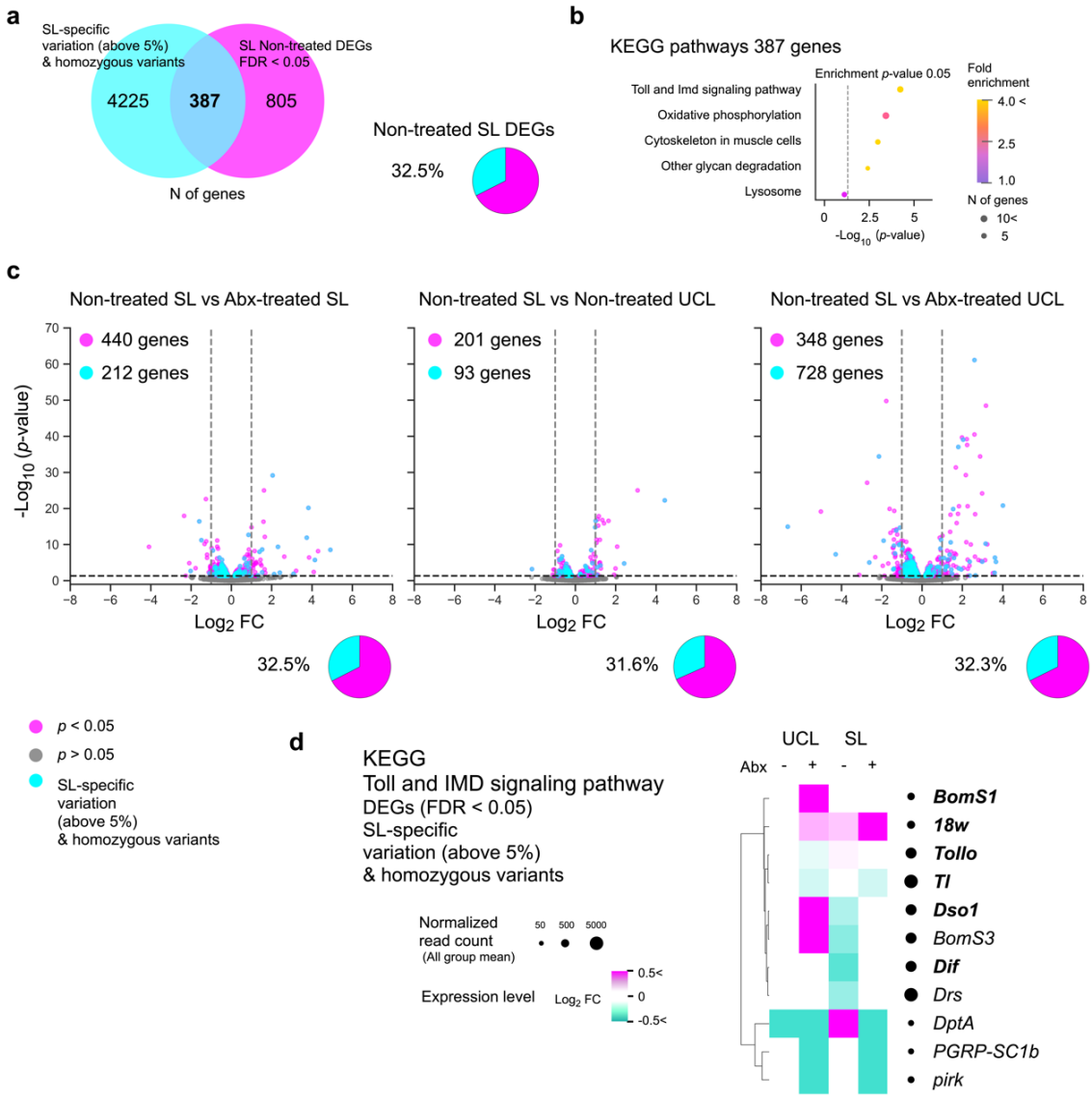


**Fig. S18: Genes shared between genetic characteristics unique to SL and non-treated SL DEGs are enriched in immune-related pathways.**

**a**, Venn diagram of genetic characteristics unique to SL and differentially expressed genes (DEGs) in non-treated SL, showing a 32.5% overlap. **b**, Enrichment analysis of 387 overlapping genes using the Kyoto Encyclopedia of Genes and Genomes (KEGG), with the top hit identified as the Toll and Imd signaling pathway. **c**, Volcano plots comparing non-treated SL with each condition, highlighting genetic characteristics unique to SL. Approximately 32% overlap was observed across all treatments. **d**, Expression levels of Toll and IMD signaling pathway genes shared between genetic characteristics unique to SL and non-treated SL DEGs. Expression levels are presented as mean $\log_2$ FC for each group, calculated by first calculating $\log_2$ FC for individual samples relative to the average

1848 expression in non-treated UCL and then averaging across groups. Circles indicate mean
1849 read counts across all groups. Homozygous variants are indicated in bold. For details, see
1850 Data S14.
1851

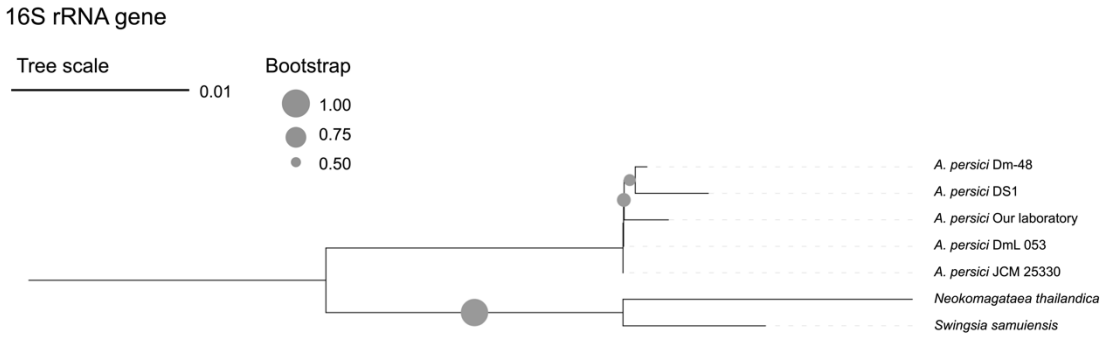


**Fig. S19: Phylogenetic tree based on the 16S rRNA gene of *A. persici***

Phylogenetic relationship between the dominant OTU ID (397 bp), which comprised 89-98% of *A. persici* in our laboratory, and other *A. persici* strains. Other bacterial species were analysed using full-length sequences (1,391-1,498 bp). *Neokomagataea thailandica* and *Swingsia samuiensi*s were used as outgroups. The tree was constructed using maximum likelihood with 1,000 bootstrap replicates.

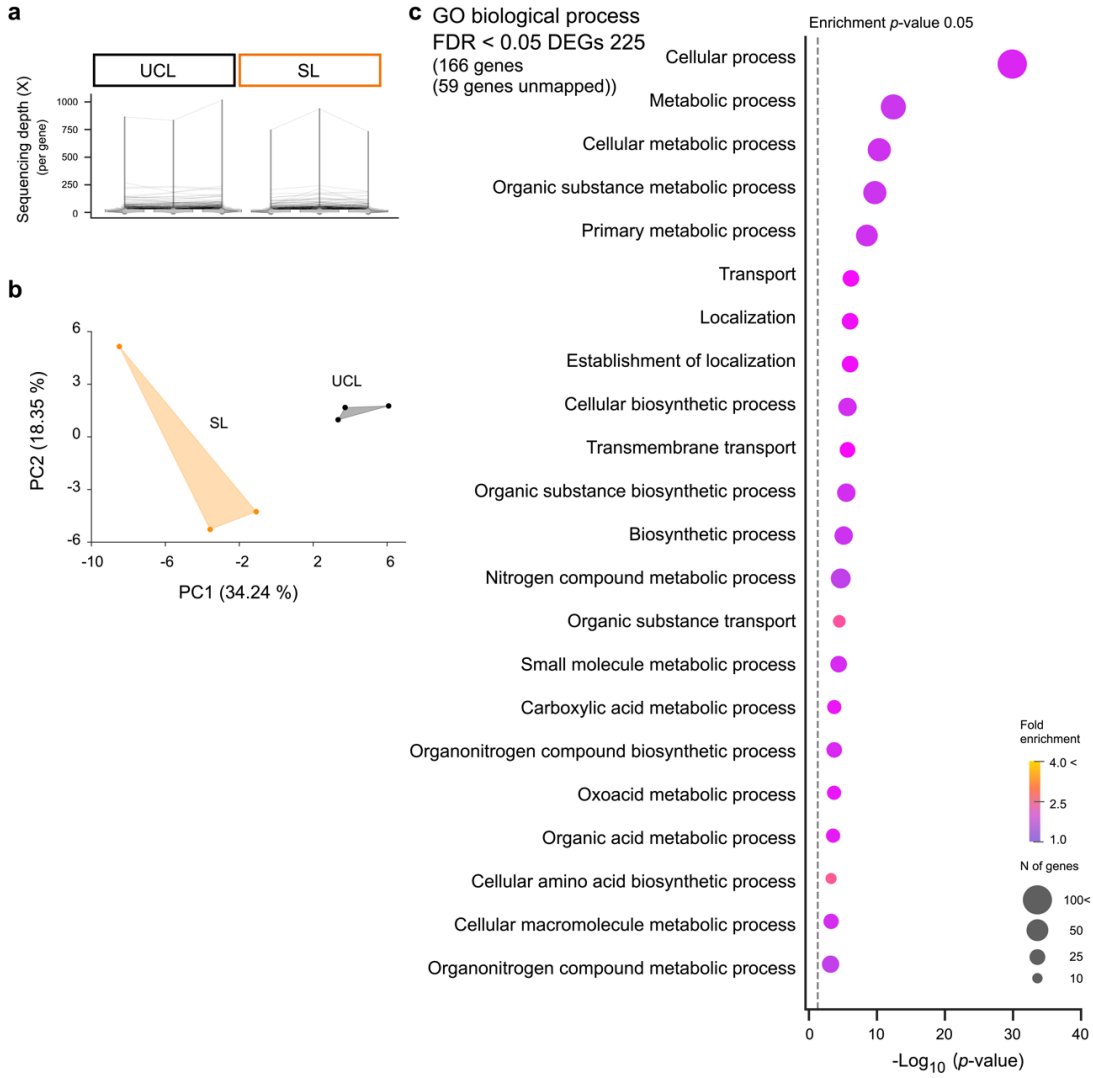


**Fig. S20: Transcriptome profile of the gut microbiota *A. persici***

**a**, Sequence depth based on mapping results. After extracting unmapped reads from the *Drosophila melanogaster* host (GCA_000001215.4), the dominant gut bacteria *A. persici* (ASM200656v1) was used as a reference for mapping. The same genes are connected by lines. The gene with the highest sequencing depth across all samples was *Large ribosomal subunit protein bL12*. See Fig 10 c for magnification and mean values. **b**, PCA based on transcripts per million (TPM). **c**, Enrichment analysis of 225 DEGs (Gene Ontology (GO); biological process), predominantly indicative of metabolic pathways. GO enrichment analysis was then performed on 166 genes mapped by DEGs to the STRING database.

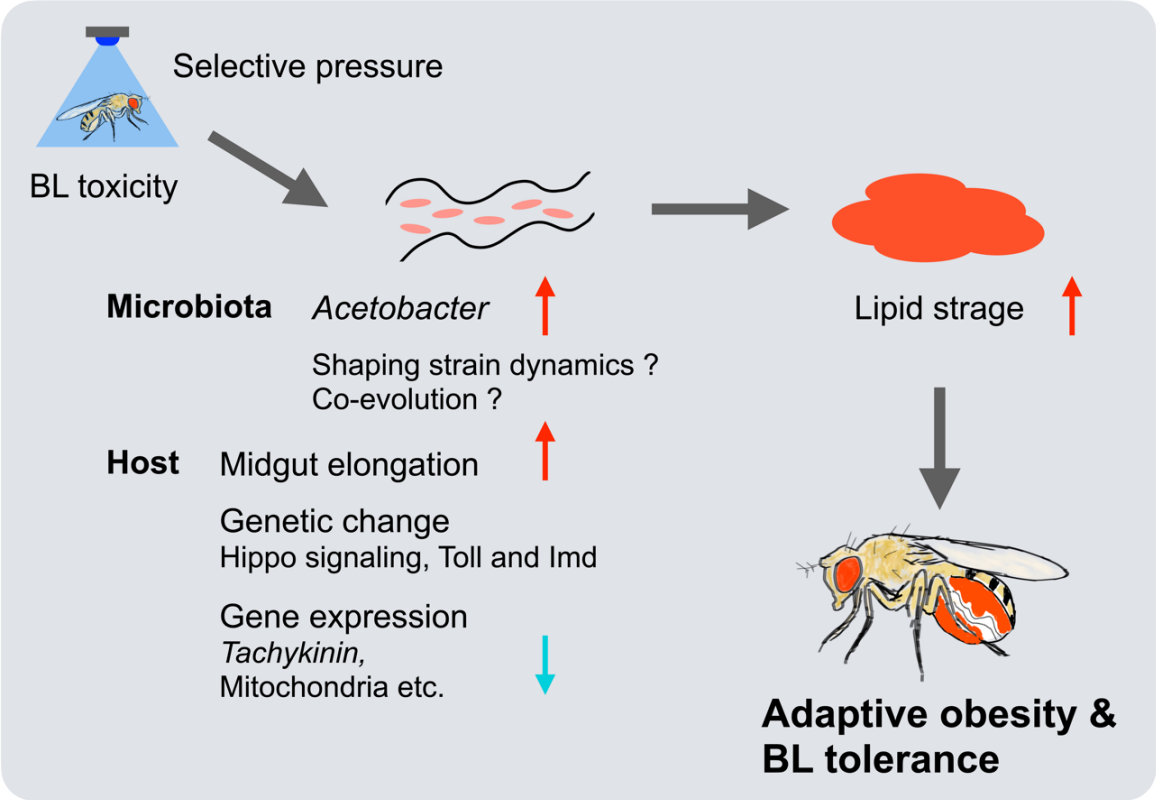


**Fig. S21: Gut microbiota–mediated obesity drives evolutionary adaptation to BL toxicity.**

Evolutionary adaptation to BL toxicity involves selective pressure and the intergenerational transmission of parental experience, which drives midgut elongation, increased bacterial abundance, and optimisation of both host genetic information and microbiota interaction. The shaping of bacterial strain dynamics or bacterial evolution may occur in parallel with host evolution. This process may be associated with increases in bacterial abundance and phenotypic changes, suggesting that both quantitative and qualitative changes in bacterial traits may alter host interactions. These changes can alter gene expression related to lipid metabolism, facilitating the formation of adaptive obesity characterised by lipid accumulation via the gut microbiota. Red arrows indicate an increase, while light blue arrows indicate a suppression.